

EFFECT OF SOLVENT CHOICE ON CELLULOSE ACETATE MEMBRANE
FABRICATION BY PHASE INVERSION AND DEACETYLATION BY
ALKALINE HYDROLYSIS

A THESIS SUBMITTED TO
THE GRADUATE SCHOOL OF NATURAL AND APPLIED SCIENCES
OF
MIDDLE EAST TECHNICAL UNIVERSITY

BY

FATMA SEDEN TEKİN

IN PARTIAL FULFILLMENT OF THE REQUIREMENTS
FOR
THE DEGREE OF MASTER OF SCIENCE
IN
CHEMICAL ENGINEERING

AUGUST 2022

Approval of the thesis:

**EFFECT OF SOLVENT CHOICE ON CELLULOSE ACETATE
MEMBRANE FABRICATION BY PHASE INVERSION AND
DEACETYLATION BY ALKALINE HYDROLYSIS**

submitted by **FATMA SEDEN TEKİN** in partial fulfillment of the requirements for
the degree of **Master of Science in Chemical Engineering, Middle East Technical
University** by,

Prof. Dr. Halil Kalıpçılar
Dean, Graduate School of **Natural and Applied Sciences**

Prof. Dr. Pınar Çalık
Head of the Department, **Chemical Engineering**

Assoc. Prof. Dr. Zeynep Çulfaz Emecen
Supervisor, **Chemical Engineering, METU**

Examining Committee Members:

Prof. Dr. Levent Yılmaz
Chemical Engineering, METU

Assoc. Prof. Dr. Zeynep Çulfaz Emecen
Chemical Engineering, METU

Assoc. Prof. Dr. Emre Büküşođlu
Chemical Engineering, METU

Prof. Dr. Akın Akdađ
Chemistry, METU

Assoc. Prof. Dr. Berna Topuz
Chemical Engineering, Ankara University

Date: 31.08.2022

I hereby declare that all information in this document has been obtained and presented in accordance with academic rules and ethical conduct. I also declare that, as required by these rules and conduct, I have fully cited and referenced all material and results that are not original to this work.

Name Last name : Fatma Seden Tekin

Signature :

ABSTRACT

EFFECT OF SOLVENT CHOICE ON CELLULOSE ACETATE MEMBRANE FABRICATION BY PHASE INVERSION AND DEACETYLATION BY ALKALINE HYDROLYSIS

Tekin, Fatma Seden
Master of Science, Chemical Engineering
Supervisor: Assoc. Prof. Dr. Zeynep Çulfaz Emecen

August 2022, 127 pages

In this study, the effect of solvent choice on cellulose acetate (CA) membrane morphology and performance was investigated to relate this to the thermodynamics and kinetics of phase inversion. Three different solvent systems were used, which are dimethyl sulfoxide (DMSO), the mixture of DMSO: acetone (DA) and DMSO: acetic acid (DHAc) in the ratio of 1:1. Water was used as non-solvent. Acetone and acetic acid were chosen due to their similar solvent quality for cellulose acetate based on Hansen solubility parameters but their different viscosities. All solvents are less harmful to the environment and human health compared to the conventional solvents used in CA membrane fabrication. The thermodynamics of the systems were investigated by the binary and ternary interactions of the components. Phase inversion kinetics was investigated by phase inversion rate observation by optical microscope, light transmission measurement, and rheological analysis of solvents and polymer solutions. The performances of the membranes were characterized by pure water permeance (PWP) and molecular weight cut-off (MWCO), and the membrane morphology was observed by scanning electron microscopy (SEM).

The phase inversion kinetics was observed to be the main parameter that controlled the morphology and performance of the membranes, even though the thermodynamic interactions between the components were also different. Phase

inversion kinetics is mainly affected by solvent viscosity. The lower viscosity of DA led to a faster phase inversion, and asymmetric membrane structure, whereas adding acetic acid to the solvent system resulted in higher viscosity of solvent system and slower phase inversion, which made the membrane structure loose, porous, and symmetrical.

The changes in the membrane properties were also investigated by applying the evaporation step to the cast polymer solution containing acetone as the volatile co-solvent for different durations. In addition, the presence of humidity in the evaporation bath was studied. As the evaporation time increased, the porosity and pore size of membranes decreased, leading to lower pure water permeance and MWCO. In addition, conducting evaporation in a humid medium resulted in a looser membrane structure.

The effect of deacetylation via alkaline hydrolysis on the membranes with different porosity was investigated. There was no significant difference observed in the morphology after alkaline hydrolysis. However, the performance of membranes changed after alkaline hydrolysis, probably due to the partial degradation of cellulose chains in the aqueous alkaline solution affecting the pore size and membrane matrix. The narrowing of pores may be considered the dominant effect on the performance of membranes conducting separation based on the pore flow mechanism. On the other hand, the effect of a loosened membrane matrix also becomes important in the performance of membranes where separation occurs through the solution-diffusion mechanism. Consequently, when both pores and membrane matrix contribute to transport in comparable amounts, the water permeance increased while MWCO decreased due to water permeating through both pores and membrane matrix, while solutes essentially permeated through the pores only. When solution diffusion mechanism became dominant for both solvent and solutes, both permeance and MWCO increased.

Hollow fiber membranes were fabricated by dry-wet spinning with the same polymer solutions to investigate the effect of membrane configuration on membrane performance. Compared with flat sheet membranes, denser selective layer, possibly resulting from molecular orientation due to shear rate in the spinning system, was obtained in the CA18-DHAc hollow fiber membrane. CA18-DA hollow fiber membrane showed similar morphology and MWCO, but higher pure water permeance. The difference in flat sheet and hollow fiber membranes with different solvent systems is attributed to the simultaneous impact of many spinning conditions in the fabrication of these membranes.

Keywords: Phase Inversion, Cellulose Acetate Membrane, Alkaline Hydrolysis, Hollow Fiber, Benign Solvents

ÖZ

ÇÖZÜCÜ SİSTEMİNİN FAZ DEĞİŞİMİ İLE ÜRETİLEN SELÜLOZ ASETAT MEMBRANLAR VE ALKALİ HİDROLİZ İLE DEASETİLYASYONA ETKİSİ

Tekin, Fatma Seden
Yüksek Lisans, Kimya Mühendisliği
Tez Yöneticisi: Assoc. Prof. Dr. Zeynep Çulfaz Emecen

Ağustos 2018, 127 sayfa

Bu çalışmada, çözücü seçiminin selüloz asetat membran morfolojisi ve performansı üzerindeki etkisi, faz değişim termodinamiği ve kinetiği ile ilişkili olarak araştırılmıştır. Dimetil sülfoksit (DMSO), 1:1 oranında DMSO: aseton (DA) ve DMSO: asetik asit (DHAc) karışımları üç farklı solvent sistemi olarak kullanılmıştır. Çözmeyen olarak su kullanılmıştır. Aseton ve asetik asit, Hansen çözünürlük parametrelerine göre selüloz asetat için benzer çözücü kaliteleri, fakat farklı viskoziteleri olması nedeniyle seçilmiştir. Tüm solventler selüloz asetat membran üretiminde kullanılan geleneksel solventlere kıyasla daha az zararlıdır. Sistemlerin termodinamiği, bileşenlerin ikili ve üçlü etkileşimleri ile incelenmiştir. Faz değişim kinetiği, optik mikroskopla faz değişim hızı gözlemi, ışık geçirgenliği ölçümü ve solvent sistemlerinin ve polimer çözeltilerinin reolojik analizi ile araştırılmıştır. Membranların performansları saf su geçirgenliği (PWP) ve moleküler ağırlık kesmesi (MWCO) ile karakterize edilmiş ve membran morfolojisi taramalı elektron mikroskobu ile gözlemlenmiştir.

Bileşenler arasındaki termodinamik etkileşimlerin de farklı olmasına rağmen, membranların morfolojisini ve performansını belirleyen ana parametrenin faz tersinme kinetiği olduğu gözlemlenmiştir. Faz değişim kinetiği esas olarak solvent

viskozitesinden etkilenmiştir. DA' nın düşük viskozitesi, daha hızlı faz değişimine ve asimetrik membran yapısına yol açarken, çözücü sistemine asetik asit eklenmesi, çözücü sisteminin daha yüksek viskozitesine ve daha yavaş faz değişimine neden olmuş ve membran yapısını gevşek, gözenekli ve simetrik hale getirmiştir.

Uçucu yardımcı çözücü olarak aseton içeren polimer çözeltisine farklı süreler boyunca buharlaştırma adımı uygulanarak membran özelliklerindeki değişiklikler araştırılmıştır. Ayrıca buharlaşma banyosunda nemin varlığı da incelenmiştir. Buharlaşma süresi arttıkça membranların gözenekliliği ve gözenek boyutu azalmıştır ve saf su geçirgenliği ve MWCO değerleri düşmüştür. Ek olarak, buharlaşmanın nemli bir ortamda gerçekleştirilmesi daha gevşek bir membran yapısı ile sonuçlanmıştır.

Alkali hidroliz yoluyla deasetilasyonun farklı gözenekliliğe sahip membranlar üzerindeki etkisi araştırılmıştır. Alkali hidroliz sonrasında membran morfolojisinde önemli bir fark gözlemlenmemiştir. Fakat alkali hidroliz selüloz zincirlerinin sulu alkali çözeltide muhtemel kısmi bozulması sonucunda gözenek boyutunu ve membran matrisini etkilemesi nedeniyle membranların performansını değiştirmiştir. Gözeneklerin daralması, gözenekte akış mekanizmasına göre ayırım yapan membranların performansı üzerindeki baskın etki olarak kabul edilebilir. Öte yandan, gevşemiş membran matrisinin etkisi ayırmanın çözünme-yayılma mekanizmasıyla gerçekleştiği membranların performansında önemli görünmektedir. Sonuç olarak, gözenekler ve membran matrisi taşınımına kıyaslanabilir miktarlarda katkı sağladığında, su hem gözeneklerden hem membran matrisinden geçtiği fakat çözünen madde esas olarak sadece gözeneklerden geçtiği için, su geçirgenliği yükselirken MWCO azalmıştır. Çözünme-yayılma mekanizması hem çözücü hem çözünen taşınımı için baskın olduğunda, geçirgenlik ve MWCO artmıştır.

Membran şeklinin membran performansı üzerindeki etkisini araştırmak için aynı polimer çözeltileri ile kuru-yaş eğirme sisteminde kavuklu elyaf membranlar üretilmiştir. Düz levha membranlarla karşılaştırıldığında, CA18-DHAc kavuklu elyaf

membran, eđirme sistemindeki kesme hızı nedeniyle moleküler y6nelimden kaynaklanan daha yođun seęici katmana sahiptir. CA18-DA ięi bođ fiber membran benzer morfoloji ve MWCO ancak daha y6ksek saf su geęirgenlięi g6stermiřtir. Sonuę olarak, kavuklu elyaf ve d6z levha yapıları, bu membranların imalatındaki farklı kořulların aynı anda etki etmesinden dolayı farklı membran 6zellikleri ile sonuęlanmıřtır.

Anahtar Kelimeler: Faz Deęiřimi, Sel6loz Asetat Membran, Alkali Hidroliz, Kavuklu Elyaf Membran, Tehlikesiz 6z6c6ler

To My Father

ACKNOWLEDGMENTS

I would like to show my acknowledgment to my advisor, Assoc. Prof. Dr. Zeynep ulfaz Emecen thankful to her for endless support, guidance, and patience. Also, I am very grateful to her for the opportunity to develop myself to be a good researcher.

My most profound appreciation also goes to the Chemical Engineering department and ulfaz-Emecen research group for all the support and help related to my study. I would like to thank Feyza for her endless support and energy when I needed.

I am thankful for having my family that supported me during my education. I would like to thank Krřat, my best friend and my better half, for her unique advice and endless support in this way.

I would like to mention my special thanks to Assoc. Prof. Dr. Emre Bkřođlu for all his support and helps.

This work is partially funded by the Scientific and Technological Research Council of Turkey (TUBİTAK) under grant numbers of 119M828 and 121M320.

TABLE OF CONTENTS

ABSTRACT.....	v
ÖZ	ix
ACKNOWLEDGMENTS	xiv
TABLE OF CONTENTS.....	xv
LIST OF TABLES	xix
LIST OF FIGURES	xxi
LIST OF ABBREVIATIONS	xxiv
INTRODUCTION	1
1.1 Pressure-Driven Membrane Processes and Transport Mechanisms	2
1.2 Types of Membranes Based on Structure	4
1.3 Phase Separation Method for Fabrication of Polymeric Membranes	6
1.3.1 Non-solvent Induced Phase Separation	7
1.4 Cellulose Membranes	10
1.4.1 Fabrication of Cellulose Membranes via Ionic Liquids.....	11
1.4.2 Fabrication of Cellulose Membranes via Alkaline Hydrolysis of Cellulose Acetate Membranes	13
1.5 Parameters for Morphology and Performance Control of Cellulose Acetate Membranes.....	15
1.6 Hollow Fiber Membranes.....	19
1.7 The Aim of Study	22
EXPERIMENTAL METHODS.....	23
2.1 Materials.....	23
2.2 Preparation of Polymer Solution	23

2.3	Fabrication of Membranes.....	24
2.3.1	Flat Sheet Membrane Fabrication	24
2.3.2	Hollow Fiber Membrane Fabrication	26
2.4	Performance Tests of Membranes	29
2.5	Morphology Characterization by Scanning Electron Microscopy (SEM) ..	31
2.6	Viscosity Measurements for Solvent Systems and Polymer Solution.....	32
2.7	Phase Inversion Front Observations via Optic Microscope	32
2.8	Light Transmission Measurements.....	33
2.9	Acetone Evaporation Experiment.....	34
2.10	Cloud Point Measurements.....	35
2.11	Relative Energy Density (RED) Calculations via Hansen Solubility Parameters	36
2.12	Excess Gibbs Free Energy Calculations	37
	RESULTS AND DISCUSSION	39
3.1	Effect of Solvents on the Thermodynamics of Phase Inversion System.....	39
3.1.1	Solvent-Polymer Interactions via Hansen Solubility Parameters	39
3.1.2	Polymer Chain Entanglement Concentrations of Polymer Solutions as A Tool to Assess Solvent-Polymer Interactions	41
3.1.3	Excess Gibbs Free Energy Calculation for Solvent-Water Interaction	44
3.1.4	Cloud Point Measurements	46
3.2	Effect of Solvent Systems on the Phase Inversion Kinetic	47
3.2.1	Instantaneous Phase Inversion Rate Observations	48
3.2.2	Cumulative Phase Inversion Rate via Light Transmittance Measurements.....	51

3.3	Morphology and Performance of Cellulose Acetate Flat Sheet Membranes.....	54
3.3.1	Effect of Solvent Systems on Membrane Morphology.....	54
3.3.2	Effect of Solvent Systems on Membrane Performance	57
3.4	Effect of Acetone Evaporation at Different Times on the Phase Inversion Rate and Properties of Membranes	58
3.4.1	Effect of Evaporation Time on Instantaneous Phase Inversion Rate...	59
3.4.2	Effect of Evaporation Time on the Cumulative Phase Inversion Rate	62
3.4.3	Effect of Evaporation Time on Membrane Properties	64
3.5	Deacetylation of Cellulose Acetate Flat Sheet Membranes by Alkaline Hydrolysis for Cellulose Membrane Fabrication.....	68
3.6	Cellulose Acetate Hollow Fiber Membranes	71
3.6.1	CA18-DHAc Polymer Dope Based Hollow Fiber Membranes	71
3.6.2	CA18-DA Polymer Dope Based Hollow Fiber Membranes.....	84
	CONCLUSIONS.....	87
	REFERENCES	91
	APPENDICES	101
A.	Gel Permeation Chromatography (GPC) Calibration Curves	101
B.	Morphologies of CA and CA-AH Parts of Flat Sheet Membranes.....	106
C.	CA18-DHAc Flat Sheet Membranes and Alkaline Hydrolysis Parts with Different Thickness.....	108
D.	Average Pore Size and Effective Skin Layer Thickness Estimation by Ferry-Renkin Equation.....	111
E.	CA18-DHAc Hollow Fiber Membranes with Different Bore Liquids	113
F.	Polymer Solutions for Cloud Point Measurements	115

G.	Viscosity of Polymer Solutions	117
H.	Excess Gibbs Free Energy Calculation for Solvent-Water Systems	119
I.	Shear Rate Calculations	122

LIST OF TABLES

TABLES

Table 1. 1. Techniques for phase separation and their brief explanation.....	7
Table 2. 1. Compositions of the polymer solutions used in the membrane preparation	24
Table 2. 2. Membrane fabrication steps with illustrations.....	25
Table 2. 3. Flat Sheet membrane codes and applied fabrication steps.....	26
Table 2. 4. Membrane codes and spinning conditions for hollow fiber membrane from CA18-DHAc and CA18-DA polymer solutions	28
Table 3. 1. RED values of individual solvent-polymer pairs and solvent mixture- polymer pairs	40
Table 3. 2. Polymer chain entanglement concentrations (C_e) of polymer solutions..	44
Table 3. 3. Cloud point water composition (wt. %) of polymer solution-water system	46
Table 3. 4. The viscosities of solvent systems and polymer solutions.....	49
Table 3. 5. Average final composition of polymer solutions after evaporation times...	67
Table 3. 6. Performances of CA18-DHAc hollow fiber membranes fabricated at different air gaps and pulling speeds with 80%DMSO-20% water (80D20W) as bore liquid and flat sheet membrane of CA18-DHAc	76
Table 3. 7. Comparison of flat sheet and hollow fiber membranes from CA18-DA polymer solution	84
Table D. 1. Calculated hydrodynamic radius of dextran molecules (r_D) and average pore diameters (r_P) of CA18-DHAc membranes with different thicknesses.....	111
Table D. 2. Effective selective layer thickness of membranes of CA18-DHAc.....	112
Table E. 1. Spinning conditions for CA18-DHAc hollow fiber membranes fabricated by different bore liquids.....	113
Table E. 2. Performance tests of CA18-DHAc hollow fiber membranes fabricated by different bore liquids.....	113

Table H. 1. R_k and Q_k values for groups included by solvents and components 120

Table H. 2. Interaction Parameters for subgroups in the components 121

LIST OF FIGURES

FIGURES

Figure 1. 1. A basic illustration of a membrane separation system	2
Figure 1. 2. Classification of membrane filtration processes according to the average pore size and rejected species removed by each class of membrane	3
Figure 1. 3. Types of membranes based on the structure.....	5
Figure 1. 4. Ternary phase diagram of NIPS including polymer-solvent-nonsolvent..	8
Figure 1. 5. H-bonding in the molecular structure of cellulose	11
Figure 1. 6. Illustration of deacetylation of cellulose acetate by alkaline hydrolysis	14
Figure 1. 7. A basic illustration of the two-orifice spinneret	20
Figure 2. 1. A basic illustration of the spinning system.....	27
Figure 2. 2. Illustration of the exit of the spinneret	27
Figure 2. 3. Cross-flow mode filtration process chart.....	29
Figure 2. 4. Hollow fiber membrane module used in the filtration tests	30
Figure 2. 6. Experimental setup for measurements of polymer solution weight and relative humidity during acetone evaporation from casting solution under nitrogen stream	35
Figure 3. 1. The relative viscosity of polymer solution systems with increased cellulose acetate (CA) concentration	43
Figure 3. 2. Excess Gibbs free energy for the interaction of water-solvent systems.	45
Figure 3. 3. Phase inversion front observations via optic microscope from t=0 to t=60 seconds	48
Figure 3. 4. (a); x^2 vs. time plot from microscope observations, and (b); graph of the slope of x^2 vs. time for estimation of effective diffusivity of water into polymer solution and diffusivity of water into solvent systems estimated by Wilke-Chang equation.....	50
Figure 3. 5. Cumulative phase inversion rate by light transmittance. (a); Light transmittance plot (b); cumulative phase inversion rate obtained by the slope of the graph (a)	53

Figure 3. 6. SEM images of cellulose acetate flat sheet membranes prepared with different solvent systems	56
Figure 3. 7. Pure water permeance (PWP) and molecular weight cut-off (MWCO) values of cellulose acetate (CA) membranes prepared with different solvent systems	57
Figure 3. 8. Effect of evaporation time on the water diffusivity observed by instantaneous phase inversion by optic microscope (a); front thickness vs time, (b); diffusivity of water from the slope of graph (a)	61
Figure 3. 9. Effect of evaporation time on the cumulative phase inversion rates (a); light transmission graph, (b); cumulative phase inversion rates from the initial slope of graph (a)	63
Figure 3. 10. Morphology of CA18-DA membrane exposure to different evaporation times	65
Figure 3. 11. Membrane performances after certain evaporation times.....	66
Figure 3. 12. Change of polymer solutions weight and relative humidity in evaporation tank with respect to time during evaporation step.....	67
Figure 3. 13. Effect of deacetylation via alkaline hydrolysis on the performances of flat sheet membranes	70
Figure 3. 14. Morphologies of CA18-DHAc based hollow fiber membranes at different spinning conditions (cont'd).....	73
Figure 3. 15. Inner surfaces of CA18-DHAc hollow fiber membranes that produced with bore liquid of 80%DMSO-20% water.....	75
Figure 3. 16. Morphology of CA18-DHAc hollow fiber membrane spun at lower-sheared conditions.	79
Figure 3. 17. SEM images of CA18-DHAc hollow fiber membrane fabricated with a hot external coagulation bath at 50°C	81
Figure 3. 18. Morphology of CA18-DA hollow fiber membrane	85
Figure A. 1. GPC universal calibration of double-column via PEG standards (Easy-Vials) for molecular weight, MW (Da) vs. retention time, RT (mins) graph	101

Figure A. 2. GPC universal calibration of single column via PEG calibration standards for molecular weight (MW, Da) vs. retention time, (RT, mins) graph....	101
Figure A. 3. Calibration curve of PEG 400 Da.....	102
Figure A. 4. Calibration curve of PEG 2 kDa.....	102
Figure A. 5. Calibration curve of PEG 6 kDa.....	103
Figure A. 6. Calibration curve of PEG 10 kDa.....	103
Figure A. 7. Calibration curve of PEG 20kDa.....	104
Figure A. 8. Calibration curve of PEG 35 kDa.....	104
Figure A. 9. Calibration curve for 40 kDa-70kDa-200kDa dextran probes	105
Figure B. 1. Effect of alkaline hydrolysis on the morphology of flat sheet membranes from porous to dense structures (cont'd).....	106
Figure C. 1. Performance results of CA18-DHAc membranes and alkaline hydrolysis parts with different thicknesses.....	108
Figure C. 2. Morphologies of CA18-DHAc membranes and alkaline hydrolysis parts with different thicknesses (cont'd).....	109
Figure E. 1. SEM Images of CA18-DHAc hollow fiber membranes fabricated by different bore liquids.....	114
Figure F. 1. CA18-D polymer solutions with different water concentrations for cloud point measurement	115
Figure F. 2. CA18-DA polymer solutions with different water concentrations for cloud point measurement	115
Figure F. 3. CA18-DHAc polymer solutions with different water concentrations for cloud point measurement	116
Figure G. 1. Viscosities of polymer solutions at different shear rates.....	117
Figure I. 1. Schematic drawn of casting of polymer solution on a glass plate	122
Figure I. 2. Basic illustration of inside of the spinneret.....	123
Figure I. 3. Viscosity versus shear rate graph of CA18-DHAc polymer solution ...	126

LIST OF ABBREVIATIONS

ABBREVIATIONS

[BMIM]Cl: 1-butyl-3-methylimidazolium chloride

[EMIM][Cl]: 1-ethyl-3-methylimidazolium chloride

[EMIM]OAc: 1-ethyl-3-methylimidazoliumacetate

2-MeTHF: 2-methyl tetrahydrofuran

CA: Cellulose acetate

DMAc: Dimethyl Acetamide

DMF: Dimethylformamide

DMSO: Dimethyl sulfoxide

GPC: Gel permeation chromatography

HAc: Acetic acid

HCl: Hydrochloric acid

HF: Hollow fiber

k_c : Mass transfer coefficient

kDa: Kilo Dalton

KOH: Potassium hydroxide

MF: Microfiltration

MWCO: Molecular weight cut-off

NaOH: Sodium hydroxide

NF: Nanofiltration

NIPS: Non-solvent induced phase separation

NMP: N-Methyl-2-pyrrolidone

PEG: Polyethylene glycol

PWP: Pure water permeance

RED: Relative energy density

RO: Reverse osmosis

SEM: Scanning electron microscopy

TIPS: Thermally-induced phase separation

TMP: Transmembrane pressure

TMSC: Trimethylsilyl cellulose

UF: Ultrafiltration

VIPS: Vapor-induced phase separation

CHAPTER 1

INTRODUCTION

Membranes have gained a crucial place in separation technology. They are used in a broad range of applications such as purification and sterilization products in the food and pharmaceutical industries, treating wastewater, purification of drinking water, desalination, fuel cells, and hemodialysis^{1,2}. Additionally, membrane technology is a method to replace conventional processes (e.g., adsorption, absorption, distillation, evaporation, extraction) for separation and purification in organic solvents due to lower energy and chemical requirements, easy processability, high safety, and operating at lower temperatures. Consequently, the membrane processes are continued to improve for more sustainable and cost-efficient separations.

A membrane functions as a selective and permeable barrier allowing the permeation of certain species while rejecting others in a mixture according to the difference in size, charge, or diffusivity into the membrane under a driving force of concentration gradient, electrical potential gradient, or pressure gradient. Unlike conventional filtration, membranes extend the filtration application from separating immiscible solids particles from a liquid or gas medium to separating dissolved solutes in liquids or separating gas mixtures³. In a membrane filtration system, as shown in Figure 1.1, the feed stream is divided into two streams named permeate and retentate, enriched by passed species through the membrane and rejected species by the membrane, respectively.

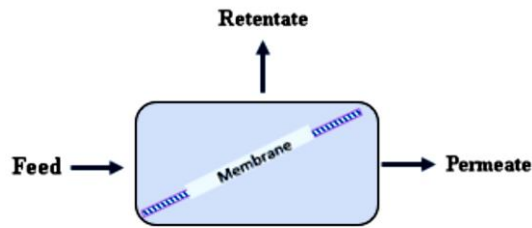


Figure 1. 1. A basic illustration of a membrane separation system

1.1 Pressure-Driven Membrane Processes and Transport Mechanisms

Membrane filtration processes driven by the pressure gradient between the feed and permeate sides are divided into four major groups based on the pore size of the membrane or size of rejected species: microfiltration (MF), ultrafiltration (UF), nanofiltration (NF), and reverse osmosis (RO). Pressure-driven membrane processes based on decreased pore size and species that membranes can retain are summarized in Figure 1.2.

The transport mechanism in porous microfiltration and ultrafiltration membranes is the pore-flow model. Based on this model, under the pressure gradient as the driving force, the separation occurs by molecular sieving, which depends on the differences in the size between species and membrane pores. The permeate stream passes through the membrane pores during separation via convective flow due to the pressure gradient across the membrane. Ultrafiltration and microfiltration, which have the same transport mechanism, are distinguished by differences in pore sizes of membranes. Membranes used in microfiltration (MF) processes are porous filtration membranes designed to retain particles in the micrometer range with diameters above $0.1\ \mu\text{m}$, such as bacteria and suspended solids. In the industry, microfiltration membranes are widely used in the clarification step of wine, beer, and fruit juices in the food industry⁴⁻⁶, in sterilization to remove microorganisms during water treatment⁷⁻⁹, or in the separation of microbial content from injectable drug solutions in pharmaceuticals^{1,10}.

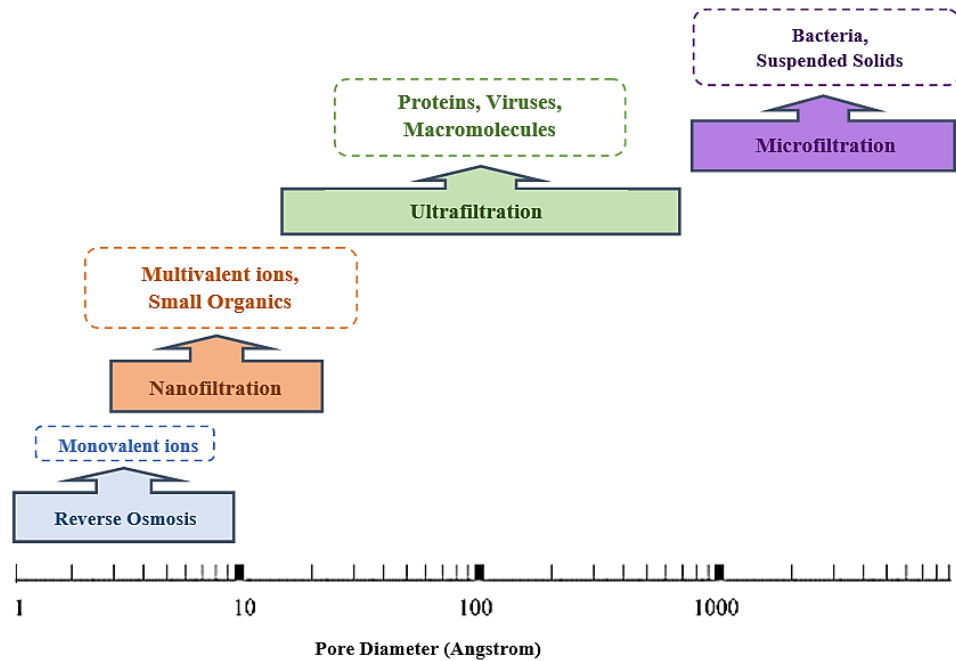


Figure 1. 2. Classification of membrane filtration processes according to the average pore size and rejected species removed by each class of membrane

Ultrafiltration (UF) membranes are finely porous membranes to separate colloidal particles, viruses, and dissolved macromolecules such as proteins within 2-100 nm. Ultrafiltration membranes are used mostly in wastewater or drinking water treatment^{9,11}, in the dairy industry for cheese production, or to separate useful protein from whey⁵. Ultrafiltration membranes are characterized by a molecular weight cut-off (MWCO) value designated as the molecular weight of macromolecule rejected by 90% through the membrane since the molecular weight of macromolecules is generally proportional to their molecular size. Poly (ethylene glycol) (PEG), proteins, and dextrans in different molecular weights are widely used to specify the MWCO value of a UF membrane¹².

The transport mechanism for dense, non-porous membranes, such as reverse osmosis membranes, is expressed by the solution-diffusion model in which the separation occurs based on solubility and diffusivity (mobility) differences of species in the membrane¹. According to this model, permeating species dissolve in the membrane

material and diffuse under a concentration gradient between feed and permeate sides at different rates through the polymer's free volume.

The reverse osmosis process is operated for desalting seawater or groundwater or purifying water with non-porous membranes permeating water but rejecting salts and monovalent ions. Nanofiltration membranes can be described as loose reverse osmosis membranes which permeate monovalent ions but retain multivalent ions and small organics such as dyes and solvent molecules. Since their separation performance is in between ultrafiltration and reverse osmosis membranes, the transport mechanism in the nanofiltration membranes can be explained by both pore-flow and solution-diffusion. In NF membranes, Donnan exclusion is another effective mechanism that conducts separation based on the interaction between charged ions and charged nanofiltration membrane.

1.2 Types of Membranes Based on Structure

The quality (extent of separation) and quantity (rate of separation) of separation are related to the morphology of the membrane. The extent or quality of separation is related to the pore size distribution on the selective layer. On the other hand, permeance depends on pore size, porosity, skin layer thickness, and pore connectivity of the membranes.

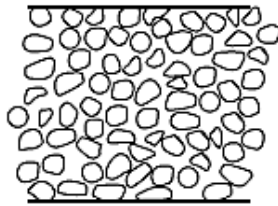
Membranes can be divided into two main groups according to morphological structures: symmetric (isotropic) or asymmetric (anisotropic), as presented in Figure 1.3. Symmetric membranes have uniform pore size and structure throughout the cross-section of the membrane. Such membranes can be porous or dense, as seen in Figure 1.3. Porous isotropic membranes have high fluxes to use in microfiltration processes. Dense isotropic membranes perform low transmembrane flux due to thicker structures causing high flow resistance and are mostly used in lab-scale characterization of new membrane materials. On the other hand, asymmetric membranes consist of different pore sizes and porosity from the top to the bottom surface. Usually, asymmetric membranes involve an ultrathin, selective top layer,

and a thicker, highly permeable, microporous substrate layer. The selective top layer of the membrane conducts separation on a microporous sublayer providing support and mechanical strength.

As a crucial point, asymmetric membranes possessing an ultrathin selective layer show higher permeability for the same separation quality (rejection against species) than thicker symmetric membranes in the same density. Therefore, asymmetric membranes are preferred in commercial usage over symmetric membranes for ultrafiltration, nanofiltration, and reverse osmosis because of their good mechanical strength against applied pressure and lower energy requirements for highly selective separation with higher flux.

Symmetric (Isotropic) Membranes

Porous Membrane

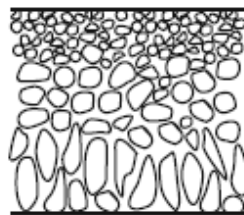


Dense Membrane



Asymmetric (Anisotropic Membrane)

Integrally Skinned



Thin-Film Composite

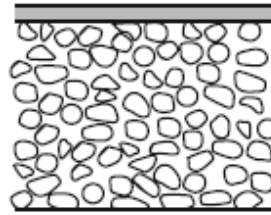


Figure 1. 3. Types of membranes based on the structure ¹

Asymmetric membranes can be divided into two subgroups named the thin-film composite membrane and integrally skinned membrane, as presented in their structure in Figure 1.3. The thin-film composite membrane consists of different materials for selective and support layers. The integrally skinned asymmetric membrane is fabricated from a single membrane material. This type is also named Loeb–Sourirajan type membrane in the literature because the Loeb and Sourirajan produced the first high-flux, integrally skinned cellulose acetate reverse osmosis membrane via the phase separation (phase inversion) method¹³.

1.3 Phase Separation Method for Fabrication of Polymeric Membranes

Phase separation (phase inversion) is one of the most common and attractive methods for producing polymeric membranes due to its simple production steps and achieving distinct structures, from asymmetric integrally skinned to symmetric membranes, according to the kinetics and thermodynamics of phase separation¹⁴. In this method, a liquid polymer solution in one phase separates into two phases by precipitation: the polymer-lean phase and the polymer-rich phase. Polymer-rich phase forms the membrane matrix while the polymer lean phase creates the membrane pores¹. The precipitation of the polymer solution can be induced in several techniques, as described briefly in Table 1.1. Also, the combination of processes can be used for membrane fabrication. The polymer solution is converted into a solid membrane in all processes, but different morphologies are obtained by different methods.

Table 1. 1. Techniques for phase separation and their brief explanations ¹

Phase Separation Technique	Description
Thermally-induced phase separation (TIPS)	Cooling the hot casting polymer solution causes precipitation.
Solvent evaporation	Evaporation of volatile solvent from casting polymer solution changes the solution composition and causes precipitation.
Non-solvent induced phase separation (NIPS)	Introducing a nonsolvent into the polymer solution leads to precipitation.
Vapor-induced phase separation	NIPS via absorption of nonsolvent vapor from humid air.
Liquid-induced phase separation (Immersion precipitation)	NIPS via immersion of polymer solution into a liquid non-solvent bath.

1.3.1 Non-solvent Induced Phase Separation

This production technique is essentially composed of three components: a polymer, a solvent that dissolves the polymer, and a non-solvent, which does not dissolve the polymer but is fully miscible with solvent. In this process, a homogeneous polymer solution consisting of a polymer and solvent (or solvent mixture) is cast in the form of a flat sheet or hollow fiber. It is precipitated by exposing to the vapor of a non-solvent or immersing in a liquid non-solvent bath, or a combination of both.

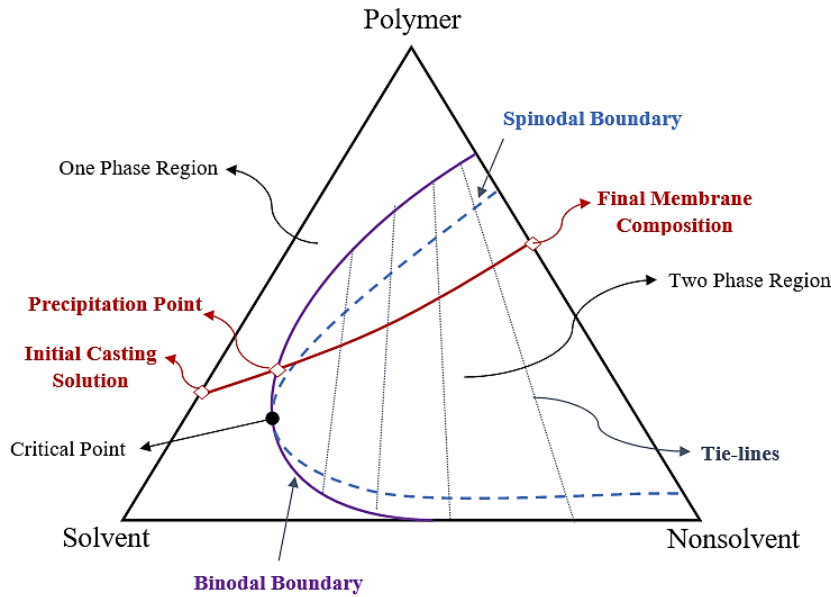


Figure 1. 4. Ternary phase diagram of NIPS including polymer-solvent-non-solvent^{1,15}

The steps of membrane fabrication by NIPS are explained by the typical ternary phase diagram shown in Figure 1.4. The corners of the diagram represent the pure components of the system, and the edges show the binary mixtures of linked components. The diagram has two main regions: the one-phase region where all components are miscible and the two-phase region where the system separates into two phases (i.e., polymer lean phase and polymer-rich phase). One-phase and two-phase regions are distinguished by the binodal boundary¹.

As represented by the red line in Figure 1.4, the membrane formation process is a series of steps beginning with a homogeneous polymer solution located on the polymer-solvent edge and finalized by the formation of the membrane. After exposure of polymer solution to a non-solvent, the thermodynamically stable casting polymer solution moves from the one-phase region to the unstable two-phase region by changing the composition: the solvent non-solvent exchange, which means solvent diffusion out of the solution and diffusion of non-solvent into the polymer solution. The decrease in the Gibbs free energy of mixing of solution causes the separation of stable-solution into two phases which are polymer-lean and polymer-rich phases producing membrane structure. These phases are in equilibrium with

each other, and the tie-lines in the two-phase region show the compositions of phases: the top of the tie-line represents the polymer-rich phase, while the bottom represents the polymer-lean phase.

Where the starting composition of the solution is compared to the binodal boundary and the rate of out-diffusion of the solvent and in-diffusion of the nonsolvent, designated as solvent non-solvent exchange rate or demixing rate in the literature, the final morphology of the membrane is determined.

Mutual diffusion between solvent and nonsolvent starts in the solution-nonsolvent interface and proceeds throughout the whole cross-section of the solution during the precipitation process. In the case of a higher demixing rate (rapid precipitation), the rate of precipitation gets increasingly slow through the cross-section. When the casting polymer solution interacts with a nonsolvent at the interface, the surface precipitates rapidly, increasing polymer concentration there. As a result, thin selective skin layer is obtained. The precipitated surface layer acts as a barrier to restrict the further loss of solvent and diffusion of nonsolvent causing slow precipitation with a lower polymer concentration to form a more porous substructure. Consequently, the rapid precipitation typically produces anisotropic membranes. By contrast, with a slow demixing rate (slow precipitation), there is enough time for diffusion of non-solvent more homogeneously along the cross-section leading to a similar precipitation stage in the different locations of the solution. As a result, a slow demixing rate during the phase separation typically results in a more symmetric membrane with either a dense or porous structure. However, estimating the effect of fabrication parameters on the overall demixing rate is complicated since many parameters have competing effects.

The thermodynamics of the ternary system and kinetics of the phase separation process are two main factors that affect how the phase inversion proceeds (in slow or rapid precipitation rate) and which membrane morphology is obtained. By altering these parameters, the morphology and properties of polymeric membranes can be controlled for the desired separation performance. The parameters that influence the

kinetics and thermodynamics of the phase separation process, and hence the performance and morphology of membranes, are explained in terms of cellulose acetate (CA) and cellulose-based membranes, which are polymers used in this study.

1.4 Cellulose Membranes

Organic solvents are widely involved in petrochemistry, pharmaceutical, food processing, electronics, and biotechnology industries. In applications, solute separation from organic solvent medium, purification, separation, or recovery of solvents are required¹⁶. After the wide applications of membranes in aqueous solution, membrane separation in organic solvents rapidly develops in membrane technology. The biggest challenge is finding a polymer to fabricate a membrane having high organic solvent resistance during separation. In addition, increasing needs for renewable materials and sustainable processes because of depleting fossil fuels and growing ecological concerns make natural polymers receive more attention for membrane fabrication.

Cellulose is the most abundant natural polymer on earth. It is a solvent-resistant material due to inter and intramolecular hydrogen bonds in its structure, as seen in Figure 1.5. This property makes it an attractive membrane material for organic solvent filtration applications. Additionally, cellulose membranes have hydrophilic and antifouling nature due to hydroxide groups on the surface. This advantage of cellulose membranes reduces the accumulation of rejected species on the membrane surface during filtration (membrane fouling), which helps to retain the separation performance to the same extent and increases the membrane's operating life.

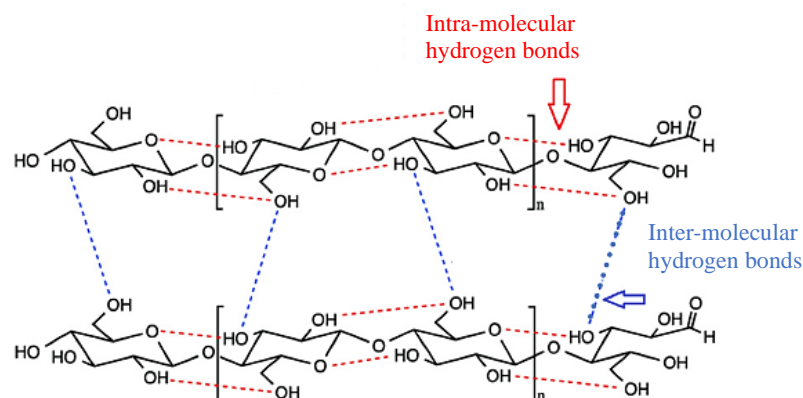


Figure 1. 5. H-bonging in the molecular structure of cellulose¹⁷

1.4.1 Fabrication of Cellulose Membranes via Ionic Liquids

Dissolving a polymer in a proper solvent or solvent mixture is required to fabricate a polymeric membrane by phase inversion method. However, it is difficult to dissolve cellulose into many conventional organic solvents including harsh polar aprotic solvents such as N-Methyl-2-pyrrolidone (NMP) and Dimethylformamide (DMF) due to the intermolecular and intramolecular hydrogen bonding in linear cellulose structure as seen in Figure 1.5.

Dissolution of cellulose in a wide range of ionic liquids makes it possible to fabricate cellulose membrane by the phase inversion method, which is the most common and simpler way of commercial membrane fabrication¹⁶. Ionic liquids are molten salts in liquid form below 100 °C. The examples of ionic liquids used for dissolving cellulose are 1-ethyl-3-methylimidazoliumacetate ([EMIM]OAc) 1-butyl-3-methylimidazolium chloride ([BMIM]Cl), 1-ethyl-3-methylimidazolium chloride ([EMIM][Cl])^{18,19}. The one of the advantages of ionic liquids is to be more benign solvents than conventional organic solvents due to their negligible vapor pressure. Also, they dissolve cellulose without derivatizing it. In 2002, Swatloski et al. investigated the solubility of cellulose in ionic liquids. They showed cellulose dissolved in several ionic liquids up to 25 wt.% concentration²⁰.

In our research group, to produce cellulose membranes for organic solvent filtration applications by phase inversion from ionic liquid solutions, [EMIM]OAc was preferred as ionic liquid because of its higher dissolution capacity and lower viscosity than others. A certain amount of cosolvent, such as acetone or dimethyl sulfoxide (DMSO), was added to the polymer solution to decrease the high viscosity of ionic liquids and increase the dissolution rate^{16,21,22}. In the study of Sukma et al., cellulose nanofiltration flat sheet membranes were fabricated with polymer solutions containing different amount of cellulose (8, 12, and 20 wt. %) dissolved in the solvent mixtures of [EMIM]OAc and acetone at different ratios. Fabrication of membranes were done by non-solvent induced phase separation in water bath. Pre-evaporation of acetone was applied in some membranes. Although used different casting solutions with or without pre-evaporation step, the morphology of all cellulose membranes was observed as dense and symmetric¹⁶. Symmetric, macrovoid-free, and nodular morphologies were obtained for all fabricated cellulose membranes also in the study of Durmaz et al. despite the changing in solvent and non-solvent. [EMIM]OAc and mixtures it with DMSO in different ratios were used for membrane fabrication by phase inversion into water or ethanol as non-solvent. Similar membrane morphologies were attributed to higher cellulose concentration (8 wt. %) than its entanglement concentration in used solvent systems and slow phase inversion even if DMSO additive to the solvent system²¹. İmir et al. produced cellulose hollow fiber membranes besides flat sheet membranes from an ionic liquid solution consisting of 25% cellulose and mixtures of [EMIM]OAc-DMSO or [EMIM]OAc-Acetone. In this study, the morphology of hollow fiber and flat sheet membranes were also symmetric and nodular.

To fabricate cellulose hollow fiber membranes for organic solvent nanofiltration in the study of Falca et al, three different ionic liquids of [EMIM][Ac], [EMIM][DEP], and [DMIM][DMP] were used. Although, different porosity was observed on the bore side of the hollow fiber membranes with changing ionic liquid; morphologies of all hollow fibers were macrovoid-free and almost symmetric especially throughout the shell side of fibers²³.

As can be seen from the studies in the literature, it is difficult to control the morphology of cellulose membranes produced with ionic liquids. Despite changing production parameters, only symmetrical morphologies, dense to microporous, are common for cellulose membranes fabricated with ionic liquids due to the high viscosity, making the demixing rate slower. The symmetric membrane structure is not preferred due to permeability restrictions; even when the desired selectivity is obtained. In addition to symmetrical narrow range membrane structure, the high viscosity of ionic liquids makes preparing and casting solutions harder. Finally, the cost of ionic liquids is higher compared to other solvents. These features of ionic liquids can be disadvantages in the large-scale fabrication of cellulose membranes.

1.4.2 Fabrication of Cellulose Membranes via Alkaline Hydrolysis of Cellulose Acetate Membranes

Another method for fabricating cellulose membrane is to produce a membrane from cellulose derivatives and convert it into cellulose membranes via deacetylation by alkaline hydrolysis. This method allows cellulose membranes to be fabricated without a casting solution prepared by ionic liquids. In the study of Puspasari et al., the cellulose membranes were obtained via acid treatment of trimethylsilyl cellulose (TMSC) membranes. The silyl groups of TMSC were converted into hydroxyl groups by exposing membranes to vapor of hydrochloric acid (HCl) solution.²⁴ Alternatively, in an alkaline solution, a cellulose acetate membrane can be converted into a cellulose membrane by exchanging the acetate groups with hydroxyl groups, as shown in Figure 1.6. The cellulose membrane after deacetylation is also called regenerated cellulose membranes in the literature.

The time required for complete deacetylation changes according to the concentration or composition of the alkaline solution. In general, the degree of deacetylation was verified via FTIR analysis by comparing the peak of C=O bonding (1740 cm^{-1}) representing the acetyl group in CA structure and the peak of O-H bonding ($3000\text{-}3600\text{ cm}^{-1}$) exhibiting the hydroxyl group in the cellulose structure.

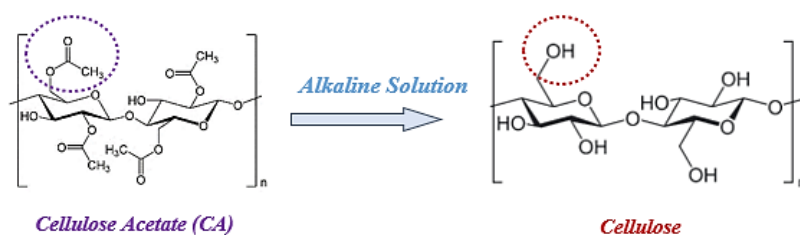


Figure 1. 6. Illustration of deacetylation of cellulose acetate by alkaline hydrolysis

In the literature, different alkaline solutions of sodium hydroxide (NaOH) or potassium hydroxide (KOH) in ethanol or water are used for the deacetylation cellulose acetate fibers or membranes. In general observation of these studies, the time needed for complete deacetylation decreases as alkaline concentration increases, or as regeneration duration increases^{18,22,25}. How the deacetylation affects the morphology and performance of cellulose acetate membranes were also investigated in the literature.

0.05 M NaOH-ethanol was used in the study of Liu et al. After 24 hours, cellulose acetate fibers were converted into cellulose completely without any changing on the morphology¹⁸. Also, 0.5 N KOH in ethanol and 1 M NaOH in ethanol solutions were used to deacetylation of electrospun CA fibers^{26,27}. For the alkaline hydrolysis of CA membranes fabricated by phase inversion, 0.1 M NaOH and 0.05 M NaOH in water with different regeneration durations were examined by İmir et al. 0.05 M NaOH-water solution achieved complete deacetylation after 24 hours²². In this study, cellulose acetate flat sheet and hollow fiber nanofiltration membranes were deacetylated by this alkaline solution. The ethanol permeance increased, and BTB rejection reduced in the regenerated cellulose membranes. The decrease in the performance of membranes did not change when regeneration occurred in 0.05 M NaOH-90% ethanol-10% water solution causing less swelling of the cellulose membrane with higher ethanol content²². Savaş-Alkan et al. showed that the entire cross-section of the densest cellulose acetate membranes was deacetylated via 0.05M NaOH aqueous after 24 hours. They observed that higher concentrations of NaOH, such as 0.1 M, made the membrane fragile and deformed the membrane structure²⁵.

Nguyen et al. reported a study on the fabrication of cellulose membranes via alkaline hydrolysis of cellulose acetate flat sheet nanofiltration membranes in 0.2 M NaOH. After deacetylation, the nanofiltration performance of cellulose membranes was observed to be less than that of cellulose acetate membranes: rejection against poly (propylene glycol) probe in ethanol decreased while the ethanol permeance increased. It was attributed to the grain boundaries between cellulose crystals, causing pathways to enhance the permeate²⁸.

There are several advantages in the fabrication of cellulose membranes via deacetylation of cellulose acetate membranes by alkaline hydrolysis: cellulose acetate can be dissolved in various conventional solvents and their mixtures, unlike cellulose, for membrane fabrication by phase inversion; the performance and morphology of cellulose acetate membranes can be tuned before converting it into cellulose membrane by controlling the parameters of the phase inversion relatively easily; cellulose acetate can be deacetylated easily in an alkaline solution to yield solvent-stable cellulose membranes.

1.5 Parameters for Morphology and Performance Control of Cellulose Acetate Membranes

The membrane performance is related to its morphology²⁹. The thermodynamics of the system and kinetics of the phase separation process determine the final membrane morphology by affecting the mechanism of phase inversion simultaneously. Thermodynamics relates to the phase equilibrium between components in the systems; kinetics relates to the mutual diffusion of solvent and non-solvent. Therefore, the relation between thermodynamics and kinetics of the phase separation process and the membrane morphology is complicated and needs to be clarified experimentally for a studied membrane system.

The different thermodynamic and kinetic conditions depending on many phase separation parameters lead to distinct membrane morphology in the literature^{30,31}. The type of polymer and its composition in the solution; solvent, cosolvent, and non-

solvent types and their compositions in the polymer solution; evaporation of volatile cosolvent; coagulation bath temperature; types of the additive in the polymer solution (such as non-solvent or pore-forming agents); annealing of the membrane are parameters mostly used for tuning the membrane morphology^{30,32}. The parameters used in this study will be explained in detail.

The solvent systems used in the polymer solution affect the morphology and performance of the membranes in terms of thermodynamics and kinetics of the phase separation process. Solvent quality for the used polymer and the affinity between solvent-nonsolvent determine the thermodynamics of the system. At the same time, the solvent also affects the phase inversion rate since they affect diffusion rate. In the study of Xing et al., the slower phase inversion rate of the CA/[BMIM]SCN system was attributed to the higher viscosity of the ionic liquid and its solution. This solution resulted in a symmetrical and nodular membrane structure with lower porosity and pore size. In contrast, the CA/NMP system yielded an asymmetrical structure along the cross-section with large microvoids due to the lower viscosity of NMP. Besides, phase separation was conducted in the CA/NMP systems with a small amount of water than the CA/[BMIM]SCN system, as shown in the phase diagram of the systems³³. There are no strict rules about how the solvents affect the final membrane features for different polymer and nonsolvent since the thermodynamics and kinetics properties influence the phase inversion mechanism at the same time. From the experimental observations, when the solvent quality is poor for the used polymer, the resultant membrane morphology is symmetric with low porosity due to delayed demixing during phase separation. On the contrary, when a good solvent is used in the polymer solution, the asymmetric structure consisting of the skin layer and porous support layers with high porosity is obtained due to instantaneous demixing¹. Therefore, the selection of solvent plays a vital role in the final properties of the membrane³⁴.

In general, for cellulose acetate, the polar aprotic solvents such as NMP, DMF, DMSO, and dimethyl acetamide (DMAc), acetone, and their mixtures are preferable

as solvent for instantaneous demixing and produce anisotropic membranes with a high porosity^{1,29,32}.

In the study of Li et al., the relatively poor solvent of GBL resulted in the delaying phase separation and sponge-like structure. In contrast, the NMP as a good solvent for cellulose acetate caused instantaneous phase separation and asymmetric morphology with microvoids. Increased GBL composition made the selective layer tighter, leading to lower pure water permeance and higher PEG rejection³⁵.

Some studies used less toxic and harmful solvents to fabricate cellulose acetate membranes instead of traditional toxic solvents such as formamide, dioxane, DMF, NMP, chloroform, or dichloromethane. Rasool et al. fabricated cellulose acetate membranes from bio-based solvents, which are glycerol derivatives. The good solvent quality of diacetin and triacetin caused the asymmetrical morphology with macrovoids. However, the lower solvent quality of monoacetin and glycerol-formal resulted in symmetrical structures³⁶.

In this study, DMSO, acetone, and acetic acid are used as solvents because of their low toxicity and benign nature. DMSO can be considered a “green” polar aprotic solvent due to its low toxicity and biodegradable nature^{37,38} and represent good solubilizing power for cellulose acetate. Acetone and acetic acid are also less harmful and toxic solvents for health and the environment³⁹.

The concentration of polymer in the casting solution is another important parameter to determine the final morphology and hence the performance of the membrane. The increasing polymer concentration in the polymer casting solution reduces the porosity and pore size of the membranes^{1,32,36,40}. Typical polymer concentrations for porous ultrafiltration membranes are 15–20 wt.%, while NF and RO membranes are typically fabricated with polymer concentrations ≥ 20 wt. %¹. Also, as the polymer concentration increases, the macro-void formation is suppressed³².

Evaporation of volatile co-solvents such as acetone, formamide, or dioxane were applied to the casting solution before immersing to the water bath for obtaining the

denser selective layer due to increased polymer concentration upon solvent evaporation⁴¹⁻⁴³.

Evaporation time is a critical parameter for adjusting the pore size of the selective layer, the porosity of the membrane, and its performance when a volatile solvent is present in the polymer solution. The polymer concentration increases as the volatile co-solvent is evaporated from the cast membrane; hence, the phase separation starts with a higher polymer ratio making the selective layer with smaller porosity, as in the case of increased polymer concentration. According to the study by Kusworo et al., with the increased evaporation times of acetone from cellulose acetate membrane, the pore size of the selective layer reduced, and the thickness of the layer increased. Accordingly, the rejection improved while the permeance of the membrane declined⁴⁴.

Adding low-solubility-parameter solvents (co-solvent) such as acetone, tetrahydrofuran, or dioxane produce denser, more retentive membranes even without evaporation^{1,33,45}. However, the kind of system co-solvent added, the solvent quality of the co-solvent for the used polymer, and the amount of co-solvent in the casting solution can be critical for final membrane properties. Kim et al. added acetone to the cellulose acetate polymer solution to improve the limiting solubility of the ionic liquid-[EMIM]OAc against CA. The presence of acetone in the polymer solution improved the mechanical and performance features of the membrane and led to the asymmetric structure of the membrane and higher porosity described by the high phase inversion rate. When only acetone was used for cellulose acetate, permeation was not observed even with higher pressure due to the denser selective layer of this membrane⁴⁵. However, a small amount of acetone remaining in the casting solution since the time is insufficient for full evaporation of acetone led to a looser skin layer due to the poorer solvent quality of acetone for cellulose acetate in the study of İmir et al.²². Also, in the study of Rasool et. al, a critical concentration of low boiling co-solvent, 2-methyl tetrahydrofuran (2-MeTHF) was detected. Until a certain concentration without any evaporation step resulted in enhanced separation performance and reduced the permeance without any change in the asymmetric

structure of the membrane. However, overuse of co-solvent led to a decrease in rejection and an increase in permeance with symmetric membrane morphology. This observation was linked with the lower solvent quality of 2-MeTHF for cellulose acetate. The poor solvent behavior of 2-MeTHF led to delayed demixing resulting from a sponge-like structure with a loose selective layer⁴⁶.

1.6 Hollow Fiber Membranes

One of the important advantages of the hollow fiber configuration over the flat sheet is to possess a higher membrane surface area to volume of the membrane module since more compact modules can be formed¹. Another is that the hollow fiber configuration allows to membrane to be cleaned by backwashing. The asymmetric integrally skinned hollow fiber membranes are produced by the phase separation method. Therefore, the phase separation mechanism, its parameters, and observed morphologies described for flat sheet membranes until this point can be adapted to this structure and used for tuning the properties of hollow fiber membranes.

The fabrication process of hollow fiber membranes is achieved by a spinning system where the polymer solution is extruded by a spinneret and immersed in a water bath. The two-orifice spinneret consists of coaxial cylinders with small radii, as shown in Figure 1.7; bore liquid (internal coagulant) passes through the inside capillary of the spinneret, and polymer solution passes across the annular gap of the spinneret simultaneously to produce this configuration. In addition to polymer solution properties, the spinning process conditions, which are air gap distance, composition, and the flow rate of bore liquid and polymer solution, temperature, and composition of external coagulant, take up speed, etc., should be considered to determine the final membrane morphology¹⁵.

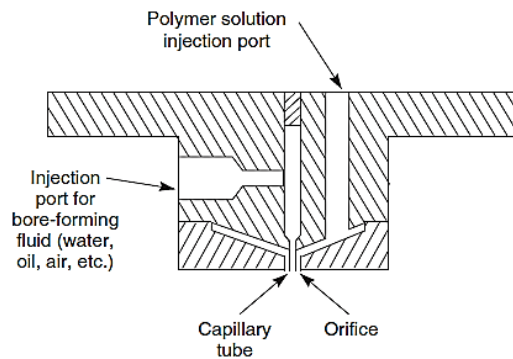


Figure 1. 7. A basic illustration of the two-orifice spinneret ¹

The integrally skinned structure is also preferred for hollow fiber membranes due to higher permeability for the desired separation and mechanical strength¹¹. The position of the selective skin layer can be adjusted by altering the composition of the bore liquid and coagulation bath. In general, where water (or other strong non-solvents) is used as a coagulant of phase separation, the skin layer tends to be formed on this side (shell side or bore side) of the hollow fiber because of the higher non-solvent quality of water for polymers. The porous morphology can be made by a coagulant containing a solvent for the other side of the hollow fiber membrane owing to the slow demixing rate. For the flat sheet membranes, there is one side for adjusting as a selective layer; however, in the case of hollow fiber, the varied structure and properties can be gained by manipulating the dense and supporting layers¹.

There are many studies about the effect of spinning conditions and components of the polymer solution on the performance and morphology of cellulose acetate membranes. Here, the studies that produce both flat sheet and hollow fiber membranes via phase separation from the same polymer solution are considered.

Kim et al. fabricated flat sheet and hollow fiber membranes with the same cellulose acetate solutions to understand the effect of acetone additive to the ionic liquid on the morphology and mechanical properties of flat sheet and hollow fiber membranes. The results showed that adding acetone to the polymer solution caused asymmetric

structure along the cross-section of HF; hence, it made the membrane more mechanically strong, as well as in flat sheet membranes⁴⁵.

Hollow fiber and flat sheet membranes were produced in the study of Xing et al. via non-solvent induced phase separation with the same polymer solution, CA/[BMIM]SCN. Compared to the morphological properties of the two configurations, the flat sheet membrane possessed a symmetric nodular structure, while hollow fiber had an asymmetric structure since the bore liquids involved solvent. Also, unlike the flat sheet membrane, the looser nodular cross-section of hollow fiber was observed. This structure was associated with the shear rate in the spinneret and elongation stress by gravity and the fiber's weight during spinning causing a looser interconnected nodular structure³³.

Another study on the morphology and performance of flat sheet and hollow fiber membranes synthesis with the same polymer solution (25% CA/DMSO: Acetone (1:1)) was conducted by İmir et al. In this study, water was used as an external coagulant at 15°C, and DMSO-water mixture was used as bore liquid with 4 cm air gap distance. The morphology of hollow fiber included macrovoids near the shell side; the asymmetric structure was obtained, unlike flat sheets. After applying the same annealing procedure to both configurations, higher permeance and lower rejection of hollow fiber were observed. The regeneration affected the flat sheet and hollow fiber membranes similarly: a decreased separation performance²².

1.7 The Aim of Study

The first aim of this study is to investigate the effect of solvent systems on the thermodynamics and kinetics of phase inversion and relate these to the morphology and performance of resulting cellulose acetate membranes. DMSO, mixtures of DMSO: acetone, and DMSO: acetic acid in the ratio of (1:1) were selected as solvent systems for membrane fabrication. Acetone and acetic acid were selected as co-solvents because of their similar solvent qualities for cellulose acetate based on Hansen solubility parameters but different viscosities: acetone is low-viscosity co-solvent and acetic acid is high-viscosity co-solvent. Cellulose acetate was selected as precursor membrane material to be converted into cellulose membranes after deacetylation via alkaline hydrolysis. Although there are many recipes for the fabrication of cellulose acetate membranes, most use quite toxic and harmful solvents to dissolve cellulose acetate such as dioxane, formamide, NMP. DMSO, acetone, and acetic acid are preferred also since they are less harmful and benign solvent and cosolvents. Secondly, the effect of acetone evaporation at different durations was studied to tune the properties of cellulose acetate membranes. Finally, the effect of deacetylation on the performance and morphology of cellulose acetate membranes with varying pore size is investigated. Consequently, this study presents the first investigation of these solvent systems for cellulose acetate and a detailed examination of deacetylation in different membrane morphology in the literature. Besides flat sheet membranes, hollow fiber membranes were produced with the same polymer solutions to investigate the effect of membrane geometry on membrane performance.

CHAPTER 2

EXPERIMENTAL METHODS

2.1 Materials

Cellulose acetate ($M_n \sim 50000$ Da by GPC), polyethylene glycol (PEG, 400 Da, 2 kDa, 10 kDa, 35 kDa), dextran (40 kDa, 70kDa, 200kDa), sodium hydroxide (NaOH) was purchased from Sigma-Aldrich. Acetone (99.5%) and glacial acetic acid were provided by Merck. Dimethyl sulfoxide (DMSO, 99.0%) was obtained from Merck and ISOLAB.

2.2 Preparation of Polymer Solution

The composition of polymer solutions used in membrane fabrication is presented in Table 2.1. Cellulose acetate (CA) and dimethyl sulfoxide (DMSO) were used as polymer and solvent, respectively. Acetone and acetic acid were used as co-solvent. The codes of D, DA, and DHAc for solvent systems refer to DMSO, the mixture of DMSO: acetone in the ratio of (1:1), and the mixture of DMSO: acetic acid in the ratio (1:1).

Before the preparation of the polymer solutions, cellulose acetate was dried under vacuum for at least 48 hours. For preparing polymer solution, the contents were mixed until a homogeneous solution was obtained on a magnetic stirrer and roller.

Table 2. 1. Compositions of the polymer solutions used in the membrane preparation

Solution	Polymer (wt. %)	Solvent (wt. %)	Co-solvent (wt. %)
CA18-D	18% CA	82% DMSO	-
CA18-DA	18% CA	41 % DMSO	41% Acetone
CA18-DHAc	18% CA	41% DMSO	41% Acetic Acid
CA25-DA	25% CA	37.5% DMSO	37.5% Acetone

2.3 Fabrication of Membranes

2.3.1 Flat Sheet Membrane Fabrication

Flat sheet membranes were fabricated via the non-solvent induced phase separation method. Fabrication steps are illustrated and described in Table 2.2.

Used flat sheet membranes were listed with their codes and applied process during fabrication in Table 2.3. Polymer solutions were cast with the 250 μm casting bar, except with the CA25-DA-30CT membrane which is cast with the 30 μm casting thickness (-CT). As listed in Table 2.3, different evaporation times were applied to the casted polymer solution including acetone. In the membrane coding, (-xE) means the evaporation step: x is evaporation duration. The deacetylation by alkaline hydrolysis step is shown by the (-AH) code.

Table 2. 2. Membrane fabrication steps with illustrations



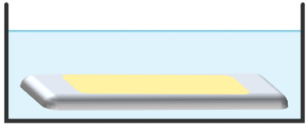
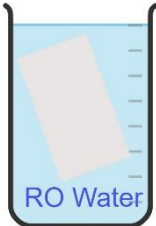
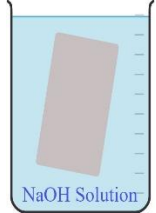
<p>Casting</p>	<p>A homogeneously mixed polymer solution was cast on a clean and smooth glass plate in the flat sheet form by a casting bar at room temperature.</p>	
<p>Pre-evaporation</p>	<p>The evaporation step was only applied to the acetone-containing polymer solution (CA18-DA) for different durations before immersing in the coagulation bath. Evaporation was done under the nitrogen flow with 0.6 L/min flow rate. Membranes were also cast from the DA solvent system with no pre-evaporation.</p>	
<p>Phase Separation</p>	<p>The casting membrane solution was immersed in a nonsolvent bath immediately or after evaporation (if used) to achieve phase separation. Type III (reverse osmosis, RO) water was used as non-solvent.</p>	
<p>Washing</p>	<p>After coagulation, membranes were washed in fresh reverse osmosis water to remove the residual solvents by changing the water three times in 24 hours. Upon washing, membranes were stored in the solution of 20% ethanol in water if the deacetylation was not applied.</p>	
<p>Alkaline Hydrolysis (Deacetylation)</p>	<p>Cellulose acetate membranes were immersed in the 0.05 M NaOH-water alkaline hydrolysis solution for 24 hours for converting to cellulose membranes. After 24 hours, regenerated cellulose membranes were washed in the RO water for one day to stop the reaction and clean the membranes. Cellulose membranes were stored in the solution of 20% ethanol in water.</p>	

Table 2. 3. Flat Sheet membrane codes and applied fabrication steps

Membrane Code	Pre-Evaporation	Alkaline Hydrolysis (Deacetylation)
CA18-D	-	-
CA18-DA	-	-
CA18-DHAc	-	-
CA25-DA-30CT	-	-
CA18-DA-1E	1 minute	-
CA18-DA-2E	2 minutes	-
CA18-DA-5E	5 minutes	-
CA18-DA-5E-RH	5 minutes (at high Relative Humidity)	-
CA18-DA-30E	30 minutes	-
CA25-DA-5E	5 minutes	-
CA18-DA-AH	-	+
CA18-DHAc-AH	-	+
CA25-DA-5E-AH	5 minutes	+
CA25-DA-30CT-AH	-	+

2.3.2 Hollow Fiber Membrane Fabrication

Hollow fiber (HF) membranes were fabricated through a dry-wet spinning process which a detailed illustration is presented in Figure 2.1. The polymer solution was filtered by metal mesh and filled into the tank at least one day before spinning for degassing. When the bubbles were removed from the solution, the polymer solution and bore liquid were fed to the spinneret simultaneously by individual gear pumps at an adjusted flow rate, as presented in the schematic diagram. For the more viscous polymer solution (CA18-DHAc), the nitrogen gas at 5 bar was used at the gear pump inlet to feed the solution at identical flow rates with other polymer solutions. Used spinneret has 1.3 mm orifice diameter and 3 mm outer diameter.

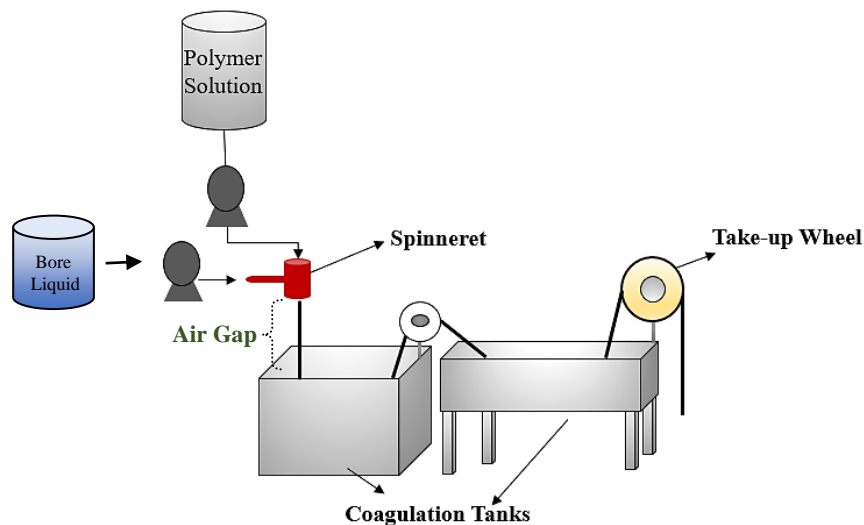


Figure 2. 1. A basic illustration of the spinning system

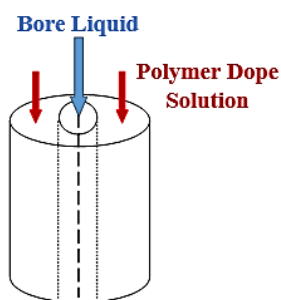


Figure 2. 2. Illustration of the exit of the spinneret

The fiber in the hollow structure was obtained by the bore liquid passing the inside capillary of the spinneret while the polymer solution falls from the annular space of the spinneret, as presented in Figure 2.2. After the fiber was extruded from the spinneret, it passed through an air gap distance and entered the first and second external coagulation tanks by drawing through a take-up wheel with a certain speed.

During the air gap, the inside of the fiber was precipitated by the bore liquid whereas the outside of the fiber was coagulated in the external coagulation baths. Tap water at different temperatures was used as external coagulant. Different bore liquids, air gap distances, and pulling speeds or free-fall conditions were applied during hollow fiber spinning. The detailed spinning conditions and membrane labels are summarized in

Table 2.4. CA18-DA and CA18-DHAc solutions were spun at different conditions. For all conditions, the ratio of dope flow rate to the bore flow rate was kept at 2:1 to obtain sufficient wall thickness required for strength during filtration experiments. Flow rates of polymer dopes were selected for continuous fiber spinning without a break since the drawing and air gap were applied together.

After spinning, the hollow fiber membranes were washed in the tap water for 24 hours by changing the water three times. Finally, hollow fiber membranes were immersed in 10% glycerol-90% pure water solution for 24 hours to prevent the pore from collapsing during drying. Fibers were dried for one day at ambient temperature before using in filtration experiments.

Table 2. 4. Membrane codes and spinning conditions for hollow fiber membrane from CA18-DHAc and CA18-DA polymer solutions

Membrane Code	Bore Liquid	Flow Rates (Dope/Bore) (ml/min)	Air Gap (cm)	Pulling Speed (m/min)	Coagulation Bath Temperature (°C)
<i>Polymer solution: CA18-DHAc</i>					
20AG-DW-3.7PS		12/6	20	10.4	
20AG-DW-10.4PS		12/6	20	3.7	
15AG-DW-3.7PS	80%DMSO 20% water	9.8/4.9	15	10.4	Ambient
15AG-DW-10.4PS		9.8/4.9	15	3.7	
4AG-DW-3.7PS		9.8/4.9	4	10.4	
4AG-DW-10.4PS		9.8/4.9	4	3.7	
2AG-DW-LFR-FF		3.8/1.9	2	Free-fall	
11AG-W-FF-HCB	Water	5.6/3.7	11	Free-fall	50
<i>Polymer solution: CA18-DA</i>					
6AG-DW-15PS	80%DMSO 20% water	15/7.5	6	15	Ambient

*(AG: Air gap distance; DW: 80%DMSO-20%water; W: pure water; PS: pulling speed; LFR: Lower flow rate; FF: free-fall; HCB; hot coagulation bath)

2.4 Performance Tests of Membranes

Performance of both hollow fiber and flat sheet membranes was observed by pure water permeance and molecular weight cut-off tests. The performance tests of the membranes were conducted in cross-flow mode, as illustrated in Figure 2.3. The feed stream was carried through the membrane module by a peristaltic pump. The back-pressure valve was used for pressurizing the feed side, and the permeate stream was obtained due to transmembrane pressure between the permeate and feed sides of the modules.

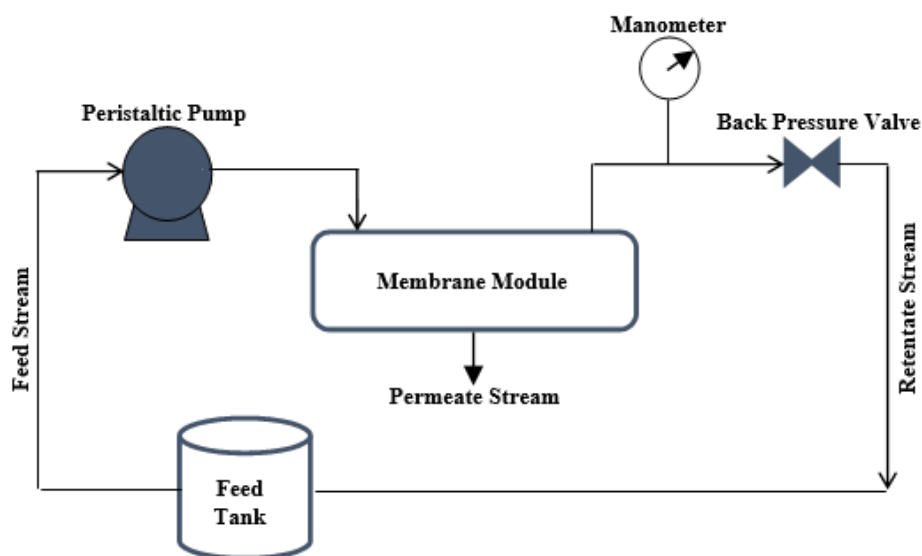


Figure 2. 3. Cross-flow mode filtration process chart

Sterlitech CF016A acrylic cross-flow module was used for the performance test of flat sheet membranes. The membrane module for hollow fiber membranes was prepared with a single dried fiber, as shown in Figure 2.4. A hollow fiber membrane is placed into a plastic pipe, and the pipe ends are closed by epoxy solution. The module is left for one day for the epoxy to cure before being used in filtration tests. Feed solution was fed to open end of one T connector when the selective layer is shell side of the fibers and permeate was collected from bore side of the fibers (outside-to-inside filtration).

When the selective layer was in bore side of the membrane, the feed solution is fed through the one end of the pipe while permeate was collected from the shell side (inside-to-outside filtration).



Figure 2. 4. Hollow fiber membrane module used in the filtration tests

Before the filtration (MWCO) experiments, the pure water permeance value was obtained. The permeate volume was collected against time at three different transmembrane pressures (1-0.5-0.3 bar), and the pure water flux values at these pressures were found. Pure water permeance (L/hm^2bar) is equal to the ratio of flux (L/hm^2) to transmembrane pressure (bar), as seen in the equation (1). After obtaining constant flux values for each pressure, the pure water permeance (PWP) value was obtained from the slope of the flux (J) versus the transmembrane pressure (TMP) graph.

$$PWP \left(\frac{L}{hm^2bar} \right) = \frac{J \left(\frac{L}{hm^2} \right)}{TMP (bar)} \quad (1)$$

After the PWP value was found, the MWCO test was applied to the same membrane to characterize the separation performance of it. The MWCO value represents the weight of the molecule that the membrane rejects at 90%. PEG molecules with different molecular weights were used to detect the MWCO value of membranes. The molecular weight of the PEG probes used in the filtration is 400 Da, 2000 Da, 6000 Da, 10000 Da, 20000 Da and 35000 Da. For looser membranes, dextran probes with higher molecular weights which are 40000 Da, 70000 Da, and 200000 Da were used. Filtration was carried out with an aqueous feed solution with a total probe concentration of 2.0 g/L. The MWCO value of a membrane strongly depends on the presence and extent of the concentration polarization altering the rejection of the membrane. The operating conditions should be adjusted to reduce the effect of

concentration polarization on the MWCO. The filtration was done in the cross-flow mode under a transmembrane pressure difference of 0.3 bar. The cross-flow velocity was adjusted at 0.02 m/s during filtration of the flat sheet membranes.

Cross-flow velocities used in the hollow fiber membrane filtration were in the range of 0.12-0.14 m/s and 1-1.2 m/s during outside-to-inside and inside-to-outside filtration modes, respectively. With these cross-flow velocities, the Peclet number (J/k_c) less than 1 was obtained; that is, the concentration polarization effect was minimized, and the obtained MWCO data was ensured to reflect the structure of the membrane regardless of filtration conditions^{12,47}.

The permeate and retentate samples began to be collected after 30 minutes of the filtration were started. Agilent 1260 Infinity II Gel Permeation Chromatography (GPC) was used to determine the probe concentrations in the permeate and retentate samples. Rejection of probes was found by Equation (2): C_p and C_R refer to permeate and retentate concentrations, respectively. The molecular weight of the probe which has 90 % rejection was marked as the MWCO value of the membranes.

$$Rejection \% = \left(1 - \frac{C_p}{C_R}\right) * 100 \quad (2)$$

2.5 Morphology Characterization by Scanning Electron Microscopy (SEM)

Membrane morphology was analyzed by scanning electron microscopy. Analyses were done in the METU Central laboratory (QUANTA 400F Field Emission SEM), and in METU Chemical Engineering Department (TESCAN VEGA3). For cross-sectional analysis of flat sheet and hollow fiber membranes, the structures of the membranes were frozen and broken in liquid nitrogen. There is no additional preparation step for the analysis of the membrane surfaces. The prepared samples were attached to conductive tape and dried in vacuum overnight. Before analysis, samples were coated with gold-palladium (Au-Pd).

2.6 Viscosity Measurements for Solvent Systems and Polymer Solution

Ubbelohde type capillary viscometer was used to measure the viscosity of used solvents and solvent mixtures at 25 ± 1 °C. Kinematic viscosities obtained by Ubbelohde viscometer were converted into dynamic viscosity by dividing by the density of solvent systems measured via pycnometer at 25 ± 1 °C. The viscosity of polymer solutions was measured by Anton Paar MCR302 model modular compact rheometer at METU Chemical Engineering Department. Analyses were done with 25 mm cone plate at 25 ± 1 °C. The viscosity of the acetone-containing solutions was measured using an evaporation blocker to prevent evaporation during analysis. All measurements were done at least three times.

2.7 Phase Inversion Front Observations via Optic Microscope

The progression rate of the phase inversion, which was started with the contact of the interface of the polymer solution with non-solvent (water), over time was observed with an optical microscope. After a drop of solution was placed between a clean microscope slide and a cover slip, 100 μ L of water was injected from one side of the solution drop. With the diffusion of water into the polymer solution, an opaque region in front of the non-solvent polymer interface formed as a result of the precipitation of polymer solution, and it progresses over time. The advancement of the precipitated region over time from the moment the interface encounters water ($t=0$ s) was recorded via the optical microscope (Zeiss AxioScope.A1). The rate of progression of this opaque region (the thickness of the opaque region formed over time) was considered as the instantaneous phase inversion rate²¹.

The square of the opaque part thickness (x^2) was measured and plotted against the relevant time (t). It was discussed by Strathmann and coworkers that, the slope of the x^2 vs. t plot is directly proportional to the effective diffusivity of water into the polymer solution^{21,48}. According to equation (3), the $(\frac{1-w_{CP}}{1+w_{CP}})$ term was considered as not dominant since it would be close to unity most of the time, and the $(\frac{\epsilon}{\tau})$ term,

which is the empirical parameters of membrane structure was considered constant for obtained membranes. Therefore, the effective diffusivity of water (D_{eff}) into polymer solution was estimated as the slope of the x^2 vs. t plot.

$$x^2 = \frac{4D_{eff}\varepsilon}{\tau} \cdot \left(\frac{1 - w_{CP}}{1 + w_{CP}} \right) \cdot t \quad (3)$$

2.8 Light Transmission Measurements

The amount of light passing through the membrane solution cast on a glass plate during phase inversion was measured against time with the experimental setup shown in Figure 2.5. After the cast polymer solution was immersed in the water bath, the light transmission across the cross-section of nascent membrane was recorded against time with the light meter located under the water bath while the phase inversion progressed. A protective box was placed around the experimental setup to prevent the light meter from being affected by ambient light. In this way, the light meter was enabled to measure only the light coming from the light source and passing through the membrane. The raw data obtained were normalized as I/I_0 : I represents the light passing through the membrane and I_0 represents the light passing in the absence of the membrane. The value found from the initial slope of the graph was calculated as cumulative phase inversion rate.

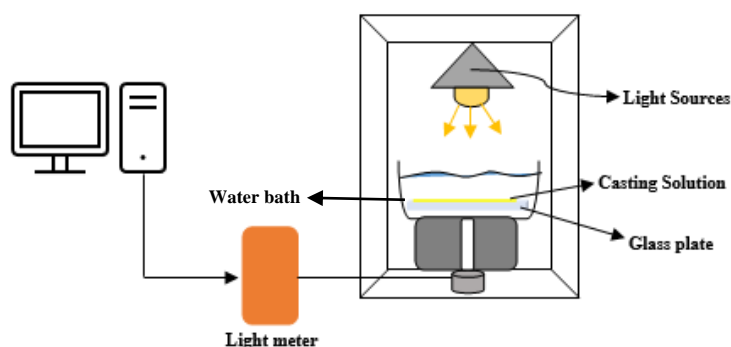


Figure 2. 5. Illustration for experimental setup of light transmission measurement

2.9 Acetone Evaporation Experiment

In order to determine the new solution composition obtained at the end of different evaporation times applied to the acetone-containing polymer solution (CA18-DA), the mass change of the casting polymer solution and the change in relative humidity in the evaporation bath were recorded over time. In order to observe the changes in the system with high accuracy, the original evaporation bath in the membrane fabrication was used with nitrogen at the same flow. A simple drawing of the experimental setup used is presented in Figure 2.6. Before starting the experiment, nitrogen was passed through the bath at a flow rate of 0.6 L/min for 10 minutes to stabilize the nitrogen flow and ambient humidity in the bath. Then, the polymer solution cast in the same thickness (250 μm) on the glass plate was quickly placed in the bath and the measurement was started. The change in the weight of the overall system over time was carried out with a precision balance connected to the computer. At the same time, while evaporation continued, the change in the % relative humidity inside the bath was measured with a % RH meter against time. The weight of the polymer solution during evaporation was calculated using equation (4).

$$W_{\text{polymer solution}} = W_{\text{total}} - W_{\text{setup w/o glass}} - W_{\text{glass}} \quad (4)$$

W_{total} represents the weight of the entire setup measured during evaporation with time, $W_{\text{setup w/o glass}}$ is the weight of the setup without glass at the beginning of the experiment with stabilized nitrogen flowing, and W_{glass} is the weight of the glass used for casting polymer solution.

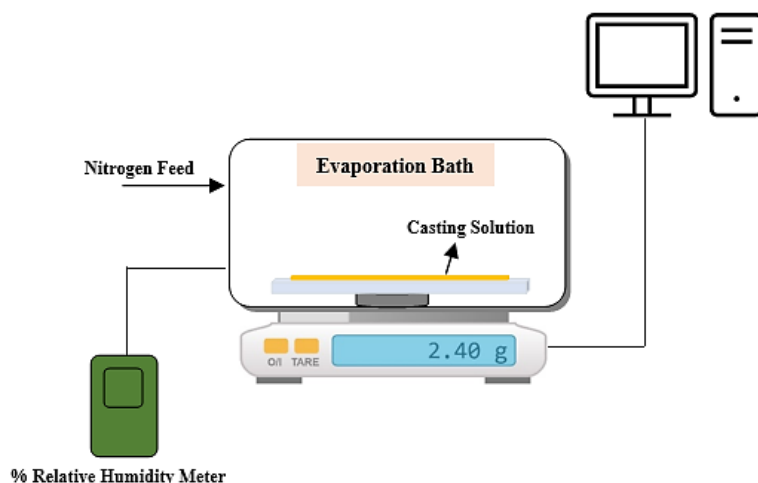


Figure 2. 6. Experimental setup for measurements of polymer solution weight and relative humidity during acetone evaporation from casting solution under nitrogen stream

2.10 Cloud Point Measurements

The cloud point is the point where the polymer solution contains the maximum amount of nonsolvent it can contain before phase separation occurs and is located on the binodal curve of the phase diagram. For determining cloud point of polymer solutions, polymer solutions were firstly prepared with 5 wt.% increased water content, and the last clear solution and the first turbid solution were determined by visual inspection. Then, solutions containing water with closer compositions were prepared between these two water concentrations (with 1 wt.% and 0.2 wt.% concentration difference, respectively). In polymer solutions with closer water content, cloud point concentration was determined with high precision by visual inspection and turbidity meter as the concentration between the final clear solution and the first turbid solution.

2.11 Relative Energy Density (RED) Calculations via Hansen Solubility Parameters

The affinity between the solvent systems and the polymer, that is, the solvent quality of the solvent systems against the polymer, was theoretically estimated by comparing the Relative Energy Density (RED) values using Hansen solubility parameters. Three different Hansen solubility parameters were used to determine the molecular interaction: permanent dipole-permanent dipole interactions (δ_P), dispersion interactions (δ_D) and hydrogen bonding (δ_H). By using these parameters, the solubility parameter distance (Ra), which is the distance between radii of solubility spheres of compared materials (polymer and solvent), was calculate by using equation (5).

$$Ra^2 = 4 (\delta_{D1} - \delta_{D2})^2 + (\delta_{P1} - \delta_{P2})^2 + (\delta_{H1} - \delta_{H2})^2 \quad (5)$$

For the determination of Ra value for solvent mixtures and polymer, the solubility parameters of solvent mixtures were calculated by equations (6),

$$\delta_{mixture} = [\varphi_1 * \delta_1] + [\varphi_2 * \delta_2] \quad (6)$$

φ is the volume fraction of each solvent in the mixture and volume change on mixing ($\Delta\hat{V}$) is assumed be zero for solvent mixtures in the calculation of volume fraction using equation (7) ⁴⁹.

$$(Vol.Fraction)_1 = \frac{\left(\frac{Wt. Fraction}{Density}\right)_1}{\left(\frac{Wt. Fraction}{Density}\right)_1 + \left(\frac{Wt. Fraction}{Density}\right)_2} \quad (7)$$

Then, the relative energy density (RED) value for two components was calculated by following equation (8). Ro is called radius of the solubility sphere, which defines a limit for solubility parameter distance. For high affinity between two components, Ra value should be less than Ro. RED equal to or close to 1.0 is a boundary condition for solubility.

$$RED = \frac{Ra}{Ro} \quad (8)$$

Hansen solubility parameters for all solvents and polymer were obtained from Hansen's book⁴⁹. Also, Ro value for cellulose acetate was taken from the same book.

2.12 Excess Gibbs Free Energy Calculations

Excess Gibbs free energy (\underline{G}^{ex}) for solvent/non-solvent systems was calculated to observe their interactions. Excess Gibbs free energy is the difference between Gibbs free energy for the real mixture and Gibbs free energy for an ideal mixture at the same temperature, pressure, and composition, as seen in the equation (9). The negative \underline{G}^{ex} implies that the interactions between unlike molecules are more favorable than those between like molecules, while in the case of positive \underline{G}^{ex} , the interactions between like molecules are more favorable than those between unlike molecules. The equation (10) was used to calculate \underline{G}^{ex} for solvent or solvent mixtures and water. Activity coefficients for components were estimated by the UNIFAC model. All interaction parameters and volume and surface area parameters (R and Q) for groups included by components were taken from Poling et al.⁵⁰. Also, \underline{G}^{ex} for the DMSO-water system was calculated with experimental activity coefficients obtained by the study of Lam et al.⁵¹.

$$\underline{G}^{ex} = \underline{G}^{real} - \underline{G}^{ideal} \quad (9)$$

$$\underline{G}^{ex} = RT \sum_{i=1}^k x_i \ln \gamma_i \quad (10)$$

CHAPTER 3

RESULTS AND DISCUSSION

3.1 Effect of Solvents on the Thermodynamics of Phase Inversion System

Changing the solvent or solvent mixture is an important parameter affecting the thermodynamics of the ternary system (polymer-solvent-non-solvent) used to fabricate membranes via phase inversion. In this part of the study, binary interactions of cellulose acetate-solvent, water-solvent, and their ternary system were investigated by combining experimental and theoretical methods.

3.1.1 Solvent-Polymer Interactions via Hansen Solubility Parameters

Using Hansen solubility parameters, the affinity between solvent and polymer can theoretically be estimated. The closer solubility parameters of components indicate the higher affinity or vice versa. The relative energy density (RED) value calculated with this approach provides convenience in comparing the solvent quality for the same polymer. The divergence of RED value from 1 determines the solvent quality for the polymer, that is, affinity or interaction between them. If the RED value of a solvent-polymer system is lower than unity, the interactions of solvent and polymer are strong, which means the solvent is a good solvent for the polymer. In contrast, the RED value higher than unity implies a lower affinity between the solvent and polymer or strong nonsolvent quality for the polymer⁴⁹.

Hansen solubility parameters of all components and RED values for polymer/solvent systems and polymer/non-solvent interaction are listed in Table 3.1. According to RED values, DMSO is a good solvent for cellulose acetate by itself. Pure solvents of acetone and acetic acid are near the solubility limit. However, in the literature, some

studies used acetone and acetic acid as solvents to dissolve 10-12 wt.% cellulose acetate^{45,52}. Thus, they can be considered as poor solvents for cellulose acetate.

Table 3. 1. RED values of individual solvent-polymer pairs and solvent mixture-polymer pairs

Materials	Solubility Parameters (MPa ^{1/2})			RED _{P-S}
	δ_D	δ_P	δ_H	
Cellulose Acetate				
(CA)	18.2	12.4	10.8	-
(Ro=7.4)				
DMSO	18.4	16.4	10.2	0.55
Acetone	15.5	10.4	7	0.93
Acetic Acid	14.5	8	13.5	1.22
DA	16.95	13.4	8.6	0.51
DHAc	16.45	12.2	11.85	0.52
				RED _{P-NS}
Water	15.5	16	42.3	4.35

Although acetic acid and acetone alone are estimated to be poor solvents, the mixtures of DMSO-acetic acid (DHAc) and DMSO-acetone (DA) in the ratio of 1:1 have lower RED values than unity like DMSO, which implies that these solvent mixtures also can show high affinity and good solvent quality for cellulose acetate. Water, used as nonsolvent for phase inversion, has the highest RED value and strong non-solvent quality for cellulose acetate. This is also expected from its low swelling ratio for CA, a property typically considered to indicate non-solvent-polymer interactions, as reported by Durmaz et al.²¹

3.1.2 Polymer Chain Entanglement Concentrations of Polymer Solutions as A Tool to Assess Solvent-Polymer Interactions

The theoretical solubility parameters approach may not be sufficient to predict the solvent mixture-polymer interactions due to the complexity of these systems. Thus, besides the RED values, the polymer chain entanglement concentrations of polymer solutions were used to understand the qualities of solvent systems against cellulose acetate experimentally.

Increasing polymer concentration leads to a gradual increase in the relative viscosity of polymer solutions and three concentration regions can be distinguished according to polymer concentration: dilute, semi-dilute, and concentrated regions. In the semi-dilute region, relative viscosity starts to change more significantly with increased polymer concentration since polymer coils are closer and interact with each other, named the entanglement of polymer chains^{53,54}. At a certain polymer concentration, a dramatic change in relative viscosity occurs due to a significant increase in the degree of chain entanglement at this point, designated as polymer chain entanglement concentration^{54,55}. Therefore, the polymer chain entanglement concentration (C_e) for a polymer solution is the threshold point where the slope of the viscosity line changes sharply from semi-dilute region to concentrated region⁵⁴.

The relative viscosity of polymer solutions in the good solvents is lower than in the poor solvents for the same polymer concentration in this region⁵³. This means that, polymer chains in the good solvents start to entangle at a higher polymer concentration (higher C_e) than in poor solvents^{34,54,55,57}. Consequently, when it comes to the same polymer, differences in entanglement concentration relates to the solvent quality⁵⁴.

The relative viscosity, which was calculated by the ratio of zero-shear viscosity of the polymer solutions to the viscosity of the solvent systems, was plotted against increasing cellulose acetate concentration to detect the polymer chain entanglement concentrations of used polymer solutions, as shown in Figure 3.1.

The entanglement concentrations for all polymer solutions obtained from the graph are listed in Table 3.2.

According to Figure 3.1, no obvious change was observed in the slope of the viscosity line for the cellulose acetate-DMSO-acetone system (CA-DA) with increasing CA concentration. This indicates that the CA-DA polymer solution has a higher polymer chain entanglement concentration than 35 wt.% cellulose acetate, which is the maximum concentration point on the graph. Since the CA-DA polymer solution couldn't be prepared due to the difficulty in mixing of polymer solution with higher cellulose acetate concentration homogeneously, the certain entanglement concentration was not measured for this system. The polymer chain entanglement concentrations for cellulose acetate-DMSO (CA-D) and cellulose acetate-DMSO-acetic acid (CA-DHAc) systems are 30 wt.% and 25 wt. %, respectively.

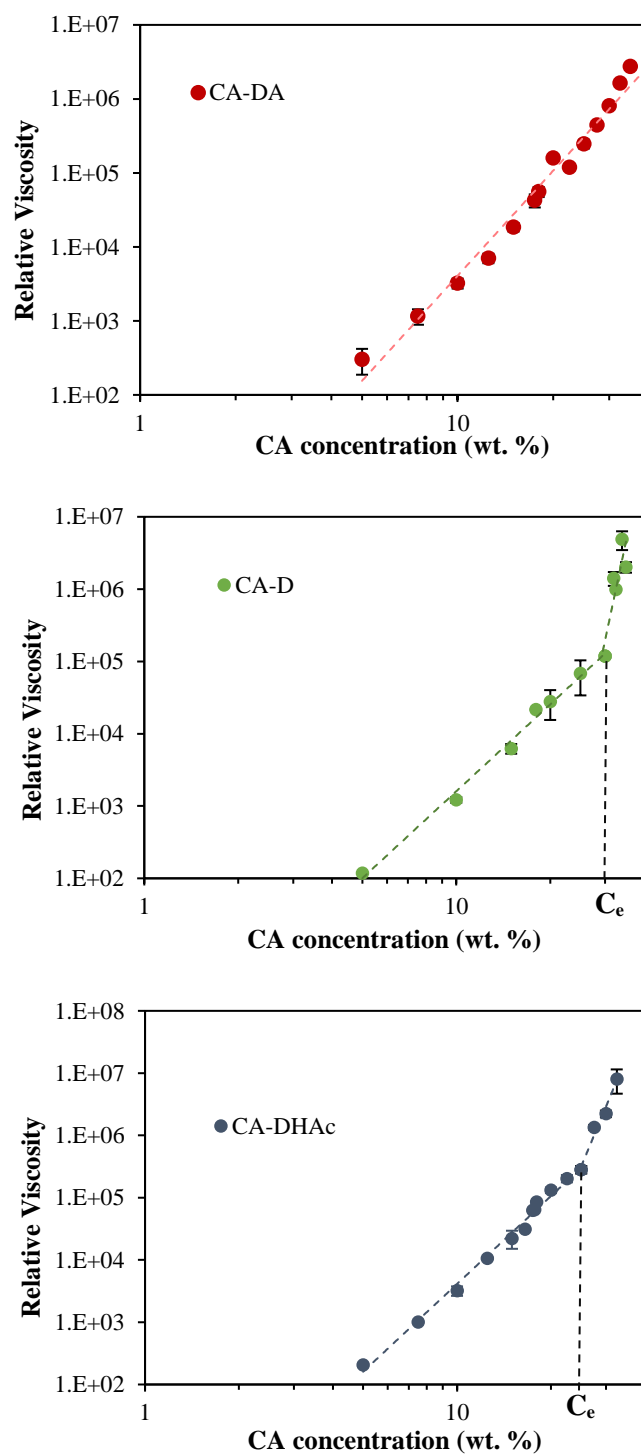


Figure 3. 1. The relative viscosity of polymer solution systems with increased cellulose acetate (CA) concentration

According to these results, the order of solvent quality for cellulose acetate from high to low is DA, DMSO, and DHAc, as listed in Table 3.2. Adding acetone to the solvent system as a co-solvent enhanced the solvent quality of DMSO; in contrast, using acetic acid as another co-solvent resulted in poorer solvent quality for cellulose acetate.

Table 3. 2. Polymer chain entanglement concentrations (C_e) of polymer solutions

Polymer solution	C_e (wt. %)
CA-DA	>35
CA-D	30
CA-DHAc	25

All solvent systems had quite similar qualities for cellulose acetate according to the theoretical RED values. Hansen solubility parameters of solvent mixtures are simply calculated as if no volume change occurs upon mixing as suggested by Hansen⁴⁹. However, molar volume change on mixing ($\Delta\tilde{V}_{mix}$) of DMSO-acetone and DMSO-acetic acid in the ratio of 1:1 was calculated as -0.24 and -0.73 cm³/mol, respectively⁵⁸. Negative volume change on mixing demonstrates more preferable interaction between unlike molecules compared to like molecules. This may affect the accuracy of Hansen solubility parameters predictions for solvent mixtures.

3.1.3 Excess Gibbs Free Energy Calculation for Solvent-Water Interaction

The excess Gibbs free energy (G^{ex}) was calculated to understand the interactions between used solvent systems and water (nonsolvent) during phase inversion process at 25 °C. The UNIFAC model was used to estimate the activity coefficients of components in the binary mixture of DMSO-water and the ternary mixtures of DMSO-acetone-water and DMSO-acetic acid-water.

Also, the experimental data for activity coefficients of the DMSO-water system obtained from the study of Lam et al. were used to compare the calculated and experimental $\underline{G}^{\text{ex}}$ ⁵¹. The plot of the excess Gibbs free energy ($\underline{G}^{\text{ex}}$) for water-solvent systems versus water mole fraction in the binary (DMSO-water) and ternary (DMSO-HAc-water or DMSO-acetone-water) is presented in Figure 3.2. The point that the water mole fraction equals zero represents the beginning of phase inversion where the water and solvent systems encounter. Thus, at this point, the $\underline{G}^{\text{ex}}$ values belong to binary mixtures of solvents in 1:1 ratio, which are DMSO-acetone and DMSO-acetic acid.

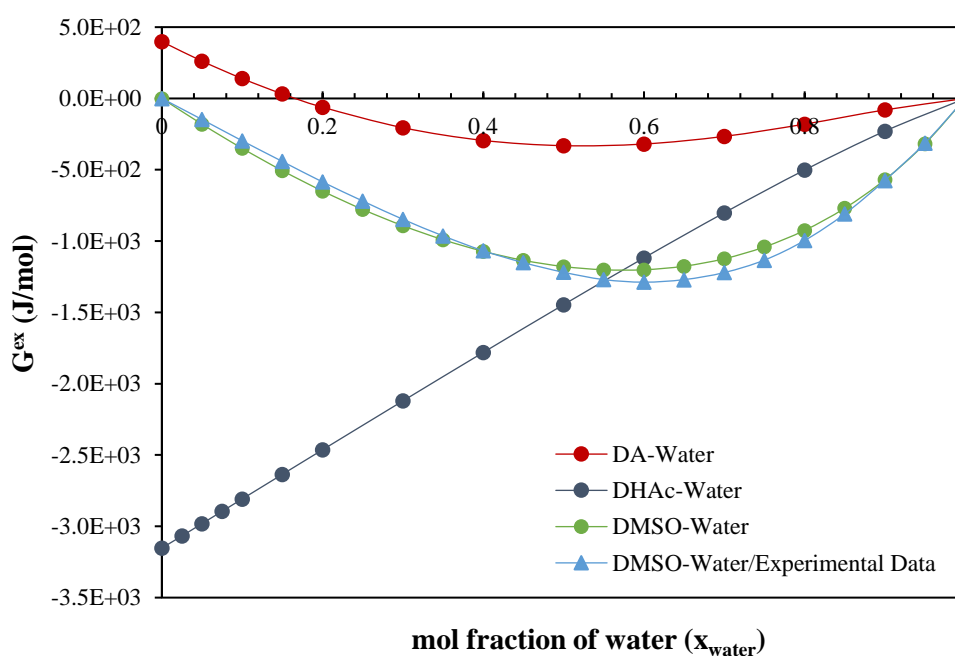


Figure 3. 2. Excess Gibbs free energy for the interaction of water-solvent systems

According to Figure 3.2., excess Gibbs free energy is negative for all water-solvent systems, except the DA-water system at low water mole fraction. Negative $\underline{G}^{\text{ex}}$ means negative deviation from Raoult's law implying unlike-unlike interactions are more favorable than like-like interactions. The highest solvent-non-solvent (S-NS) affinity is estimated in the DHAc-water system, probably due to the higher hydrogen

bonding capacity of acetic acid in this system. DMSO-water system shows second high affinity, while DA-water system exhibits almost ideal behavior. In addition, $\underline{G}^{\text{ex}}$ of DMSO-water mixture calculated by the activity coefficient data from literature overlaps quite well with $\underline{G}^{\text{ex}}$ found with activity coefficients from the UNIFAC group contribution method.

Overall, solvent-nonsolvent (S-NS) interactions for the three systems appear to be quite different, where the highest S-NS affinity is in the DHAc-water system and lowest is in DA-water system.

3.1.4 Cloud Point Measurements

The cloud point (or binodal composition) is the point on the binodal curve; the polymer solution is not stable in one phase on that point¹⁴. The cloud point, which is the maximum water composition of polymer solutions before phase separation initiates, gives an idea about the thermodynamic stability of the ternary polymer-solvent-non-solvent system. Less stable systems possess a lower cloud point which means a small amount of non-solvent is sufficient for starting the precipitation of the polymer solution in phase inversion⁴⁵.

Table 3. 3. Cloud point water composition (wt. %) of polymer solution-water system

Polymer Solution	Cloud Point (wt. % water)
CA18-D	10.3
CA18-DA	13.3
CA18-DHAc	8.1

The cloud points of polymer solutions are tabulated in Table 3.3. The order of cloud points from low to high is as follows: CA18-DHAc, CA18-D, CA18-DA, which means adding acetone made the system more stable against phase separation with water compared to the acetic acid.

For these systems where water was used as non-solvent, differences in cloud points of polymer solutions containing the same cellulose acetate amount (18 wt.%) follow the interaction between the solvent systems and cellulose acetate. In the literature, the cloud point measurements were done to understand the qualities of solvents and non-solvents^{21,36,45,59}. Generally, a lower cloud point is explained by the lower solvent-polymer affinity or strong non-solvent quality because the presence of weak solvents or strong non-solvents in the polymer solution requires a lower amount of nonsolvent for phase inversion. In other words, the stronger solvent power requires a higher amount of nonsolvent to induce precipitation^{60,61}. The cloud points are in accordance with the solvent strength estimated from entanglement concentrations. Also, S-NS interactions obtained from $\underline{G}^{\text{ex}}$ data explain this order of cloud point for polymer solutions; the stability of polymer solutions against the non-solvent (water) decreases as the affinity between S-NS gets higher. Overall, the least stable cellulose acetate solution is CA18-DHAc, whereas the most stable one appears to be CA18-DA.

3.2 Effect of Solvent Systems on the Phase Inversion Kinetic

In membrane fabrication via phase inversion, phase inversion rate which occurs by the counter-diffusion of solvent and nonsolvent affects the final morphology and performance of membranes. In this section, the effect of solvent systems on the phase inversion rate was discussed by rheological data as well as phase inversion rate observations via optical microscope and light transmittance measurements.

3.2.1 Instantaneous Phase Inversion Rate Observations

The instantaneous phase inversion rate of polymer solutions can be observed by an optical microscope. As seen in Figure 3.3, when time equals zero, water injected into the interface of the polymer solution starts to interact with polymer solutions. As time progressed, the opaque part, the precipitated part, of polymer solutions moved towards the inner parts of the polymer solution.

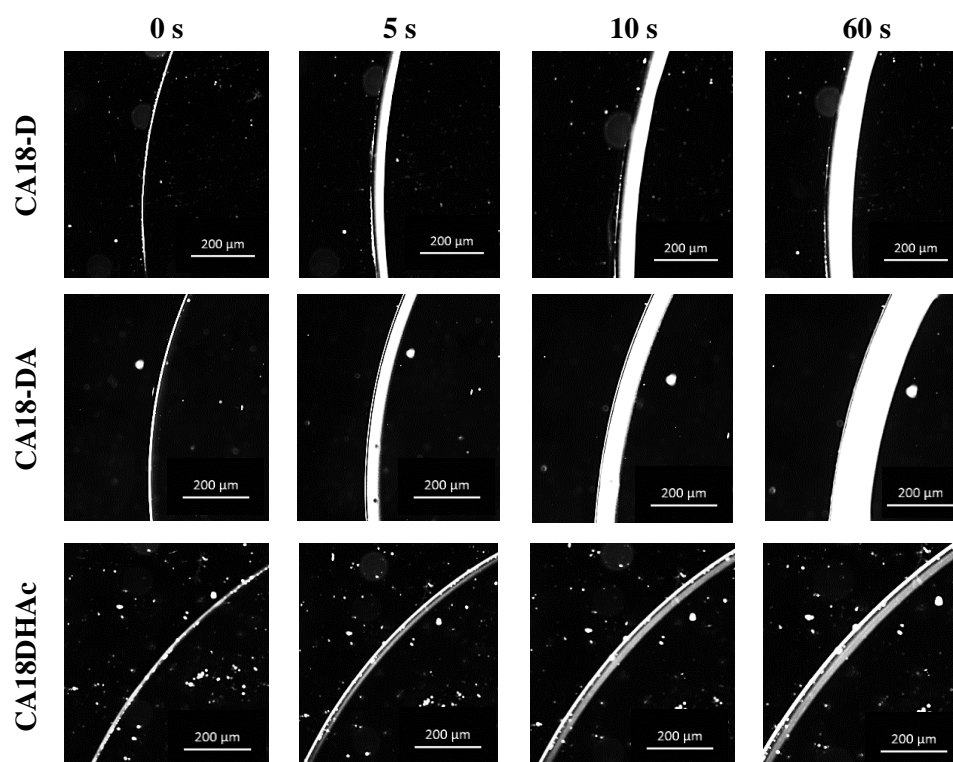


Figure 3. 3. Phase inversion front observations via optic microscope from t=0 to t=60 seconds

When the progress of opaque parts for polymer solutions is compared, the front of the CA18-DA system moves faster than in others. CA18-DHAc has the slowest front rate. As a result, adding acetone to the polymer solution enhanced the front rate, while acetic acid decreased the advancement of precipitation when the CA18-D was considered. The square of the thickness of the precipitated part (x^2) of polymer solutions was plotted with respect to time in Figure 3.4 (a).

The effective diffusivity of a non-solvent (water) into a polymer solution is proportional to the slope of x^2 vs. time graph according to the approach of Strathmann and coworkers described in the experimental method. The comparison of the slope of x^2 versus time lines for polymer solutions is presented in Figure 3.4 (b). In addition, the diffusivity of water into the solvent systems were estimated by Wilke-Chang equation as shown in the same figure. The viscosity of solvent systems is reported in Table 3.4 and are used in this calculation. In the same table are also shown viscosities of the starting polymer solutions.

The effective diffusivity of water into the polymer solutions, which are estimated from the slope of x^2 versus time data, from high to low can be ordered as CA18-DA, CA18-D, and CA18-DHAc, as shown in Figure 3.4. As a result, this effective diffusivity of water into polymer solutions and diffusivity of water into the solvent systems estimated by Wilke-Chang equation are in the same order of magnitude. This implies that the dominant factor that affects the phase inversion rates in these systems is solvent medium (solvent viscosity), and phase inversion rates are inversely proportional to the viscosity of solvent systems.

Table 3. 4. The viscosities of solvent systems and polymer solutions

Solvent or Polymer Solution	Viscosity (cP)
DMSO	1.97
DA	0.70
DHAc	2.77
CA18-D	42,600
CA18-DA	44,400
CA18-DHAc	235,000

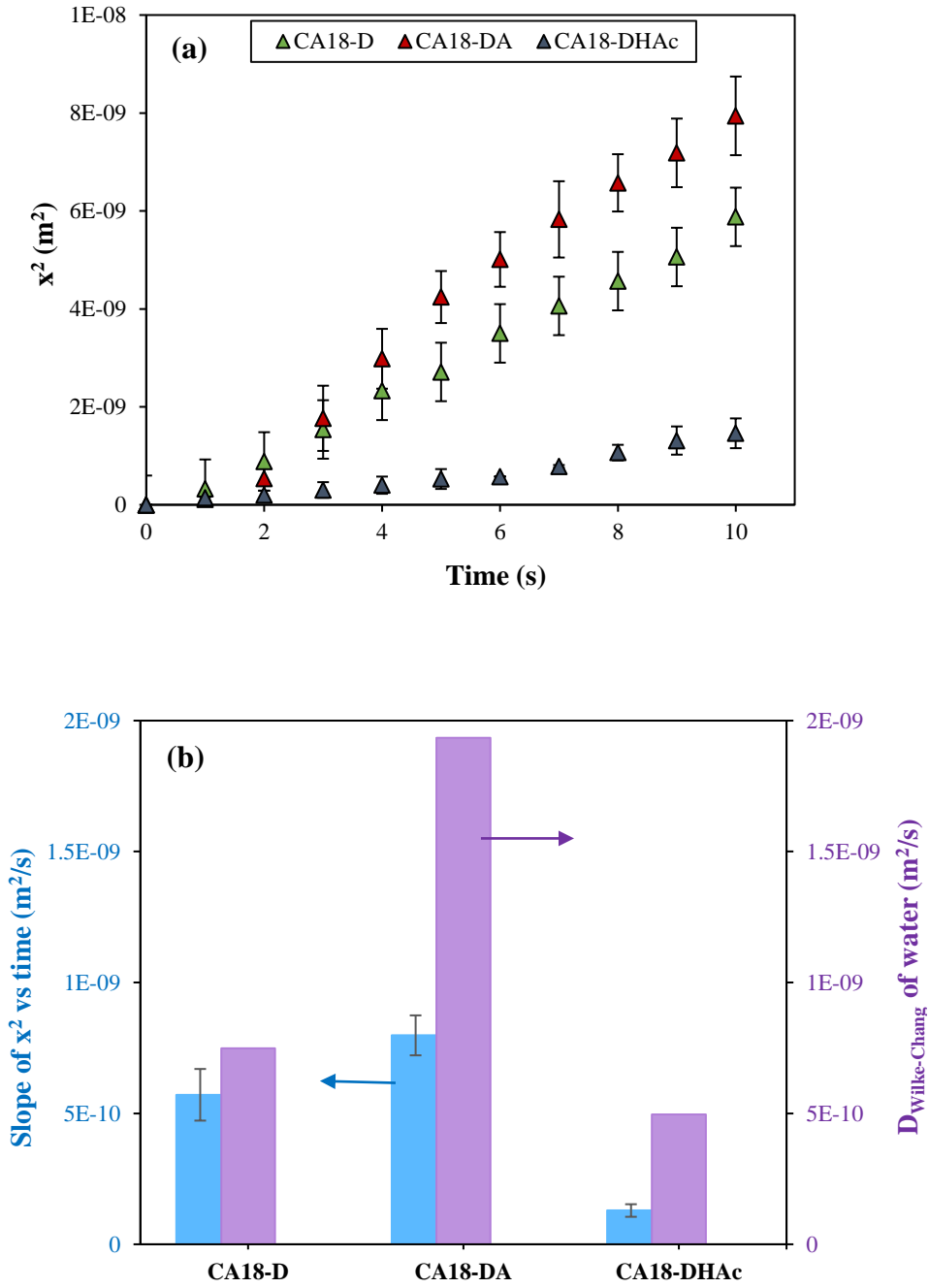


Figure 3. 4. (a); x^2 vs. time plot from microscope observations, and (b); graph of the slope of x^2 vs. time for estimation of effective diffusivity of water into polymer solution and diffusivity of water into solvent systems estimated by Wilke-Chang equation

3.2.2 Cumulative Phase Inversion Rate via Light Transmittance Measurements

Light transmittance measurement was used to measure the cumulative phase separation rate in solutions during the coagulation in water. After the polymer solution was cast as flat film, it was immediately immersed in a water bath, and light transmittance passing through the solution was measured in time. The obtained phase inversion rate is designated as “cumulative” since the progress of phase inversion is measured by light transmittance through the whole cross-section of the cast film instead of interface observation such as in the optical microscope observation.

The normalized light transmission (I/I_0) curves over time are given in Figure 3.5 (a). The normalized data was calculated by the ratio of the amount of light during measurement (I) to the amount before immersing the polymer solution in the water bath (I_0). As shown in the graph, the amount of light decreases as the phase inversion proceeds and reaches a constant I/I_0 value when the membrane is produced at the end of the phase inversion. The slope of the linear part of the light transmittance curve is taken as the cumulative phase inversion rate. The average cumulative phase inversion rates obtained by initial slopes of the light transmission plots were compared in Figure 3.5 (b).

It can be seen that there is no delay time during phase inversion for all polymer solutions despite the different cloud points of systems; that is, phase inversion started almost immediately after polymer solutions were immersed in the water bath. The delay time is related to the solvent quality and the S-NS interaction. Although there are differences in the solvent qualities and S-NS interactions in used systems, any of these differences did not cause an observable delay time during the phase inversion.

CA18-DA system possesses the highest cumulative phase inversion rate, whereas the rate of the CA18-D is lower than that of the CA18-DA, and the lowest cumulative phase inversion rate is observed in the CA18-DHAc system.

In other words, adding acetone as the co-solvent to the solvent systems leads to a higher cumulative rate, while acetic acid addition slows it down. The cumulative phase inversion rates follow the same order with the instantaneous phase inversion rates of polymer solutions. But the distinctions in the cumulative phase inversion rates of polymer solutions are more drastic due to the porosity effect on the cumulative phase inversion results. Measured cumulative phase inversion rates are significantly affected by the porosity or pore size occurring in the membrane structures. In the study by Durmaz et al., the cumulative phase inversion rates were shown to be directly proportional to the porosity or pore size of the final membrane. They showed that higher porosity or pore size in the membrane structure causes higher opaqueness creating extra turbidity, and it is reflected as higher cumulative phase inversion rates in the light transmission measurement¹⁴. Consequently, the cumulative phase inversion rate gives reliable final membrane porosity and pore size results. Especially in the morphology with macrovoids, the time interval for the formation of macrovoids is small compared to the time interval used to calculate the cumulative rate. Thus, the macrovoids already exist at the time interval considered for calculating the cumulative phase inversion rate, and the obtained cumulative rate represents the porosity and pore size completely¹⁴.

In our systems, the cumulative phase inversion rates can be related both to the actual phase inversion rate and to the porosity and pore size of the membranes shown in the next section. However, while instantaneous phase inversion rates are at the same order of magnitude for all three solvent systems, the cumulative phase inversion rate of CA18-DHAc is two orders of magnitude lower than the other two solvent systems. This implies that the pore morphology in this membrane is different and has significant effect on the observed cumulative phase inversion rate, as will be verified in the coming sections.

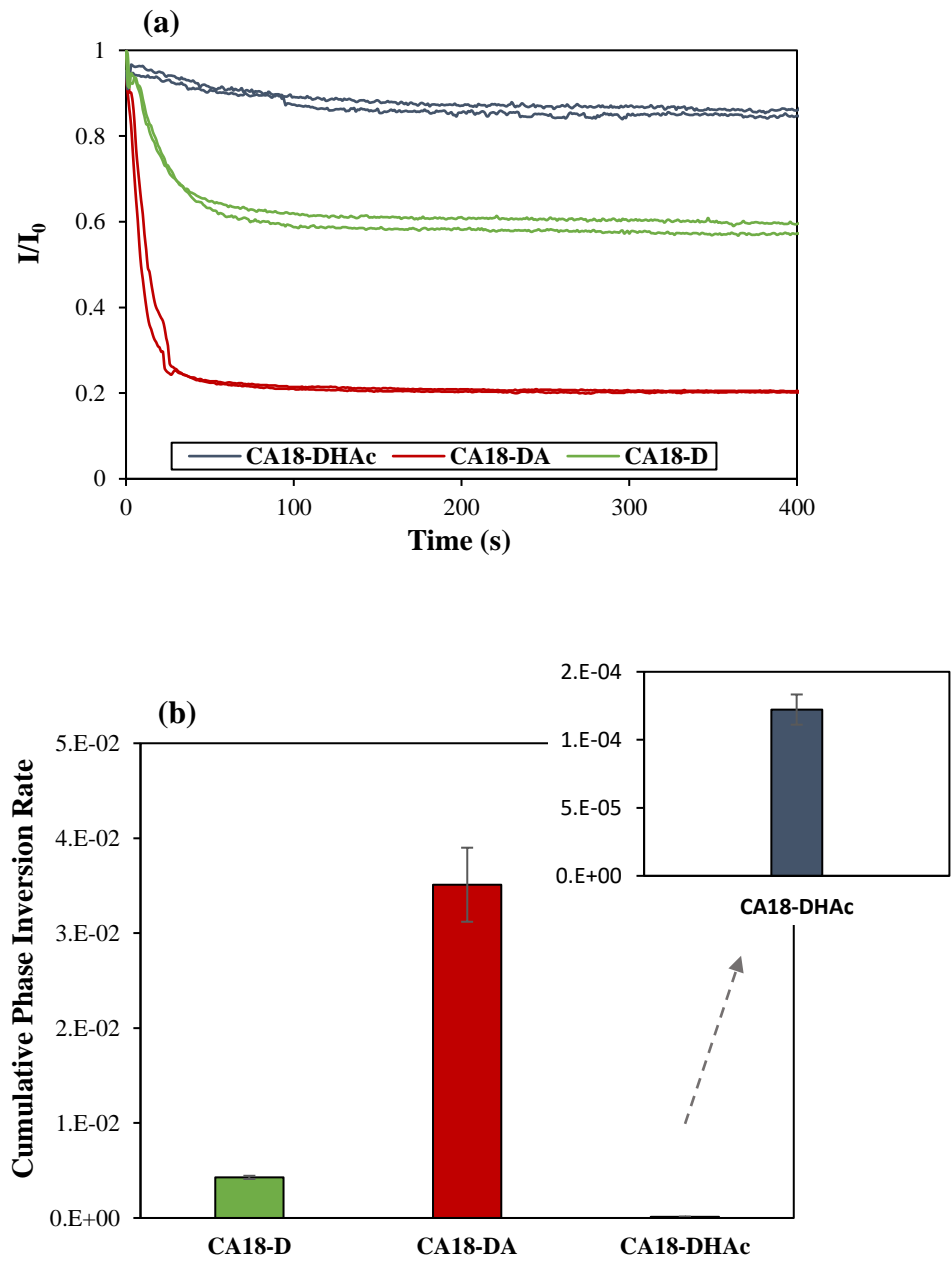


Figure 3. 5. Cumulative phase inversion rate by light transmittance. (a); Light transmittance plot (b); cumulative phase inversion rate obtained by the slope of the graph (a)

3.3 Morphology and Performance of Cellulose Acetate Flat Sheet Membranes

Fabricated flat sheet membranes from CA18-DA, CA18-D, and CA18-DHAc polymer solutions were characterized in terms of morphology and performance. The scanning electron microscope (SEM) was used to evaluate the morphologies of membranes. Pure water permeance and MWCO test were conducted to evaluate the performance of the membranes.

3.3.1 Effect of Solvent Systems on Membrane Morphology

Figure 3.6. shows the morphologies of the fabricated cellulose acetate membranes using three different solvent systems. Changing the solvent system resulted in significant differences in membrane morphology. CA18-D is an asymmetric membrane with large macrovoids in the support layer. CA18-DA membrane also has an asymmetric morphology consisting of a thinner selective layer above the substrate layer with somewhat larger pores and more macrovoids. The CA18-DHAc membrane shows a symmetric and porous structure throughout the cross-section. As a result, adding acetone to the solution as the co-solvent resulted in a more asymmetric structure; while acetic acid was used as the co-solvent instead of acetone, the asymmetry disappeared.

The asymmetric structure of the CA18-DA membrane containing a dense selective layer on the macro-sized porous substrate can be explained by the high phase inversion rate (instantaneous demixing) in the CA18-DA polymer solution as shown via phase inversion rate observations before. The instantaneous phase inversion rate causes the formation of asymmetric membrane structure with macrovoids. The lower viscosity of solvent system favors the fast phase inversion of that membrane.

While instantaneous phase inversion also occurs in the CA18-DHAc system due to the low thermodynamic stability based on its lower cloud point; the higher viscosity of solvent mixture led to a lower phase inversion rate and resulted in symmetric and

porous membrane structure. To summarize, it appears that the differences in the morphology of CA18-DA and CA18-DHAc systems can be explained mostly by the differences in viscosity of solvent systems which vary the phase inversion kinetics. The membrane structure of CA18-D reveals that the viscosity of DMSO favored the sufficiently high demixing rate to result in an asymmetric structure. The result of SEM and cumulative phase inversion rate measurement is consistent with the porosity of the final membrane structure for all systems.

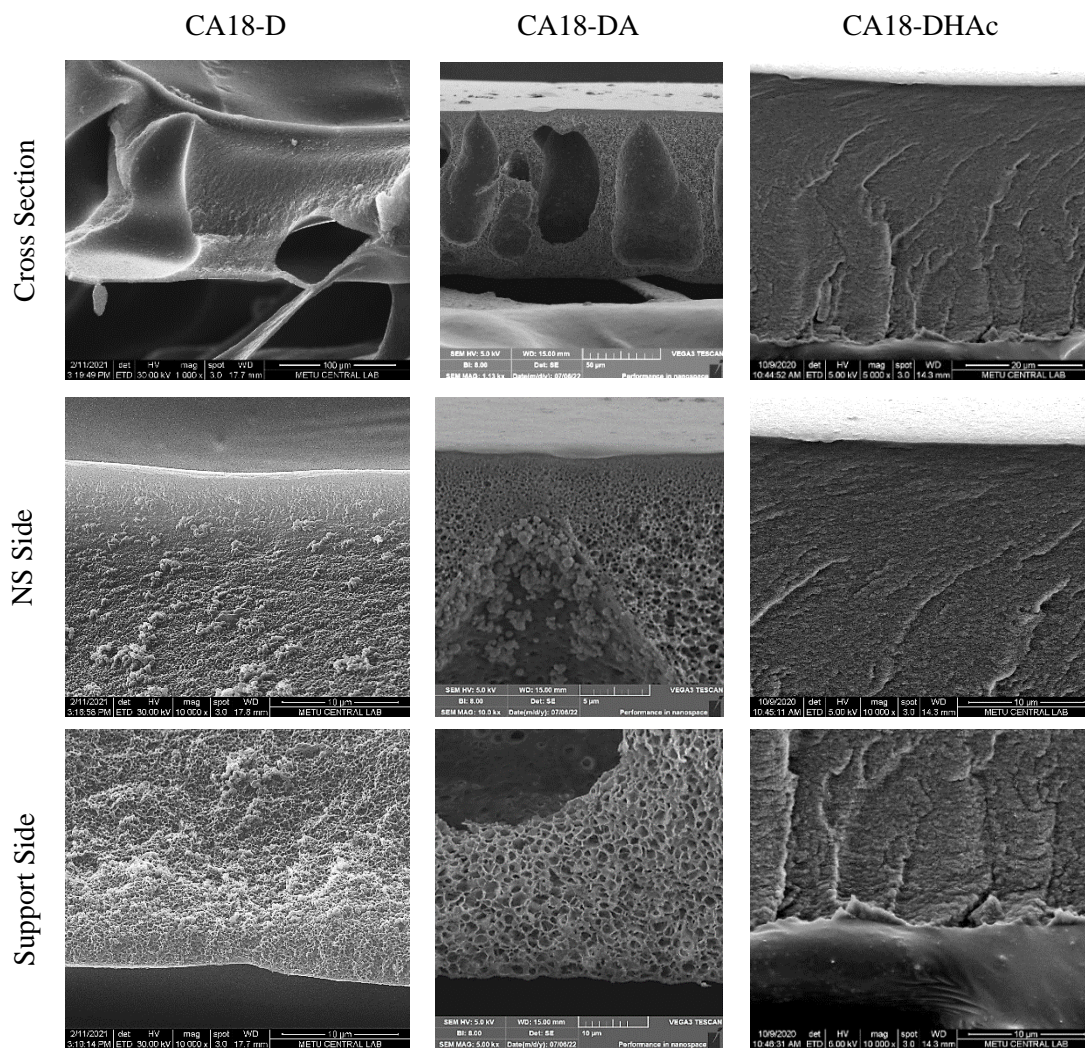


Figure 3. 6. SEM images of cellulose acetate flat sheet membranes prepared with different solvent systems

3.3.2 Effect of Solvent Systems on Membrane Performance

The average pure water permeances of membranes measured before rejection tests and average MWCO values are illustrated in Figure 3.7.

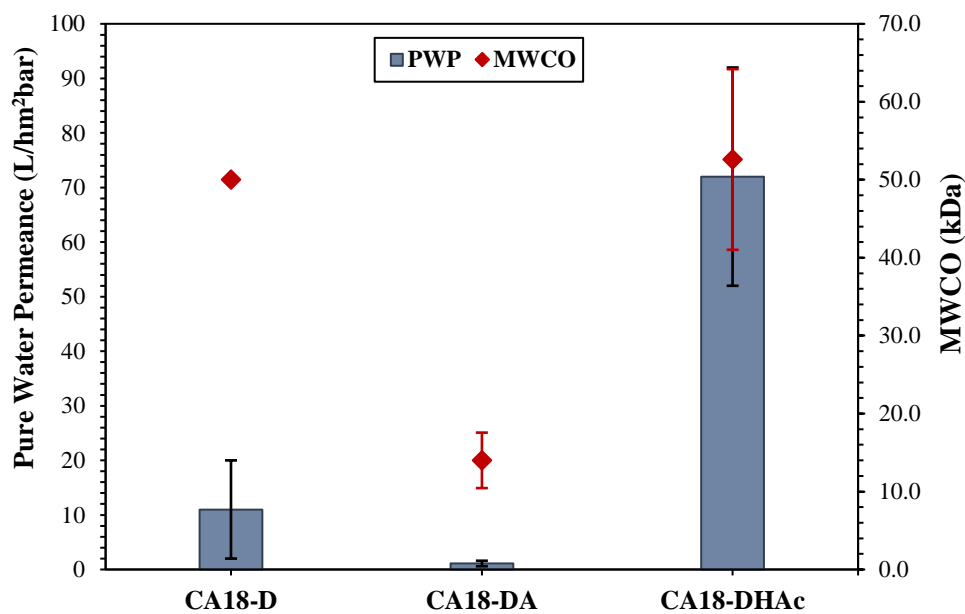


Figure 3. 7. Pure water permeance (PWP) and molecular weight cut-off (MWCO) values of cellulose acetate (CA) membranes prepared with different solvent systems

Considering the graph, the CA18-DA membrane has the lowest pure water permeance (1.0 ± 0.5 L/hm²bar) and MWCO (14 ± 4 kDa) value indicating a denser selective layer consistent with SEM observations. The membrane without a co-solvent additive, i.e., CA18-D, showed higher PWP and higher MWCO than the membrane containing acetone as the co-solvent. Thus, the performance and morphology are considered together; the CA18-D membrane has a looser selective layer than the CA18-DA, which likely resulted from a slower phase inversion rate in the CA18-D system.

Adding acetic acid to the solvent system turned the membrane morphology into a loose and porous symmetric from asymmetric as shown in the previous section. The membrane permeance and MWCO value increased when the CA18-DHAc and CA18-DA membranes were compared.

When the performance results of CA18-DHAc and CA18-D membranes are considered, the PWP value increased, but MWCO value remained constant. The higher permeance may be caused by the higher porosity and/or pore-connectivity in the CA18-DHAc membrane structure resulting from the slow phase inversion rate. This is in agreement with the significantly lower cumulative phase inversion rate of this solution, indicating the effect of phase separation rate together with a large amount of pore formation, as shown in the previous chapter.

To conclude, the phase inversion kinetics is the dominant factor that significantly alters the morphology and performance of the membranes in this study, and it is affected by the viscosity of solvent systems. Slow phase inversion caused by higher solvent viscosity resulted in a looser and symmetric membrane structure in the CA18-DHAc system. The lower viscosity of the solvent system led to the asymmetric membrane with a dense selective layer of CA18-DA, resulting from a faster phase inversion rate. The performances of membranes are coherent with their structures.

3.4 Effect of Acetone Evaporation at Different Times on the Phase Inversion Rate and Properties of Membranes

An evaporation step was applied to the CA18-DA flat sheet membrane with different durations (1, 2, 5, and 30 minutes) before immersion in the coagulation bath. The effects of increasing evaporation times on phase inversion kinetics after evaporation and final membrane performance were investigated. At the same time, to examine the effect of relative humidity during the evaporation step, evaporation was applied to the CA18-DA membrane in a relatively high humidity environment

(79% relative humidity obtained with water vapor) for 5 minutes. Phase inversion kinetics for these membrane systems were studied with instantaneous phase inversion rate by optical microscope and cumulative phase inversion rate by light transmission. The effect of evaporation times on the performance of the membrane was investigated by pure water permeance and MWCO experiments.

3.4.1 Effect of Evaporation Time on Instantaneous Phase Inversion Rate

After the evaporation step was applied for the specified times in the evaporation chamber to the cast polymer solution, the instantaneous phase inversion rates were measured under the optical microscope. The x^2 versus time graph is shown in Figure 3.8 (a). The effective diffusivity of water into the polymer solution obtained from the slope of the previous graph is given in Figure 3.8 (b). Although the change in phase inversion front rate is not clearly visible from the first graph, the effective water diffusivity obtained from its slope can be used for comparison. When the results were compared only for the membranes with different evaporation times at the same relative humidity and for the membrane made with no evaporation step, it was observed that the effective water diffusivity estimated by the slope of x^2 versus time graph (phase inversion front rate) slightly increased as the evaporation time increased until 5 minutes, while after 30 minutes evaporation, the rate was lower than at 5 minutes. As acetone was moved away from the polymer solution during the evaporation, the DMSO concentration in the solvent system of DA gets higher. When DMSO was the solvent for cellulose acetate, the phase inversion front rate was lower than the rate in the polymer solution in which DA was used as the solvent system (Figure 3.4.). Thus, a reduction in the phase inversion rate could be expected when the evaporation time increases. Small increases in phase inversion rates observed with increased evaporation durations may be because the polymer solution adsorbed a small amount of moisture during the evaporation process, even though the relative humidity was not high in the evaporation chamber. The water vapor absorption of the polymer solution may result in a faster phase inversion rate since

the composition of the polymer solution gets closer to the cloud point^{54,62}. After 1-minute of evaporation, there was no significant differences in diffusivity of water. The highest water diffusivity rate was observed in the membrane that was evaporated for 5 minutes; with a longer evaporation time (30 minutes), the rate of water diffusivity was relatively reduced. This may be the effect of a much higher cellulose acetate concentration at the onset of phase separation, which may have affected the phase inversion rate through the increased viscosity of the medium.

While in section 3.2.1., phase inversion rates corresponded well to diffusivities of water in the solvents, as the solution gets more concentrated, the increase in solution viscosity may also become a determining factor in diffusion of the nonsolvent.

The cast polymer solution that was applied 5-minutes evaporation in the evaporation bath having high relative humidity (79%) were compared with the polymer solution that was 5-minutes evaporation step was employed, it was seen that the former membrane had a higher phase inversion front rate and water diffusivity. This result may be attributed to the same reason: the polymer solution absorbed water vapor because of the high relative humidity while it loses acetone, and composition of polymer solution approach its cloud point. Reduced thermodynamic stability of the system caused fast phase separation of the membrane due to the lower amount of non-solvent requirement for phase separation⁵⁴.

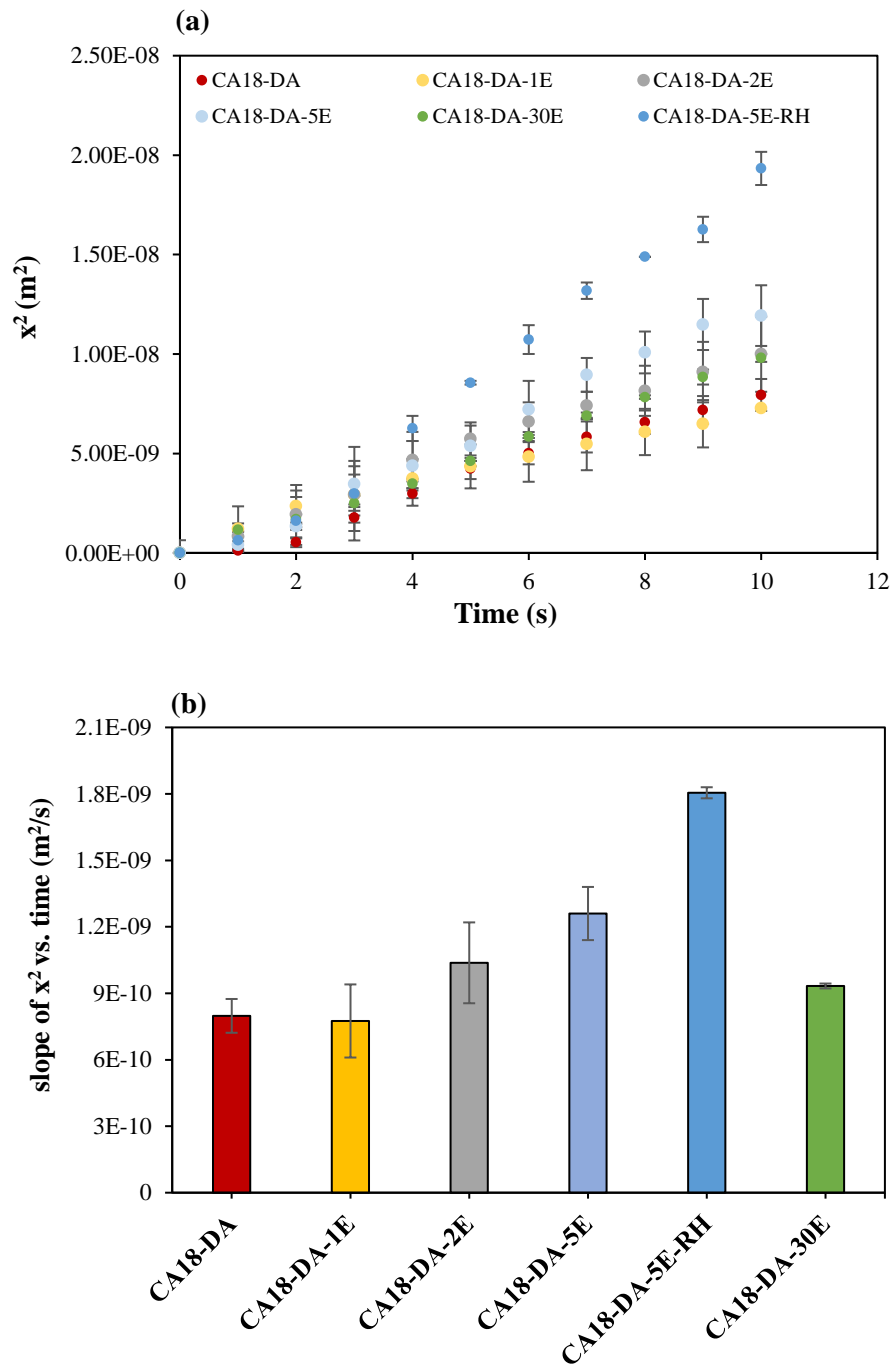


Figure 3. 8. Effect of evaporation time on the water diffusivity observed by instantaneous phase inversion by optic microscope (a); front thickness vs time, (b); diffusivity of water from the slope of graph (a)

3.4.2 Effect of Evaporation Time on the Cumulative Phase Inversion Rate

Figure 3.9 (a) and Figure 3.9 (b) present respectively the light transmission graph and cumulative phase inversion rate of the polymer solutions that were applied evaporation step with different durations. It was observed that the cumulative phase inversion rate decreased as a result of evaporation on the contrary to instantaneous phase inversion rate trends. As explained earlier, the cumulative phase inversion rate obtained with light transmittance gives more reliable information about the final membrane morphology (porosity and pore size). From this point of view, this can be attributed to decreasing porosity and/or pore size until 2 minutes. The cumulative phase inversion rate of the membrane which was applied evaporation for 5 minutes in an environment with high relative humidity, is almost the same as other membranes. The predictions about membrane morphologies are consistent with SEM images (Figure 3.10) of the membranes shown in the next section.

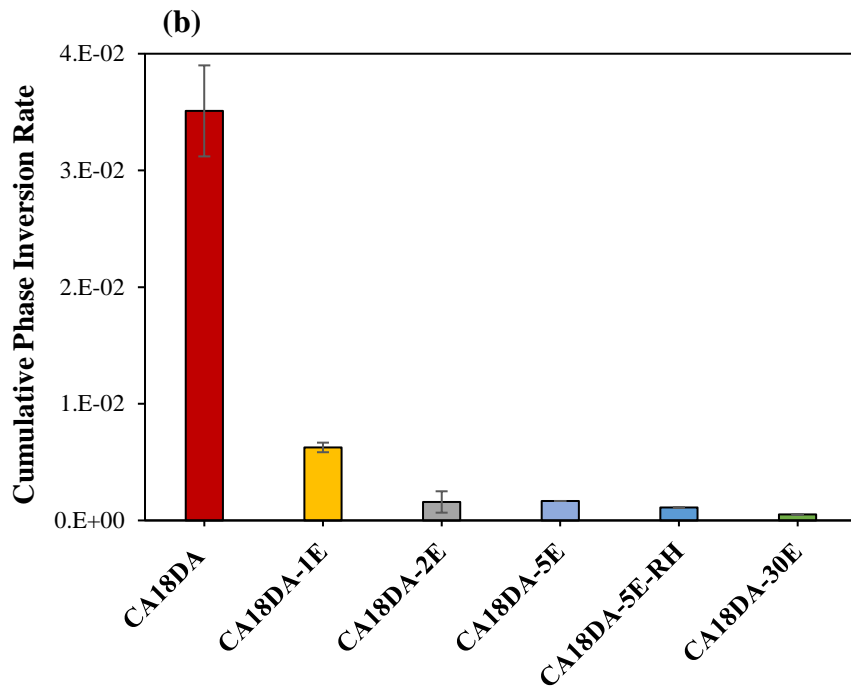
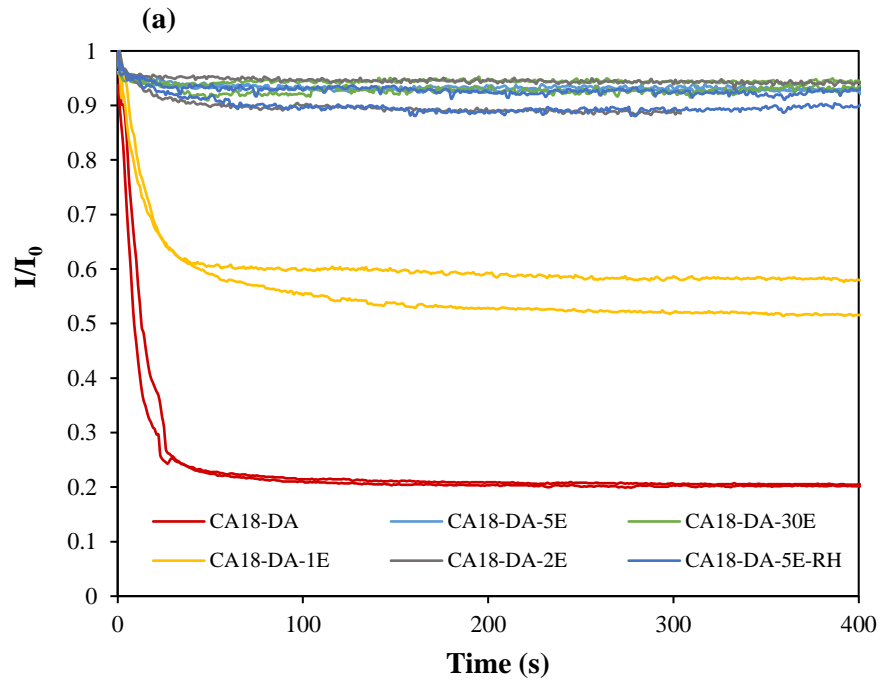


Figure 3. 9. Effect of evaporation time on the cumulative phase inversion rates (a); light transmission graph, (b); cumulative phase inversion rates from the initial slope of graph (a)

3.4.3 Effect of Evaporation Time on Membrane Properties

As the evaporation time increased, the macrovoids in the CA18-DA membrane structure disappeared, and the pore size and porosity decreased throughout the entire structure, as inferred from the light transmission measurement result. Symmetric and quite dense membrane structure was observed in the membranes exposed to evaporation times of 5 minutes and 30 minutes. As a result, the membrane structure changed from asymmetrical to symmetrical structure as the evaporation time increased. When the performance of membranes fabricated without an evaporation step and with applying an evaporation step were compared, it was observed that permeance and MWCO values decreased when the applied evaporation time increased, except for the membrane with 1 minute evaporation time. As acetone moves away from the cast solution during the evaporation period, the concentration of cellulose acetate in the surface layer of the polymer solution increases, and the membrane enters the water bath for phase separation with a higher polymer concentration⁶³. High polymer concentration leads to a higher volume of polymer-rich phase and a lower volume of polymer-lean phase during phase separation: the result is a denser membrane with a lower porosity and pore size leading to lower permeance and MWCO value^{25,61}. The performance of the membranes supports the dense and symmetrical structure seen in the morphology because of increased evaporation time. The membrane produced with a 1-minute evaporation step on the other hand, has higher permeance and MWCO value than the membrane fabricated with no evaporation step. Although porosity appears to be reduced in the SEM image, it appears that the selective layer becomes looser after 1 minute of evaporation according to the performance result. The fact that a looser structure is obtained despite the application of evaporation can perhaps be explained by the changing composition of the polymer solution due to evaporation duration. The final solution composition of the CA-DA flat sheet membrane at the end of the applied evaporation period before being immersed in the water bath was approximately found by mass measurement, as presented in Figure 3.12 and Table 3.5

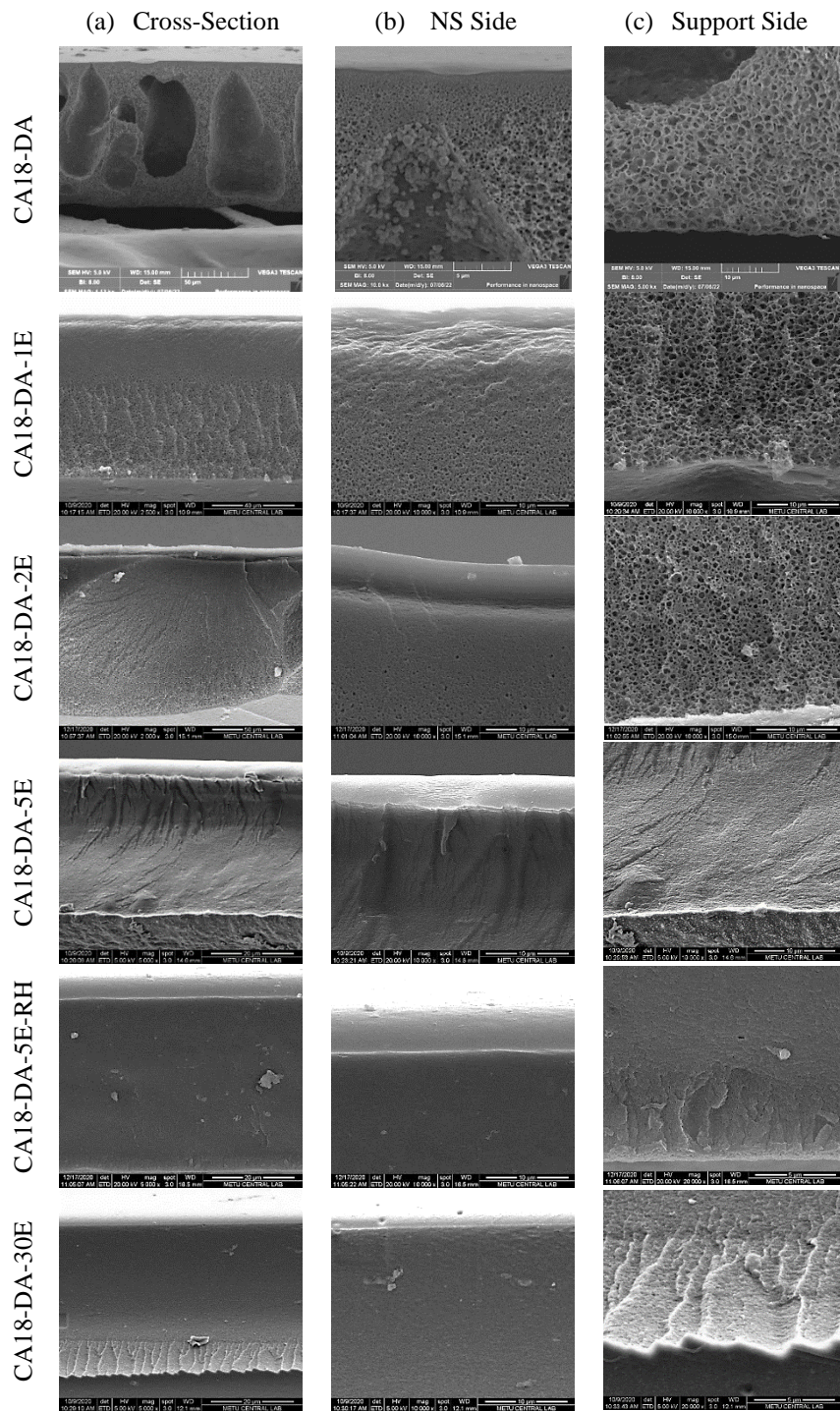


Figure 3. 10. Morphology of CA18-DA membrane exposure to different evaporation times

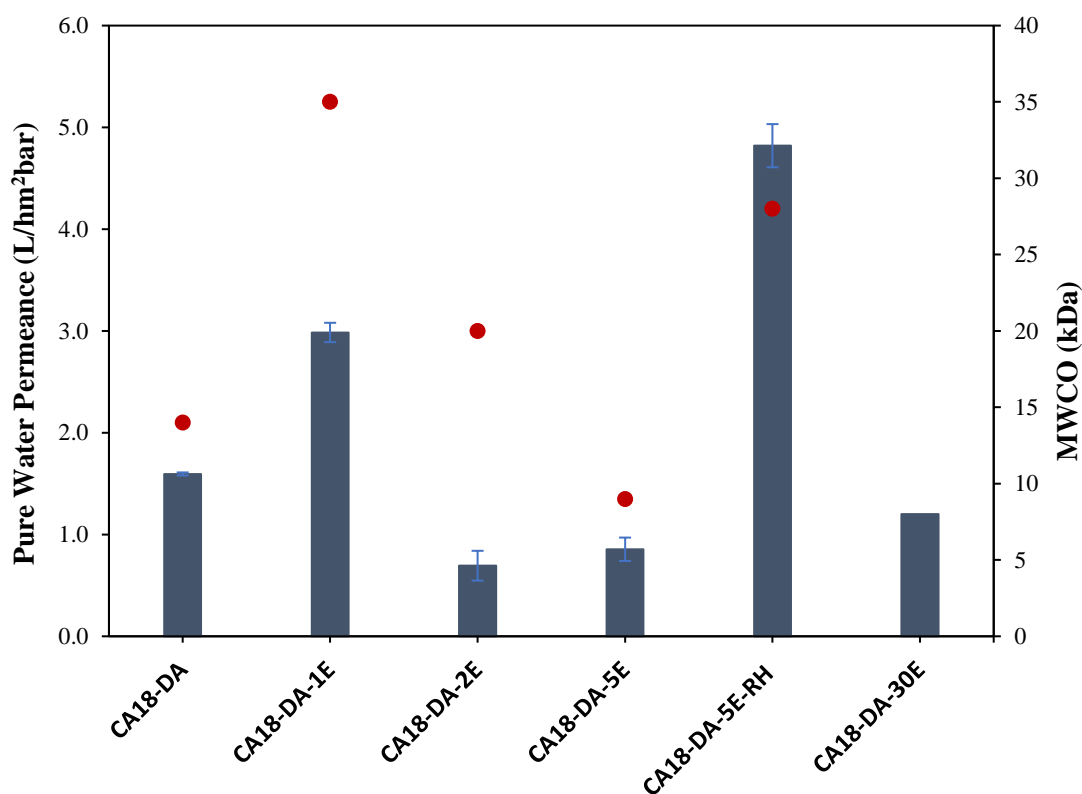


Figure 3. 11. Membrane performances after certain evaporation times

For the control experiment, the CA18-D polymer solution not including a volatile compound was also exposed to nitrogen flow. As expected, no changes were observed in the CA18-D membrane mass over time, except for the change caused by weight sensitivity. The relative humidity in the evaporation bath decreased at the same rate in all experiments.

As seen in Table 3.5, with increasing evaporation time, cellulose acetate concentration increases together with DMSO: acetone ratio of the solvent. Since DMSO alone as solvent gave looser membranes (Section 3.3.2.), the observed performance can be due to the opposing effect of increased CA concentration in the solution and increasing DMSO: acetone ratio.

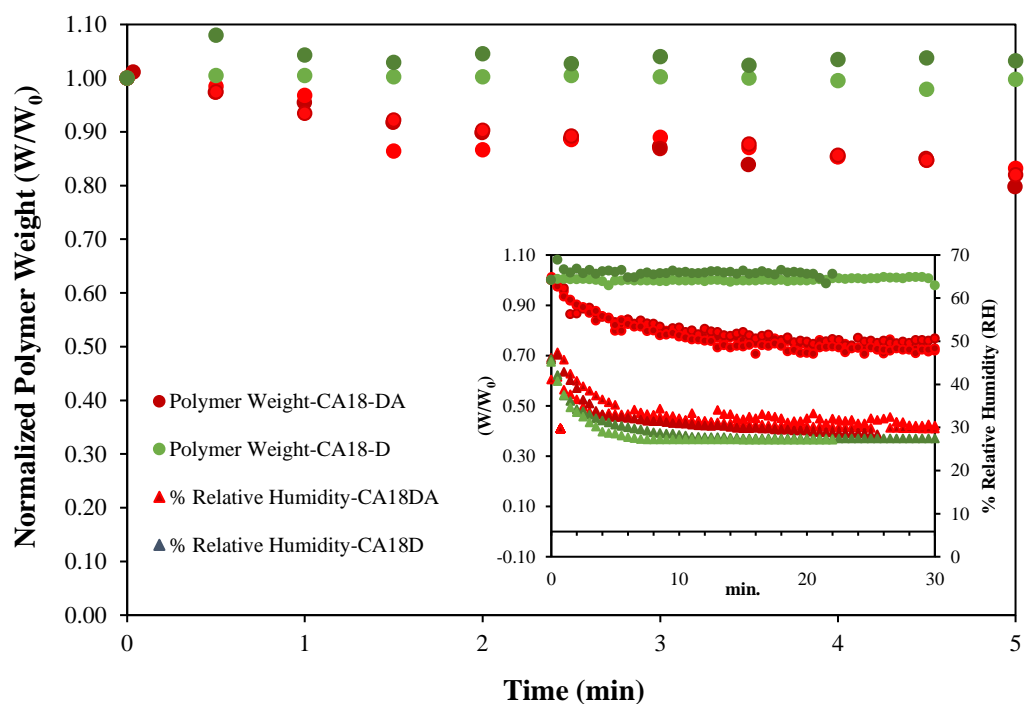


Figure 3. 12. Change of polymer solutions weight and relative humidity in evaporation tank with respect to time during evaporation step

Table 3. 5. Average final composition of polymer solutions after evaporation times

Evaporation time (min)	Average Final Solution Composition after Evaporation (wt. %)			
	CA	DMSO	Acetone	DMSO: Acetone
0	18.0	41	41	1
1	18.9± 0.3	43.1± 1	38.0± 0.9	1.13
2	20.2± 0.4	46.1± 1	33.6± 1	1.37
5	22±0.4	50.3± 1	27.7± 1	1.81
30	24.4± 0.7	55.6± 2	20.0± 2	2.78

When the effect of humidity in the evaporation bath was investigated, the CA18-DA-5E and CA18-DA-5E-RH membranes showed very similar morphologies, as predicted from the cumulative phase inversion rate results: symmetrical and dense. On the other hand, the instantaneous phase inversion rate of CA18-DA-5E-RH was higher. When their performance is compared, this membrane also shows higher permeance and MWCO. Both can be explained with water absorption of the polymer solution before coagulation in water which brought it closer to the cloud point composition. Non-solvent content in the polymer solution generally results in a looser membrane structure^{61,64,65}. The membrane from CA18-DA polymer solution with 95 % coagulation value (which means the water content in the polymer solution is 95% of the value at the cloud point) was fabricated. The permeance of the CA18-DA membrane close to the cloud point increased to 179 L/hm²bar, which is almost hundred times higher than that of CA18-DA.

3.5 Deacetylation of Cellulose Acetate Flat Sheet Membranes by Alkaline Hydrolysis for Cellulose Membrane Fabrication

To produce cellulose membranes, deacetylation of cellulose acetate by alkaline hydrolysis is used. As explained earlier, in this method, acetate groups of cellulose acetate membranes are converted into hydroxyl groups in an alkaline environment and cellulose structure is obtained across the entire membrane. During this process, changes in the performance of the final cellulose membranes can be observed after the alkaline hydrolysis of cellulose acetate^{22,28}. In this study, the effect of alkaline hydrolysis on cellulose acetate membranes tuned with different properties from porous to the dense structure was investigated. To investigate the effect of alkaline hydrolysis, half of a flat sheet membrane was deacetylated by alkaline hydrolysis, while the other half was used without alkaline hydrolysis: all morphology and performance tests were performed with these membrane pairs. Thus, batch-to-batch differences between membranes were eliminated, and only the alkaline hydrolysis effect was investigated.

The morphologies of the obtained CA (membrane parts not applied alkaline hydrolysis) and CA-AH (membrane parts applied alkaline hydrolysis) membranes are shown in Appendix-B. According to the SEM images, there was no significant difference in the morphology of the membranes after alkaline hydrolysis. The resulting cellulose membrane structure seems very similar to the original membrane structure.

The performances of membranes of CA and CA-AH are compared in Figure 3.13. As seen from the graph, both permeance and MWCO values decreased after alkaline hydrolysis of CA18-DHAc membrane. CA18-DHAc membranes fabricated with different thickness also showed the same changes in the performance after alkaline hydrolysis (Appendix-C). When the both CA18-DA and CA25-DA-30CT membranes are considered, permeance values increased whereas MWCO values decreased after the alkali hydrolysis was applied. On the other hand, the alkaline hydrolysis caused to increasing in the both of permeance and MWCO value of the CA25-DA-5E membrane. These results imply that there are morphological changes in the membranes after alkaline hydrolysis. To clarify the different direction of changes in different membrane structures, it is necessary to consider the membrane structure and transport mechanism together. High alkalinity is known to induce several degradation reactions along the cellulose backbone, which may have partly occurred during alkaline hydrolysis of these membranes^{66,67}. Partial degradation of cellulose chains would likely induce rearrangement of the membrane structure immersed in aqueous alkali solution. This can have effects both on the pore size and the membrane matrix. While the pore size is important in pore flow mechanism, the membrane matrix is important in solution-diffusion mechanism.

CA18-DHAc membranes consists of a porous structure and separates based on the pore-flow model: the decrease in performance after alkaline hydrolysis can be explained by the narrowing of the pores in the membrane structure. This results in reduced permeation through the pores and increased rejection to probe molecules (i.e., reduced MWCO).

However, in the CA18-DA and CA25-DA-5E-30CT membranes, which are tighter, the pore flow and solution diffusion models may be simultaneously effective²⁵. In this case, narrowing of pores can decrease the MWCO, considering probe molecules would mostly permeate through the pores. Water, on the other hand, permeates through both the pores and the matrix²⁵. Higher permeance through the loosened membrane matrix may be more dominant in determining the overall permeance than reduced permeance through the pores. CA25-DA-5E membrane is almost completely dense as seen in its SEM images and from the very low PWP. In this membrane, we can consider transport of water and solutes to occur through the membrane matrix, and hence upon partial degradation both PWP and MWCO increase.

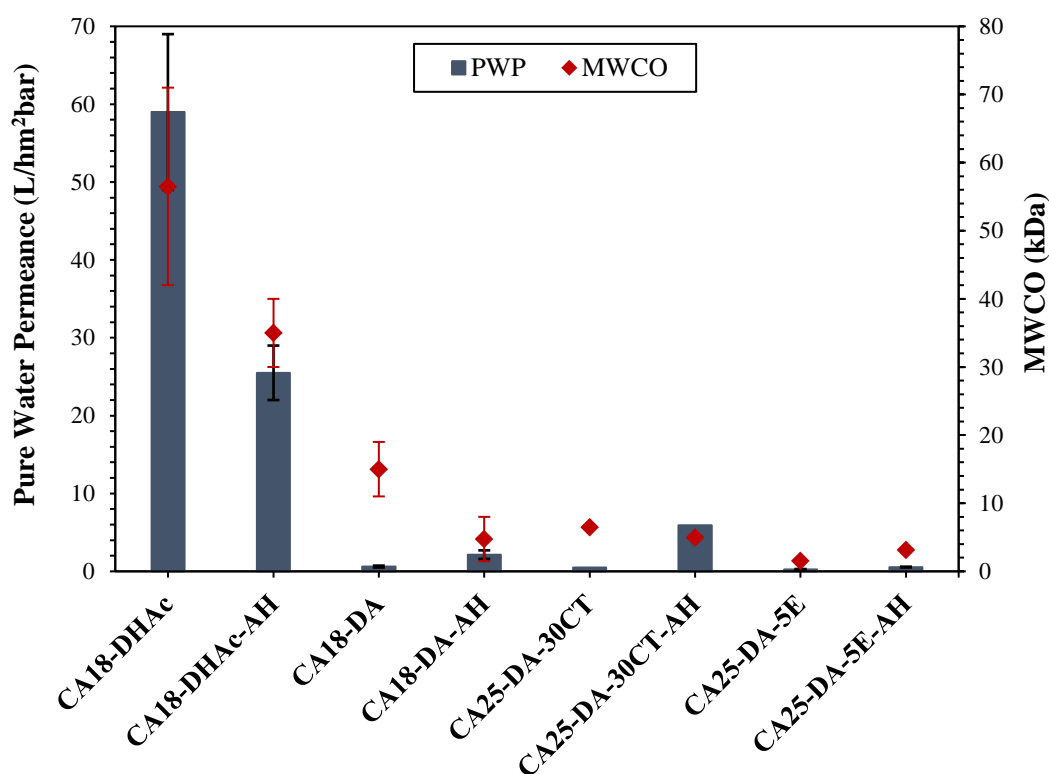


Figure 3. 13. Effect of deacetylation via alkaline hydrolysis on the performances of flat sheet membranes

3.6 Cellulose Acetate Hollow Fiber Membranes

Hollow fiber membranes from CA18-DA and CA18-DHAc solutions were produced using dry-wet spinning system with different spinning conditions. The effect of these two different polymer solution systems on the hollow fiber structure was investigated. The morphologies of obtained hollow fiber membranes were observed by SEM. Pure water permeance and MWCO tests were performed to evaluate the performance of hollow fibers membranes.

3.6.1 CA18-DHAc Polymer Dope Based Hollow Fiber Membranes

One of the advantages of hollow fiber membranes is to be able to change the location of the selective layer of the membrane by using two different coagulants at the outer and inner surfaces of the membrane. In general, using a strong non-solvent, such as water, as an internal or external coagulant leads to a denser skin layer on the non-solvent side due to instantaneous phase inversion. On the other hand, using solvent-nonsolvent mixtures as a coagulant decreases the non-solvent concentration gradient between coagulant and polymer dope and makes the surface more porous due to the slow mass transfer rate (slow phase inversion rate) between coagulant and polymer solution. Due to slow precipitation of the membrane, there is sufficient time for the growth of the pores after the nucleation occurs⁶⁸.

In the case of CA18-DHAc solution, to obtain a selective skin layer on the outer surface (shell side) of the CA18-DHAc hollow fiber membranes, 80%DMSO-20%water solution (80D20W) was used as bore liquid and water as external coagulant at room temperature (approximately 20°C). The more open porous inner substrate decreases the resistance to flow and supplies mechanical strength to hollow fiber membranes during filtration⁶⁹.

During the spinning of CA18-DHAc hollow fiber membranes, different air gap distances (AG) (from 4 to 20 cm) at a certain pulling speed (PS) and two pulling speeds (10.4 and 3.7 m/min.) were employed to observe the effect of spinning

conditions on the properties of hollow fibers. The morphologies of CA18-DHAc hollow fiber membranes are illustrated in Figures 3.14 and 3.15. It was observed that from SEM results, there are no significant effects of the varied air gap distances and applied pulling speeds on the structure of hollow fiber membranes; all membranes have a denser shell side and a porous bore side. The outer side of hollow fibers that are exposed to water as non-solvent showed similar morphology to the flat sheet membranes of CA18-DHAc solution. The high viscosity of the CA18-DHAc solution made the membranes less porous and hindered the macrovoid formation by the slower phase inversion rate. High solvent concentration in the bore liquid led to a slower diffusion rate (precipitation) due to a lower concentration gradient between bore liquid and polymer solution and a fully porous inner surface formed.

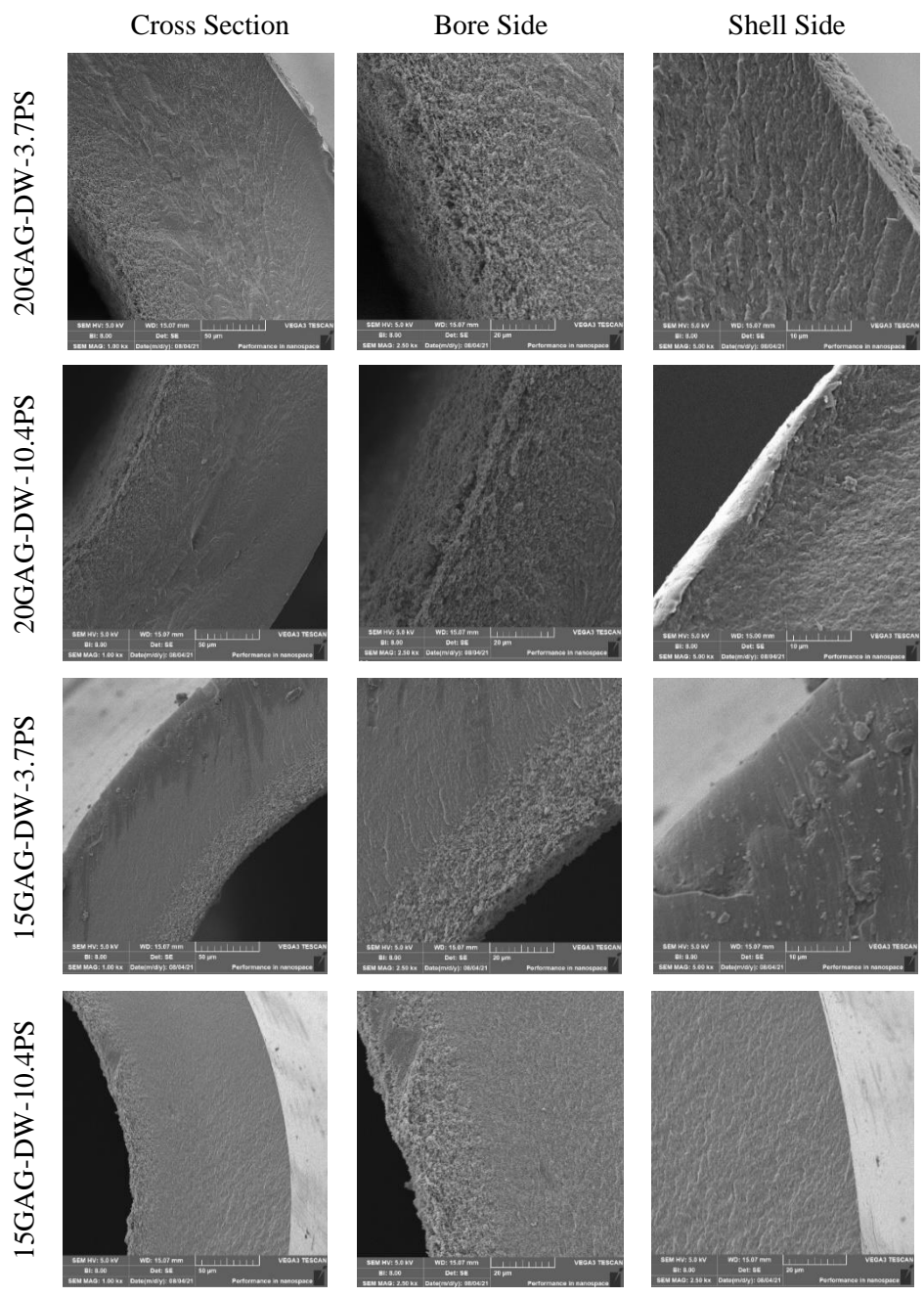


Figure 3. 14. Morphologies of CA18-DHAc based hollow fiber membranes at different spinning conditions (cont'd)

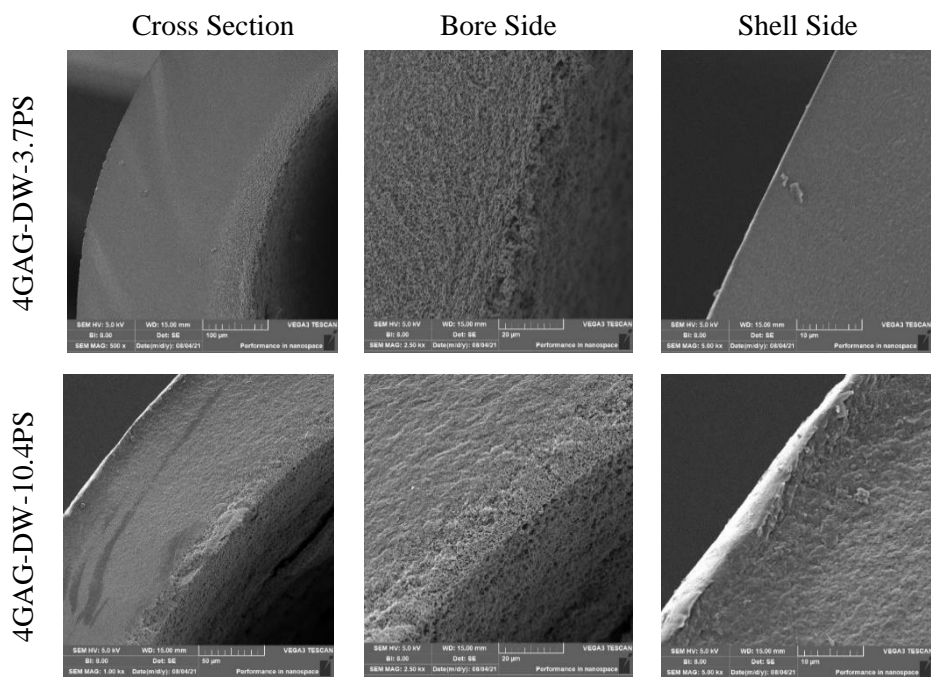


Figure 3. 14. (cont'd)

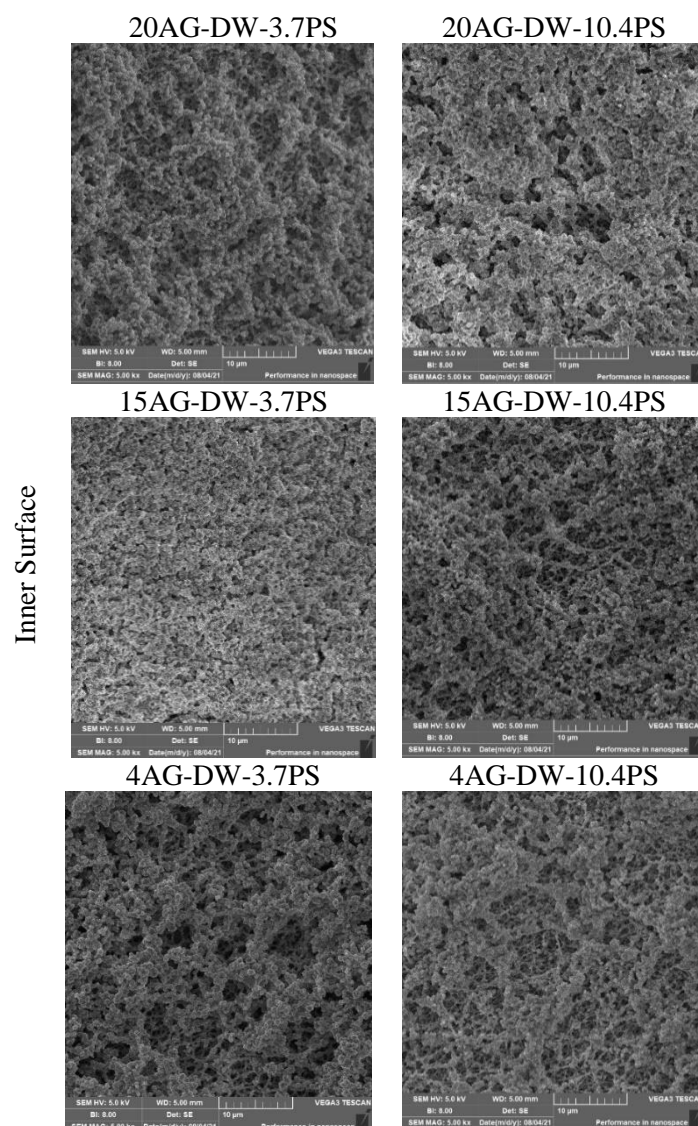


Figure 3. 15. Inner surfaces of CA18-DHAc hollow fiber membranes that produced with bore liquid of 80%DMSO-20% water

The pure water permeances and MWCO values of hollow fiber membranes are listed in Table 3.6. The direction of flow during performance tests is from the outside to the inside of hollow fiber because the skin layer located at the outside surface should be faced the feed filtration for separation. As in the morphologies of the membrane, change in air gap distance or pulling speed at a certain air gap did not make any difference in the performance of hollow fiber membranes.

Table 3. 6. Performances of CA18-DHAc hollow fiber membranes fabricated at different air gaps and pulling speeds with 80%DMSO-20% water (80D20W) as bore liquid and flat sheet membrane of CA18-DHAc

Membrane	Air Gap (cm)	Pulling Speed (m/min.)	Pure Water Permeance (Lh⁻¹m⁻²bar⁻¹)	MWCO (kgmol⁻¹)
20AG-DW-3.7PS	20	3.7	4±3	8 ± 3
20AG-DW-10.4PS	20	10.4	9±4	8 ± 2
15AG-DW-3.7PS	15	3.7	5 ± 1	8 ± 3
15AG-DW-10.4PS	15	10.4	3 ± 2	9 ± 3
4AG-DW-3.7PS	4	3.7	2±1	11 ± 2
4AG-DW-10.4PS	4	10.4	3 ± 2	7 ± 2
CA18-DHAc	-	-	72 ± 20	52 ± 12

The last row of Table 3.6 is the performance result of the flat sheet membrane fabricated with the same polymer solution (CA18-DHAc) and coagulated with the same non-solvent, water. Filtration experiment conditions are identical for hollow fiber and flat sheet membranes. Although the morphologies of flat sheet and hollow membranes coagulating at the same conditions seem similar, hollow fiber configuration resulted in lower PWP and MWCO, which implies the denser selective layer of hollow fiber membranes than that of the flat sheet membrane.

The distinction between the performance and structure of hollow fiber and flat sheet membranes fabricated from the same polymer solution can be associated with different shear rates during the spinning process induced by air gap distance, pulling speed, and flow rate of the polymer solution. The applied shear rate during the spinning of hollow fiber membranes can enhance the molecular orientation of polymer chains and densify the skin layer structure of the nascent hollow fiber membranes⁷⁰.

When a polymer solution is fed through the annular space of the spinneret, shear stress is produced at the outer wall of the spinneret due to the flow rate of the polymer solution. The shear rate at the highest value at the outer wall of the spinneret

may dramatically increase the molecular orientation of polymer chains at the outer skin of the nascent hollow fiber membranes^{71,72}. In the literature, the effect of shear rate within the spinneret produced by the flow rate of polymer solution was investigated for PES, polyimide, and polysulfone gas separation and ultrafiltration hollow fiber membranes produced in wet and dry-wet spinning^{71,73–77}. Similar results were reported that the high flow rates resulted in low membrane permeances and high rejection values of hollow fiber membranes due to the increased orientation induced by the high shear rate applied to the outer skin (shell side) of hollow fibers before it was immersed in an external coagulation bath.

The shear rate within the spinneret (at the outer wall of the spinneret) applied to CA18-DHAc polymer solution during hollow fiber spinning was calculated. Also, the shear rate applied to polymer solution as the casting of flat sheet membranes was calculated approximately (Appendix-I). The flow rate of polymer solution was 12 ml/min when an air gap of 20 cm was used, and 9.8 mL/min at the lower air gap distances to obtain continuous spinning without any fiber break.

For the maximum volumetric flow rate of polymer solution used for spinning (12 ml/min), the shear rate at the spinneret outer wall is 237 s^{-1} whereas the approximate shear rate applied during casting of a flat sheet with a thickness of $250\text{ }\mu\text{m}$ on a glass plate is calculated about 400 s^{-1} . Although the higher shear rate is applied to polymer solution during film casting, a time is available for relaxation of polymer chains between casting and immersion in the coagulation bath. Furthermore, hollow fiber membranes are exposed to measured shear also in air gap distance due to take-up creating additional gravitational and elongational stress on the outer skin during spinning process⁷⁰. The slower precipitation rate of CA18-DHAc solution in water inhibits immediate solidification and freezing of the structure; therefore, the molecular orientation of hollow fiber may be continued partly even in the external coagulation bath by elongation stress. In the study of Hasbullah and coworkers, it was shown that increasing air gap distance induced molecular orientation and made the skin layer structure tighter and thicker with increased selectivity performance⁷⁸.

To reduce the effect of shear rate, a hollow fiber membrane with a lower air gap (2 cm) and lower dope flow rate (LFR=3.8 ml/min) without drawing (freefall-FF) by take-up drum was fabricated. The morphology of 2AG-DW-LFR-FF membrane is in Figure 3.16. The hollow fiber membrane of 2AG-DW-LFR-FF that was produced under a lower shear rate resulted in nearly the same morphology and performance (its PWP value is 4 L/hm²bar and MWCO is 10 kDa) with the higher-shear-induced hollow fiber membranes. The shear rate induced by the flow of the polymer solution at the outer wall of the spinneret reduced to 75 s⁻¹ from 237 s⁻¹ with decreasing in dope flow rate from 12 ml/min to 3.8 ml/min. However, there were no significant differences appeared in membrane properties after changing the shear rate effect. The 2 cm air gap applied in the free-fall of fiber still appears to cause enhanced alignment and close packing of polymer chains at the shell side of the hollow fiber membranes.

2AG-DW-LFR-FF

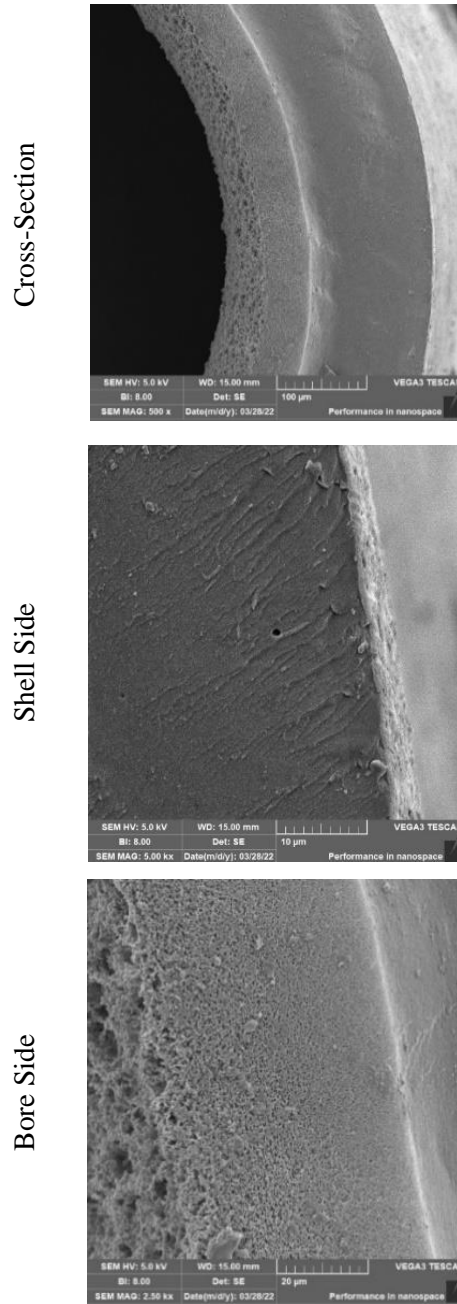


Figure 3. 16. Morphology of CA18-DHAc hollow fiber membrane spun at lower-sheared conditions.

The performance of these hollow fiber membranes of CA18-DHAc all being very similar despite difference in shear rate may be because of the shear-thinning effect on the polymer solution and enhanced molecular orientation of polymer chains affecting simultaneously at the applied shear rate range. In our spinning system, the polymer solution of CA18-DHAc shows a non-Newtonian fluid (shear-thinning) characteristic with a 0.73 power-law index (n) obtained from its rheological measurement (Appendix-I). The increased molecular orientation by increased shear rate in the spinning system may cause formation of denser skin layer until a point; however, after a certain shear, besides molecular orientation effect, reduction in the viscosity of shear-thinning polymer solution occurs with applied shear may causes the formation of a looser skin layer. Thus, these opposite factors may act simultaneously and cancel out each other after a certain shear rate⁷¹. This may explain why an apparent change is not observed in the hollow fiber membrane properties upon altering the shear rate. However, the question of why these hollow fiber membranes are all tighter than the flat sheet counterpart still remains.

The wet-spinning process generally are preferred to reduce the effect of extra shear rate due to air gap^{72,74,79}. In this study, to produce hollow fiber membrane without subjecting it to the molecular orientation formed in the air gap, water in the bore liquid and a hot water in external coagulation bath were used. This production method was preferred over the zero air gap distance and weak coagulant (DW) conditions due to the practical difficulties in the wet spinning system. Vapor-induced phase separation (VIPS) on the shell side before immersion precipitation occurring in the external coagulation bath is one way to prevent skin formation on the outside. When the outer skin of hollow fiber is exposed to water vapor throughout a certain air gap distance before reaching a coagulation bath, the average pore size and porosity on the skin layer increases since the water vapor causes a slower precipitation rate in the outer layer⁷². In the slower precipitation, the time is increased to further progress of formed pores via water vapor, and larger pores form. Hot water in the coagulation bath is used to generate water vapor introducing hollow fiber during the air gap²².

Considering this information, a hot water coagulation bath (HCB) at 50 °C was used as an external coagulant to obtain an open-pored shell side and water was used as bore liquid to obtain selective inner skin layer in the CA18-DHAc hollow fiber membrane. An air gap of 11 cm was used for applying sufficient water exposure time to the shell side. The final membrane morphology of the hollow fiber membrane is presented in Figure 3.17.

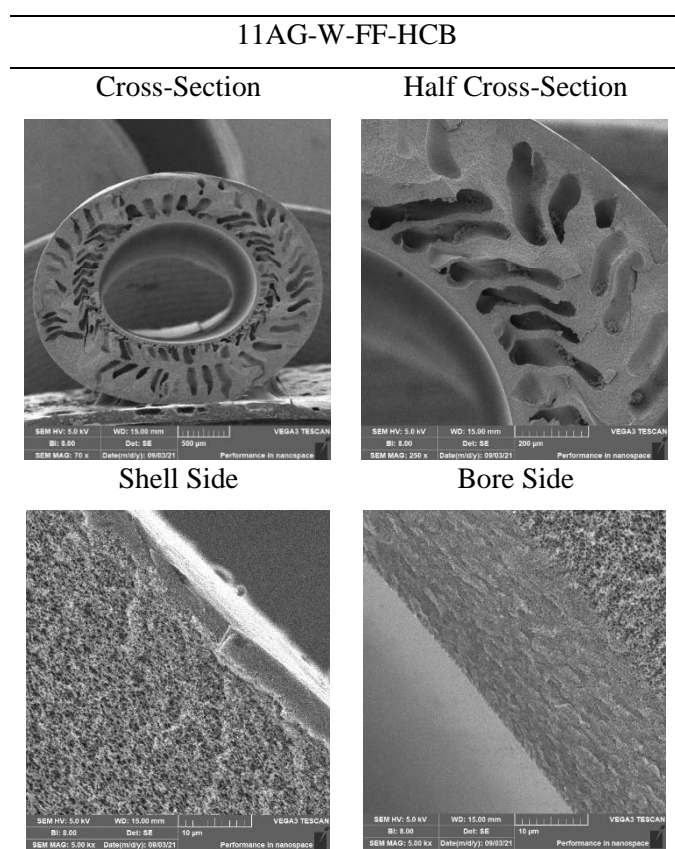


Figure 3. 17. SEM images of CA18-DHAc hollow fiber membrane fabricated with a hot external coagulation bath at 50°C

As seen from SEM images of the shell side and bore side of the membrane, the pore size on the outside is larger than the pore size in the inside of the membrane, as expected. The skin layer was formed on bore side by using water as strong-coagulant while outer surface was exposed to water vapor to produce open-pore structure. The performance of the membrane coagulated in the hot water bath (11AG-W-FF-HCB) was conducted from the inside to the outside of the membrane. It has a pure water performance of 545 L/hm²bar and its MWCO value is 199 kDa. The performance data was also consistent with the morphological feature of the membrane. In addition, a closer performance of CA18-DHAc hollow fiber to the flat sheet membrane from the same solution was observed. A looser selective layer of the hollow fiber than the flat sheet membrane may be explained by the changed demixing rate at the hot coagulation bath. The hot water in the external coagulation bath may decrease the viscosity of the spun CA18-DHAc polymer solution, which does not precipitate immediately after contact with water, and the looser selective layer on the bore side may result from the decreased polymer viscosity since the lower viscosity of polymer solution generally results in loose skin layer^{45,61}. In addition to temperature, the looser hollow fiber membrane may be caused by applied shear rate during spinning as explained before and casting thickness differences between hollow fiber and flat sheet membranes.

The casting thickness can change the final membrane morphology and performance with the same casting solution and coagulant⁵⁴. The hollow fiber membrane was fabricated at higher thickness due to the annular space in the spinneret. To investigate effect of casting thickness on the differences between the flat sheet and hollow fiber membranes of CA18-DHAc solution fabricated with water as coagulant, 30 and 1030 μm of casting thicknesses (CT) besides 250 μm were used to the flat sheet membrane fabrication (Appendix-C). A change in the morphology of the membranes could not be observed by the changing casting thickness: all CA18-DHAc membranes have still symmetric and porous structure. However, the PWP and MWCO values of membranes decreased as the casting thickness increased. Using Ferry-Rankin equation¹, the rejection of dextran molecules and hydrodynamic radius

correlation for dextran molecules as a function of molecular weight¹², the average pore size in the selective layer of these membranes were estimated as 8.3 nm, 6.8 nm, and 6.3 nm for increased casting thickness, respectively. Then using this average pore size, the pure water permeance, porosity of 0.05, pore tortuosity of 2.5¹, and the Hagen-Poiseuille equation arranged for porous membranes, the effective skin layer thicknesses were estimated as 0.6 μm , 0.7 μm , and 1.3 μm for increasing casting thickness, respectively (Appendix-D). Increasing casting thickness also decreased MWCO, implying smaller pores, especially from 30 μm to 250 μm casting thickness. However, this is contrary to the difference between flat sheet membrane and 11AG-W-FF-HCB hollow fiber membrane with larger initial wall thickness during spinning, implying that the polymer solution thickness alone also does not explain difference^{33,81}.

In addition, different bore liquids having different coagulant strengths were used at lower shear rate conditions to understand whether the bore liquid strength is a factor in the differences between hollow fiber and flat sheet membrane where the polymer solution faces the nonsolvent on one side, similar to the shell side of the hollow fiber, and an impermeable glass plate on the other side (Appendix-E). The strength of bore liquid was decreased by decreasing water content from 100 wt.% to 20 wt.% to slow down the phase inversion rate. The MWCO test could not be conducted with the membrane fabricated by pure water as bore liquid due to lower PWP, likely due to a double skinned morphology with skin layers on both inner and outer sides. As bore liquid strength decreased, the surface on the bore side became porous, and the permeance and MWCO values of membranes increased due to more porous substrate. Using ethylene glycol in the bore liquid with the water in the ratio of 1:1 was done since ethylene glycol has higher viscosity which can slow down solvent out-diffusion to simulate the effect of the impermeable glass substrate used in the fabrication of the flat sheet membrane. However, the morphology did not change, and the permeance of the membrane was lowered, which is probably because of the high non-solvent quality of the ethylene glycol and water mixture for CA (RED=3.2).

Consequently, CA18-DHAc hollow fiber membranes produced with different bore liquids also showed similar morphology with flat sheet configuration but lower permeances and MWCO values due to the bore liquid coagulant being different from the of glass substrate.

3.6.2 CA18-DA Polymer Dope Based Hollow Fiber Membranes

A hollow fiber membrane was fabricated from CA18-DA solution with the 6 cm of air gap distance and 15 m/min pulling speed. The mixture of 80%DMSO-20%water (DW) was preferred as bore liquid to obtain porous structure on the bore side of the fiber, whereas water at ambient temperature was used in the external coagulation bath for the selective skin layer on the outer. When the morphology of the membrane was considered in Figure 3.18, the structure of the hollow fiber membrane consisted of an outer skin layer on a porous substrate. Additionally, finger-like macrovoid pores were formed just below the selective layer. When comparing hollow fiber and flat sheet membranes produced from the same solution, it is seen that their morphologies are very similar. The flat sheet membrane of the CA18-DA solution has macro voids under the selective layer and porous substrate. Performance comparison of hollow fiber and flat sheet membranes is presented in Table 3.7. Hollow fiber membrane shows similar separation performance (MWCO) to flat sheet membrane; however, it has much higher permeance than the flat sheet membrane. In the SEM images (Figures 3.18 and 3.6), the skin layer of the hollow fiber membrane seems relatively thinner than that of the flat sheet membrane. This is probably why the hollow fiber membrane has higher pure water permeance.

Table 3. 7. Comparison of flat sheet and hollow fiber membranes from CA18-DA polymer solution

Membrane	Pure Water Permeance (Lh ⁻¹ m ² bar ⁻¹)	MWCO (kgmol ⁻¹)
6AG-DW-15PS	167	18
CA18-DA	1 ±0.5	14±4

6AG-DW-15PS

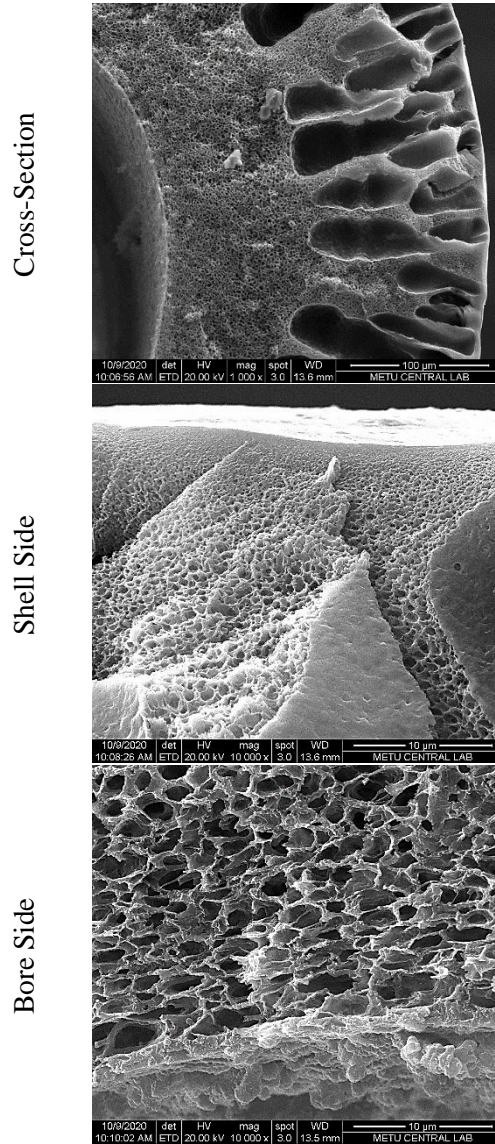


Figure 3. 18. Morphology of CA18-DA hollow fiber membrane

In general, there are differences in the properties of flat sheet and hollow fiber membranes. The continuous shear rate affecting the selective layer of hollow fiber during the spinning, different initial casting thicknesses, and bore side coagulants used in the hollow fiber membrane fabrication are important parameters creating differences between these two configurations. Since the effects of these are simultaneous, it is not straightforward to transform relationships on membrane formation obtained from flat sheet structures to hollow fibers.

CHAPTER 4

CONCLUSIONS

In this study, cellulose acetate membranes were fabricated by three solvent systems to understand the effect of solvent on the membrane morphology and performance. 18 wt. % cellulose acetate was dissolved in the solvent systems of dimethyl sulfoxide (DMSO), the mixture of DMSO: acetone (DA) and DMSO: acetic acid (DHAc) in the ratio of 1:1. The non-solvent induced phase separation was used for membrane fabrication with water as non-solvent. The membrane properties were associated with the thermodynamics and kinetics of phase inversion process since these parameters are affected to how the phase inversion process proceeds.

Thermodynamics of phase separation systems were investigated by both theoretical and experimental methods. Relative energy density (RED) values calculated via Hansen solubility parameters for interactions of polymer/solvent systems implied that all three solvent systems show high affinity and good solvent quality for cellulose acetate, although acetone and acetic acid alone are poor solvents. According to polymer chain entanglement concentration measurements, the solvent qualities can be listed as follows from high to low: DMSO-acetone (DA), DMSO (D), DMSO-acetic acid (DHAc). The excess Gibbs free energy (\underline{G}^{ex}) was calculated to understand the interactions between used solvent systems and water (non-solvent). DHAc-water system showed the highest solvent-nonsolvent (S-NS) affinity possibly due to higher hydrogen bonding capacity of acetic acid, and DMSO-water system have second highest affinity assessed by the magnitude of the negative \underline{G}^{ex} values. DA-water system exhibits almost ideal behavior. Results of cloud point measurements were consistent with the results of solvent-polymer and solvent-nonsolvent interactions: the least stable cellulose acetate solution is CA18-DHAc, whereas CA18-DA is the most stable system against phase inversion.

The phase inversion front rates and diffusivity of water into the solvent systems estimated by the Wilke-Chang equation were considered, the viscosity of solvent systems affects the phase inversion rates and final membrane morphology. The lower viscosity of the solvent system of DA led to faster phase inversion rate: an asymmetric membrane with a dense selective layer was obtained. Adding acetic acid to the solvent system turned the membrane morphology into a loose and porous symmetric because of the higher solvent viscosity of DHAc causing slow phase inversion. When all thermodynamic and kinetic findings were evaluated together, the phase inversion kinetics was seen as dominant factor for determining the final membrane properties. The performances of membranes are consistent with their structures: CA18-DA showed lower pure water permeance of 1 L/hm²bar and MWCO of 14 kDa. Higher pure water permeance of 72 L/hm²bar and MWCO of 52 kDa were obtained by CA18-DHAc membrane. The different pure water permeances of CA18-D and CA18-DHAc membranes despite their similar MWCO values can be explained by the higher porosity of CA18-DHAc membrane which was observed also in cumulative phase inversion rate.

The changes in the membrane properties of CA18-DA with evaporation step at different durations (1, 2, 5, and 30 minutes) were investigated in detail by phase inversion kinetics and performance tests. MWCO and permeance of membrane increased after 1-minute evaporation. As the evaporation duration was further increased, the porosity and pore size of membranes decreased, leading to lowered pure water permeance and MWCO. These performances of membranes can be explained by the opposing effects of increasing CA concentration with increasing DMSO: acetone ratio in increased evaporation times. A looser membrane structure was observed after the evaporation step in a humid medium, probably due to the water absorption of polymer solution and becoming closer to the cloud point composition.

After cellulose acetate membranes were obtained with different pore size, the effect of deacetylation via alkaline hydrolysis on the performance and morphology of membranes was investigated. No change in the morphologies of membranes after alkaline hydrolysis was observed according to SEM images. However, the changed performance of membranes after alkaline hydrolysis implied changes in the membrane structure (pores and matrix), which are probably induced by the partial degradation of cellulose chains in the alkaline medium. Narrowing pore size after alkaline hydrolysis can be effective in increasing rejection and decreasing permeance of the porous membranes since the pore-flow mechanism is effective in separation through the membrane. Increasing permeance and MWCO after alkaline hydrolysis in almost completely dense membranes can be attributed to the loosed membrane matrix since it can be considered that the separation occurs through the membrane matrix. In the membranes that both mechanisms employ together, the narrowing pore size resulted in a decrease in MWCO, while the loosened matrix is effective in increased permeance. These observations give a detailed examination for alkaline hydrolysis of cellulose acetate membranes having different properties.

Using the same polymer solutions (CA18-DA and CA18-DHAc), hollow fiber membranes were produced by dry-wet spinning method. The air gap distance, pulling speed and coagulation bath temperature were changed during spinning of CA18-DHAc. Although the morphologies of flat sheet and hollow membranes coagulating at the same conditions seem similar, hollow fibers resulted in lower PWP and MWCO values, which implies the denser selective layer possibly due to the applied shear rate during the spinning. All hollow fiber membranes of CA18-DHAc have similar morphologies and performance produced by varied spinning conditions. A closer performance of hollow fiber to the flat sheet membrane from CA18-DHAc solution was observed when hot external coagulation bath was used during spinning to reduce the shear rate effect on the selective layer. The hollow fiber membrane obtained with the CA18-DA solution showed similar morphology and MWCO but higher pure water permeance attributed to the thinner selective layer of hollow fiber membrane.

REFERENCES

1. Baker RW, Richard W. *Membrane Technology and Applications*. 3rd ed. John Wiley & Sons; 2012.
2. Liang B, He X, Hou J, Li L, Tang Z. Membrane separation in organic liquid: Technologies, achievements, and opportunities. *Advanced Materials*. 2019; 31(45):1-14.
3. Cheryan M. *Ultrafiltration and Microfiltration: Handbook*. 2nd ed. CRC Press; 1998.
4. Czekaj P, López F, Güell C. Membrane fouling during microfiltration of fermented beverages. *Journal of Membrane Science*. 2000; 166(2):199-212
5. Charcosset C. Classical and recent applications of membrane processes in the food industry. *Food Engineering Reviews*. 2021; 13:322-343.
6. Girard B, Fukumoto LR. Critical reviews in food science nutrition membrane processing of fruit juices and beverages: A review. *Critical Reviews in Food Science Nutrition*. 2000; 40(2):91-157.
7. Hakami MW, Alkhudhiri A, Al-Batty S, Zacharof MP, Maddy J, Hilal N. Ceramic microfiltration membranes in wastewater treatment: Filtration behavior, fouling and prevention. *Membranes*. 2020; 10(248).
8. Liu S, Zeng J, Tao D, et al. Microfiltration performance of regenerated cellulose membrane prepared at low temperature for wastewater treatment. *Cellulose*. 2010; 17:1159-1169.
9. Bruggen BVD, Vandecasteele C, Gestel TV, Doyen W, Leysen R. A review of pressure-driven membrane processes in wastewater treatment and drinking water production. *Environmental Progress*. 2004; 22(1):46-56.

10. McKinnon BT, Avis KE. Membrane filtration of pharmaceutical solutions. *American Journal of Hospital Pharmacy*. 1993; 50(9):1921-1936.
11. Lee SJ, Kim JH. Differential natural organic matter fouling of ceramic versus polymeric ultrafiltration membranes. *Water Research*. 2014;48(1): 43-51.
12. Zeman LJ, Zydney A.L. *Microfiltration and Ultrafiltration: Principles and applications*. CRC Press; 1996.
13. Loeb S, Sourirajan S. Sea water demineralization by means of an osmotic membrane. *Advanced in Chemistry; American Chemical Society*. 1963; 117-132.
14. Durmaz EN. Investigation of phase inversion behavior of cellulose-ionic liquid solutions in relationship with membrane formation. *Master Thesis*. The Graduate School of Natural and Applied Sciences of Middle East Technical University. Ankara; 2017.
15. Çulfaz PZ. Microstructured hollow fibers and microsieves: Fabrication, characterization, and filtration applications. *PhD Thesis*. University of Twente; 2010.
16. Sukma FM, Çulfaz-Emecen PZ. Cellulose membranes for organic solvent nanofiltration. *Journal of Membrane Science*. 2018; 545:329-336.
17. Baghaei B, Skrifvars M. All-cellulose composites: A review of recent studies on structure, properties and applications. *Molecules*. 2020;25(12).
18. Liu H, Hsieh YL. Ultrafine fibrous cellulose membranes from electrospinning of cellulose acetate. *Journal of Polymer Science: Part B: Polymer Physics*. 2002; 40(18):2119-2129.
19. Vallejos ME, Peresin MS, Rojas OJ. All-cellulose composite fibers obtained by electrospinning dispersions of cellulose acetate and cellulose nanocrystals. *Journal of Polymers and the Environment*. 2012; 20(4):1075-1083.

20. Swatloski RP, Spear SK, Holbrey JD, Rogers RD. Dissolution of cellulose with ionic liquids. *Journal of the American Chemical Society*. 2002; 124(18):4974-4975.
21. Durmaz EN, Çulfaz-Emecen PZ. Cellulose-based membranes via phase inversion using [EMIM]OAc-DMSO mixtures as solvent. *Chemical Engineering Science*. 2018; 178:93-103.
22. İmir Z. Cellulose membranes via alkaline hydrolysis of cellulose acetate membranes and their application in organic solvents. *Master Thesis*. The Graduate School of Natural and Applied Sciences of Middle East Technical University. Ankara; 2019.
23. Falca G, Musteata VE, Behzad AR, Chisca S, Nunes SP. Cellulose hollow fibers for organic resistant nanofiltration. *Journal of Membrane Science*. 2019; 586:151-161.
24. Puspasari T, Pradeep N, Peinemann KV. Crosslinked cellulose thin film composite nanofiltration membranes with zero salt rejection. *Journal of Membrane Science*. 2015; 491:132-137.
25. Savaş-Alkan A, Çulfaz-Emecen PZ. Solvent recovery from photolithography wastes using cellulose ultrafiltration membranes. *Journal of Membrane Science*. 2022; 647.
26. Son WK, Youk JH, Lee TS, Park WH. Electrospinning of ultrafine cellulose acetate fibers: Studies of a new solvent system and deacetylation of ultrafine cellulose acetate fibers. *Journal of Polymer Science: Part B: Polymer Physics*. 2004; 42(1):5-11.
27. Tulos N, Harbottle D, Hebden A, Goswami P, Blackburn RS. Kinetic analysis of cellulose acetate/cellulose II hybrid fiber formation by alkaline hydrolysis. *ACS Omega*. 2019; 4(3):4936-4942.

28. Thi HYN, Kim S, Nguyen BTD, et al. Closing the sustainable life cycle loop of membrane technology via a cellulose biomass platform. *ACS Sustainable Chemistry & Engineering*. 2022; 10(7):2532-2544.
29. Rasool MA, Vankelecom IFJ. Preparation of full-bio-based nanofiltration membranes. *Journal of Membrane Science*. 2021; 618.
30. Vatanpour V, Pasaoglu ME, Barzegar H, et al. Cellulose acetate in fabrication of polymeric membranes: A review. *Chemosphere*. 2022; 295.
31. Pinnau I, Freeman BD. Formation and modification of polymeric membranes: Overview. *ACS Symposium Series; American Chemical Society*. 1999.
32. Lalia BS, Kochkodan V, Hashaikeh R, Hilal N. A review on membrane fabrication: Structure, properties, and performance relationship. *Desalination*. 2013; 326:77-95.
33. Xing DY, Peng N, Chung TS. Formation of cellulose acetate membranes via phase inversion using ionic liquid, [BMIM]SCN, as the solvent. *Industrial & Engineering Chemistry Research*. 2010; 49(18):8761-8769.
34. Mousavi SM, Zadhoush A. Investigation of the relation between viscoelastic properties of polysulfone solutions, phase inversion process and membrane morphology: The effect of solvent power. *Journal of Membrane Science*. 2017; 532:47-57.
35. Li Z, Ren J, Fane AG, Li DF, Wong FS. Influence of solvent on the structure and performance of cellulose acetate membranes. *Journal of Membrane Science*. 2006; 279(1-2):601-607.
36. Rasool MA, Vankelecom IFJ. Preparation of full-bio-based nanofiltration membranes. *Journal of Membrane Science*. 2021; 618.
37. Baldoni-Andrey P, Commarieu A, Plisson-Saune S. Treatment of Wastewater Containing Dimethyl Sulfoxide (DMSO). Lichtfouse E, Schwarzbauer J, Robert D. (eds). *Environmental Chemistry*. Springer, Berlin; 2005

38. Nu DTT, Hung NP, Hoang VC, Bruggen VDB. Preparation of an asymmetric membrane from sugarcane bagasse using DMSO as green solvent. *Applied Sciences (Switzerland)*. 2019; 9(16).
39. Soroko I, Bhole Y, Livingston AG. Environmentally friendly route for the preparation of solvent resistant polyimide nanofiltration membranes. *Green Chemistry*. 2011; 13(1):162-168.
40. Mohammadi T, Saljoughi E. Effect of production conditions on morphology and permeability of asymmetric cellulose acetate membranes. *Desalination*. 2009; 243:1-7.
41. Loeb S, Sourirajan S. Sea water demineralization by means of an osmotic membrane. *Advanced in Chemistry; American Chemical Society*. 1963; 117-132.
42. Ohya H, Konuma H, Negishi Y. Posttreatment effects on pore size distribution of Loeb-Sourirajan-type modified cellulose acetate ultrathin membranes. *Journal of Applied Polymer Science*. 1977;21.
43. Kunst B, Sourirajan S. An approach to the development of cellulose acetate ultrafiltration membranes. *Journal of Applied Polymer Science*. 1974; 18:3423-3434
44. Kusworo TD, Budiyo, Ikhsan D, Rokhati N, Prasetyaningrum A, Mutiara FR, Sofiana NR. Effect of combination dope composition and evaporation time on the separation performance of cellulose acetate membrane for demak brackish water treatment. *MATEC Web of Conferences*. 2017: 101; 6.
45. Kim DL, Le NL, Nunes SP. The effects of a co-solvent on fabrication of cellulose acetate membranes from solutions in 1-ethyl-3-methylimidazolium acetate. *Journal of Membrane Science*. 2016; 520:540-549.

46. Rasool MA, Goethem CV, Vankelecom IFJ. Green preparation process using methyl lactate for cellulose-acetate-based nanofiltration membranes. *Separation and Purification Technology*. 2020; 232.
47. Platt S, Mauramo M, Butylina S, Nyström M. Retention of pegs in cross-flow ultrafiltration through membranes. *Desalination*. 2002; 149 (1-3):417-422.
48. Strathmann H, Kock K, Amar P, Baker RW. The formation mechanism of asymmetric membranes. *Desalination*. 1975; 16(2):179-203.
49. Hansen C M. *Hansen Solubility Parameters: A user's handbook*. 2nd ed. CRC Press; 2007.
50. Poling BE, Prausnitz JM, O'Connell JP. *The Properties of Gases and Liquids*. 5th ed. McGraw-Hill; 2001.
51. Lam SY, Benoit RL. Some thermodynamic properties of the dimethyl sulfoxide-water and propylene carbonate-water systems at 25°C. *Canadian Journal of Chemistry*. 1974; 52.
52. Zhang XR, Zhang LZ, Liu HM, Pei LX. One-step fabrication and analysis of an asymmetric cellulose acetate membrane for heat and moisture recovery. *Journal of Membrane Science*. 2011; 366(1-2):158-165.
53. Lambourne R, Strivens TA. *Paint and Surface Coatings: Theory and practice*. 2nd ed. Woodhead Publishing Ltd Cambridge; 1999.
54. Hung WL, Wang DM, Lai JY, Chou SC. On the initiation of macrovoids in polymeric membranes: Effect of polymer chain entanglement. *Journal of Membrane Science*. 2016; 505:70-81
55. Chung TS, Teoh SK, Hu X. Formation of ultrathin high-performance polyethersulfone hollow-fiber membranes. *Journal of Membrane Science*. 1997; 133:161-175.

56. Lambourne R, Strivens TA. *Paint and Surface Coatings: Theory and practice*. 2nd ed. Woodhead Publishing Ltd Cambridge; 1999.
57. Isono Y, Nagasawa M. Solvent effects on rheological properties of polymer solutions. *Macromolecules*. 1980; 13:862-867.
58. Tosun I. *The Thermodynamics of Phase and Reaction Equilibria*. 1st ed. Elsevier; 2012.
59. Tasselli F, Drioli E. Tuning of hollow fiber membrane properties using different bore fluids. *Journal of Membrane Science*. 2007; 301(1-2):11-18.
60. Fernández GL, García-Payo MC, Khayet M. Effects of mixed solvents on the structural morphology and membrane distillation performance of PVDF-HFP hollow fiber membranes. *Journal of Membrane Science*. 2014; 468:324-338.
61. Kahrs C, Gühlstorf T, Schwellenbach J. Influences of different preparation variables on polymeric membrane formation via nonsolvent induced phase separation. *Journal of Applied Polymer Science*. 2019; 137(28).
62. Gençal Y, Durmaz EN, Çulfaz-Emecen PZ. Preparation of patterned microfiltration membranes and their performance in crossflow yeast filtration. *Journal of Membrane Science*. 2015; 476:224-233.
63. Kusworo TD, Budiyo, Ikhsan D, Rokhati N, Prasetyaningrum A, Mutiara FR, Sofiana NR. Effect of combination dope composition and evaporation time on the separation performance of cellulose acetate membrane for demak brackish water treatment. *MATEC Web of Conferences*. 2017; 101; 6.
64. Chaturvedi BK, Ghosh AK, Ramachandran V, Trivedi MK, Hanra MS, Misra BM. Preparation, characterization and performance of polyethersulfone ultrafiltration membranes. *Desalination*. 2001; 133(1):31-40.

65. Torrestiana-Sanchez B, Ortiz-Basurto RI, Brito-De La Fuente E. Effect of nonsolvents on properties of spinning solutions and polyethersulfone hollow fiber ultrafiltration membranes. *Journal of Membrane Science*. 1999; 152(1):19-28.
66. Knill CJ, Kennedy JF. Degradation of cellulose under alkaline conditions. *Carbohydrate Polymers*. 2003; 52:281-300.
67. Pavasars I, Hagberg J, Borén H, Allard B. Alkaline Degradation of Cellulose: Mechanisms and Kinetics. *Journal of Polymers and the Environment*. 2003; 11 (2): 39-47.
68. Shieh JJ, Chung TS. Effect of liquid-liquid demixing on the membrane morphology, gas permeation, thermal and mechanical properties of cellulose acetate hollow fibers. *Journal of Membrane Science*. 1998; 140(1): 67-79.
69. Rahbari-Sisakht M, Ismail AF, Matsuura T. Effect of bore fluid composition on structure and performance of asymmetric polysulfone hollow fiber membrane contactor for CO₂ absorption. *Separation and Purification Technology*. 2012; 88:99-106.
70. Ahmad AL, Otitoju TA, Ooi BS. Hollow fiber (HF) membrane fabrication: A review on the effects of solution spinning conditions on morphology and performance. *Journal of Industrial and Engineering Chemistry*. 2019;70:35-50.
71. Qin JJ, Wang R, Chung TS. Investigation of shear stress effect within a spinneret on flux, separation, and thermomechanical properties of hollow fiber ultrafiltration membranes. *Journal of Membrane Science*. 2000; 175(2):197-213.
72. Qin J, Chung TS. Effect of dope flow rate on the morphology, separation performance, thermal and mechanical properties of ultrafiltration hollow fibre membranes. *Journal of Membrane Science*. 1999; 157(1):35-51.

73. East GC, McIntyre JE, Rogers V, Senn SC. Production of porous hollow polysulphone fibres for gas separation; 1986.
74. Chung TS, Qin JJ, Gu J. Effect of shear rate within the spinneret on morphology, separation performance and mechanical properties of ultrafiltration polyethersulfone hollow fiber membranes. *Chemical Engineering Science*. 2000; 55(6):1077-1091 .
75. Qin J, Chung TS. Effect of dope flow rate on the morphology, separation performance, thermal and mechanical properties of ultrafiltration hollow fibre membranes. *Journal of Membrane Science*. 1999; 157(1):35-51.
76. Chung TS, Lin WH, Vora RH. The effect of shear rates on gas separation performance of 6FDA-durene polyimide hollow fibers. *Journal of Membrane Science*. 2000; 167(1):55-66.
77. Chung TS, Teoh SK, Lau WWY, Srinivasan MP. Effect of shear stress within the spinneret on hollow fiber membrane morphology and separation performance. *Industrial & Engineering Chemistry Research*. 1998; 37(10):3930-3938.
78. Hasbullah H, Kumbharkar S, Ismail AF, Li K. Preparation of polyaniline asymmetric hollow fiber membranes and investigation towards gas separation performance. *Journal of Membrane Science*. 2011; 366(1-2):116-124.
79. Qin J, Chung TS. Effect of dope flow rate on the morphology, separation performance, thermal and mechanical properties of ultrafiltration hollow fibre membranes. *Journal of Membrane Science*. 1999; 157(1):35-51.
80. Tsai HA, Kuo CY, Lin JH, et al. Morphology control of polysulfone hollow fiber membranes via water vapor induced phase separation. *Journal of Membrane Science*. 2006; 278(1-2):390-400.

81. Widjojo N, Chung TS. Thickness and air gap dependence of macrovoid evolution in phase-inversion asymmetric hollow fiber membranes. *Industrial & Engineering Chemistry Research*. 2006; 45(22):7618-7626.

APPENDICES

A. Gel Permeation Chromatography (GPC) Calibration Curves

GPC Universal Calibrations

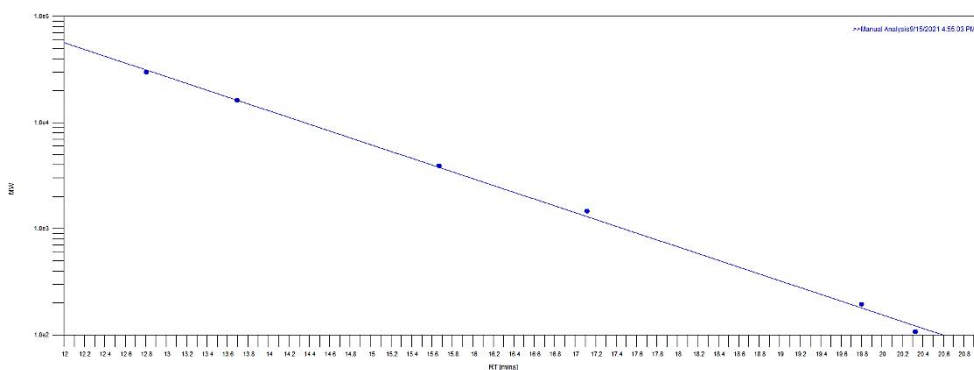


Figure A. 1. GPC universal calibration of double-column via PEG standards (Easy-Vials) for molecular weight, MW (Da) vs. retention time, RT (mins) graph

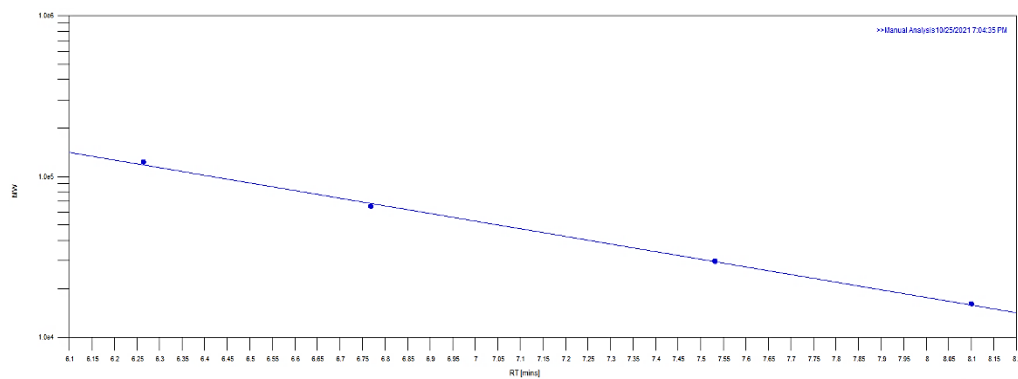


Figure A. 2. GPC universal calibration of single column via PEG calibration standards for molecular weight (MW, Da) vs. retention time, (RT, mins) graph

PEG Probes Calibrations

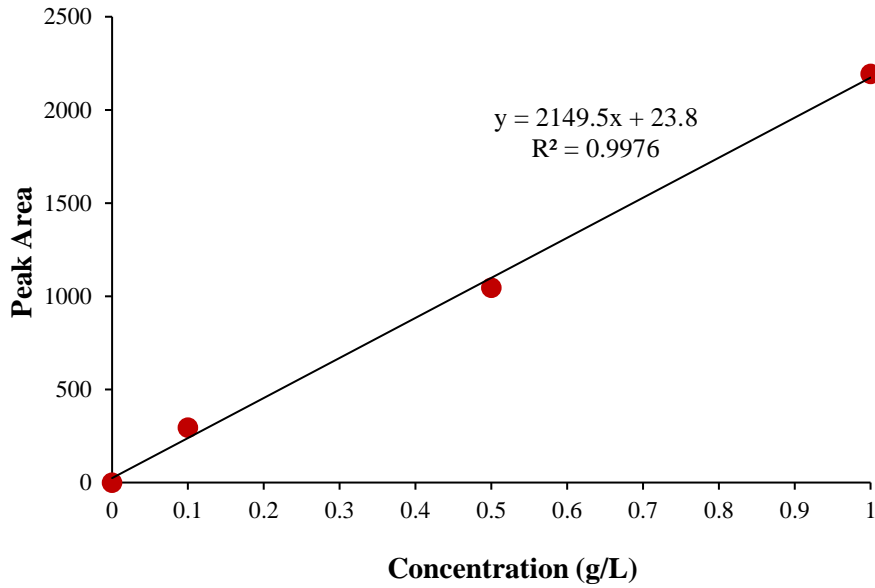


Figure A. 3. Calibration curve of PEG 400 Da

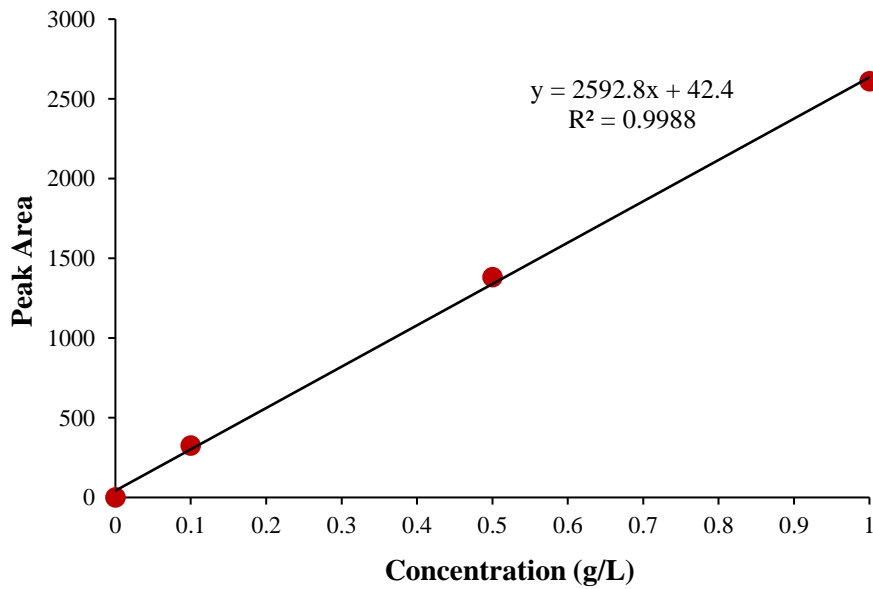


Figure A. 4. Calibration curve of PEG 2 kDa

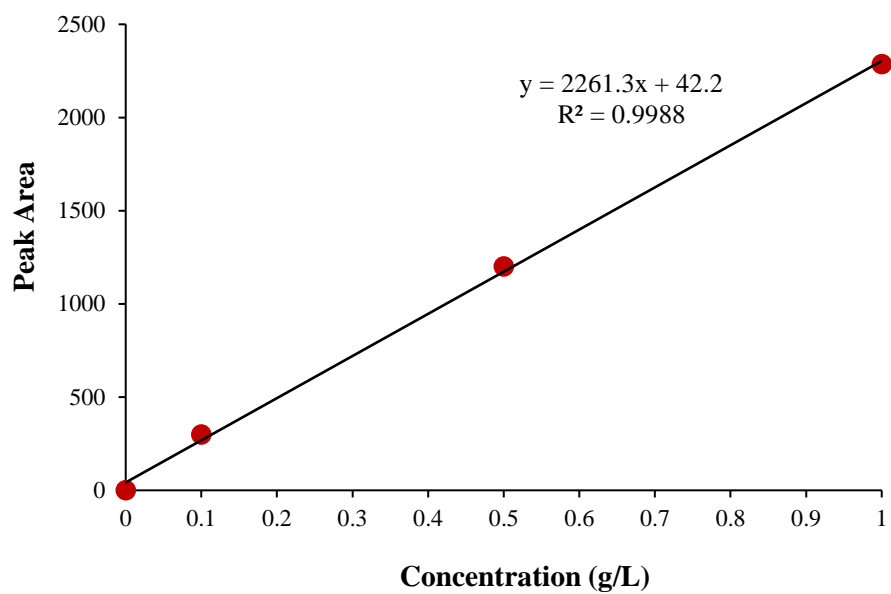


Figure A. 5. Calibration curve of PEG 6 kDa

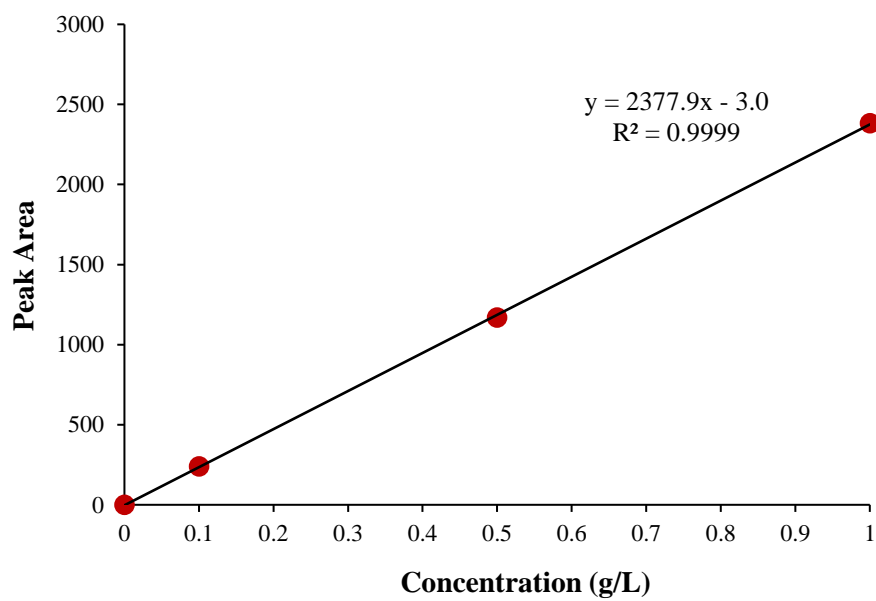


Figure A. 6. Calibration curve of PEG 10 kDa

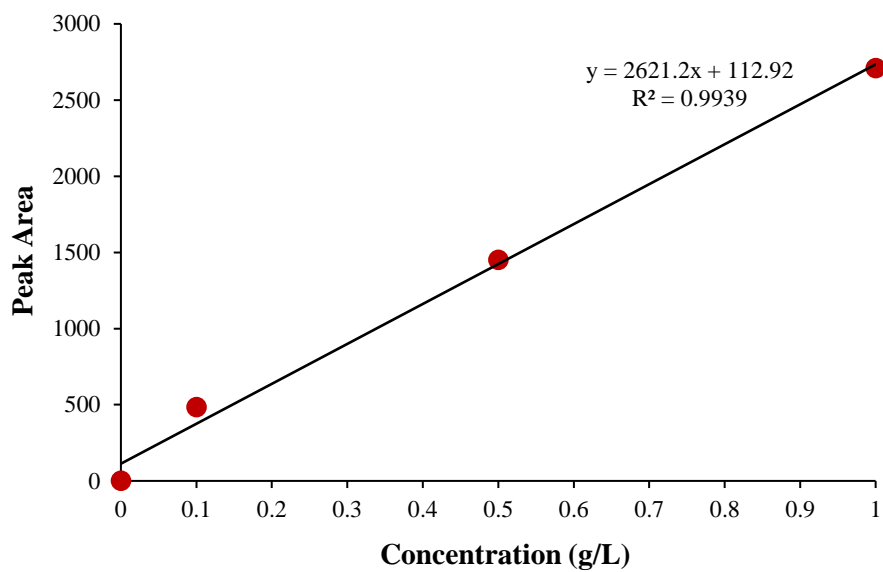


Figure A. 7. Calibration curve of PEG 20kDa

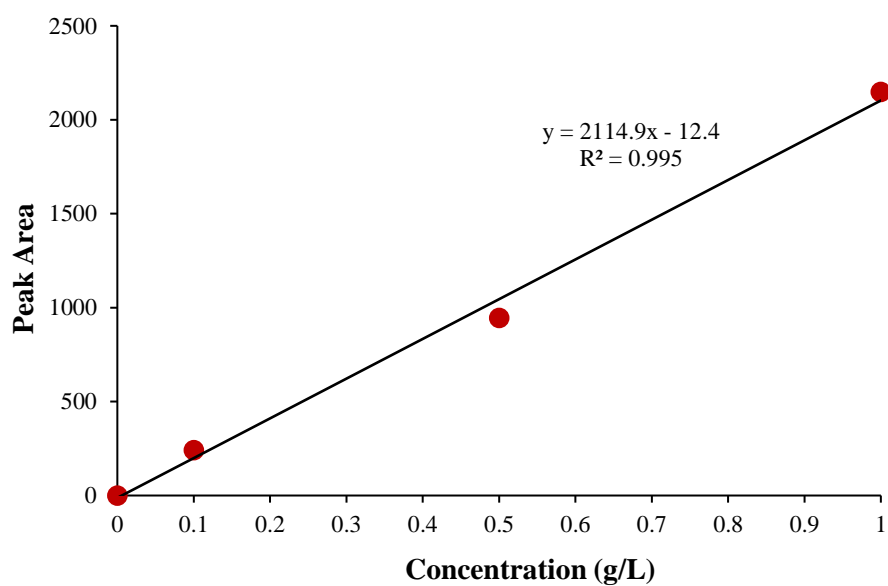


Figure A. 8. Calibration curve of PEG 35 kDa

Dextran Probes Calibration Curve

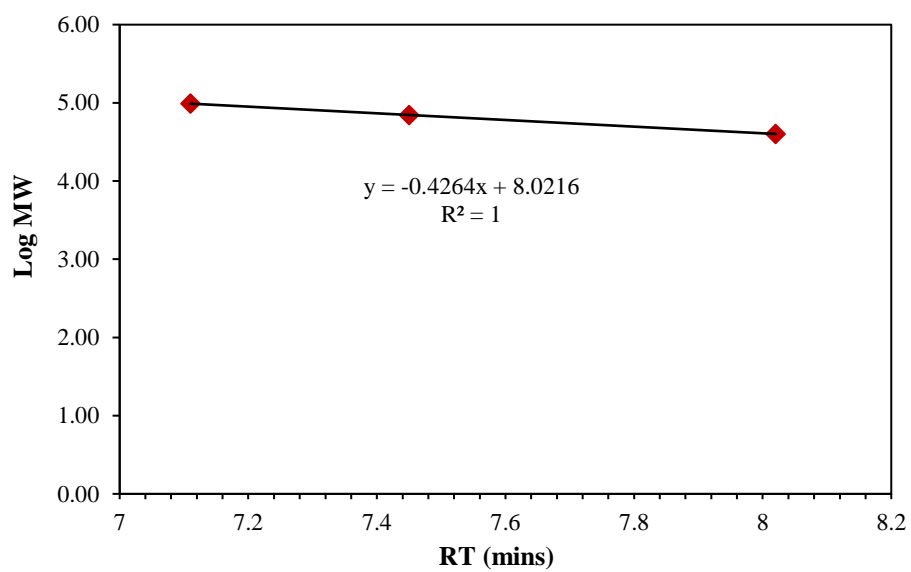


Figure A. 9. Calibration curve for 40 kDa-70kDa-200kDa dextran probes

B. Morphologies of CA and CA-AH Parts of Flat Sheet Membranes

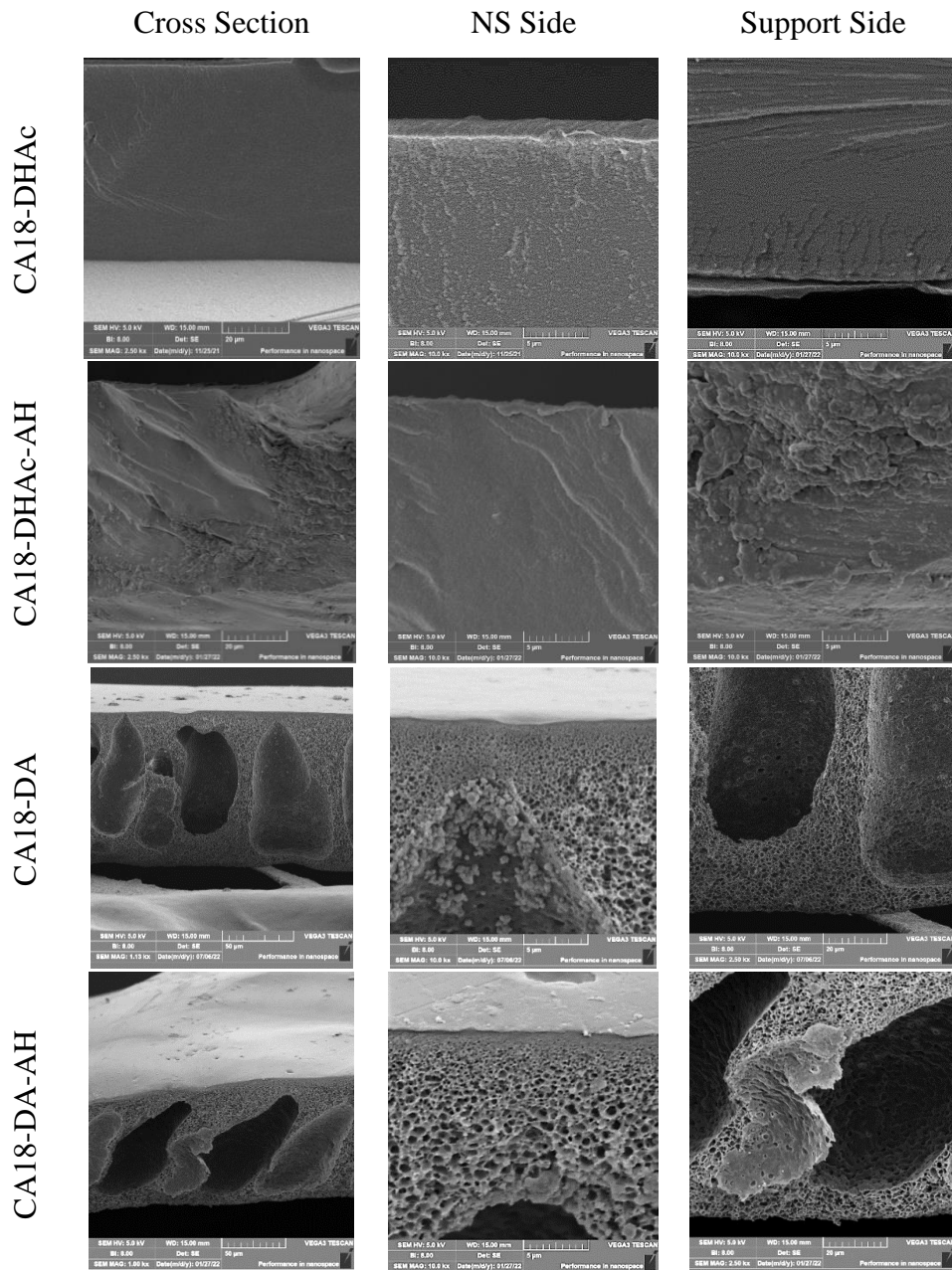
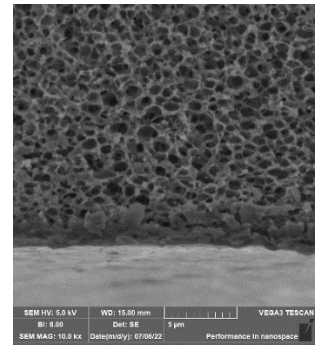
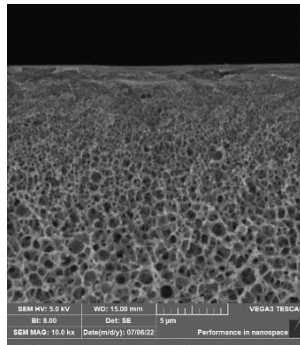
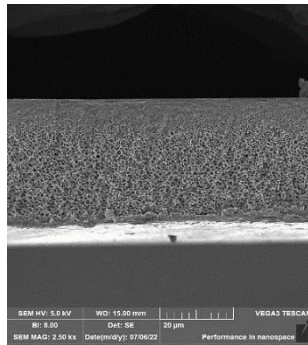
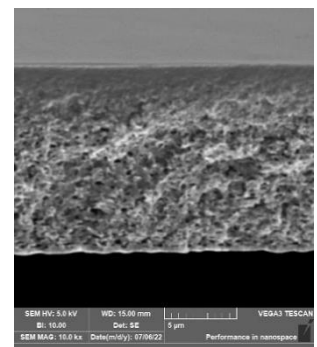
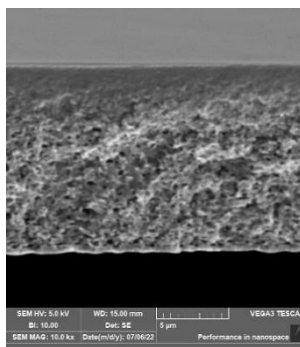
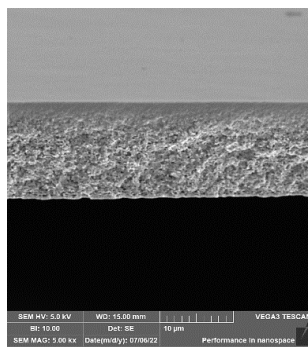


Figure B. 1. Effect of alkaline hydrolysis on the morphology of flat sheet membranes from porous to dense structures (cont'd)

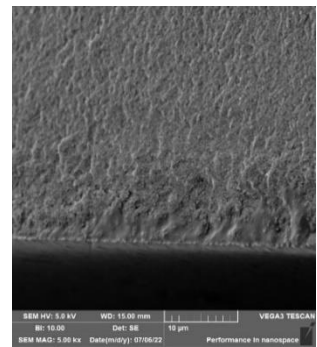
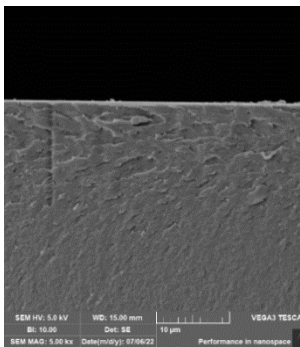
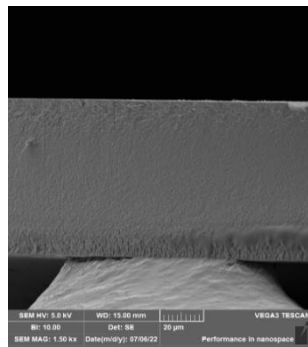
CA25-DA-30CT



CA25-DA-30CT-AH



CA25-DA-5E



CA25-DA-5E-AH

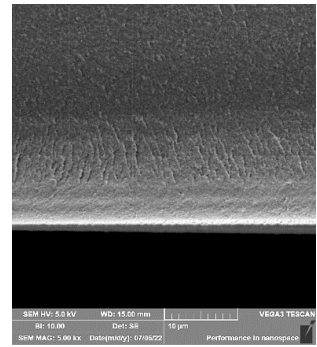
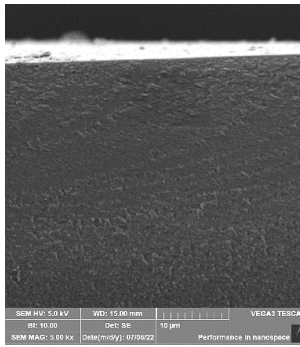
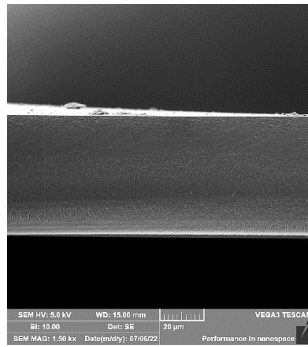


Figure B.1. (cont'd)

C. CA18-DHAc Flat Sheet Membranes and Alkaline Hydrolysis Parts with Different Thickness

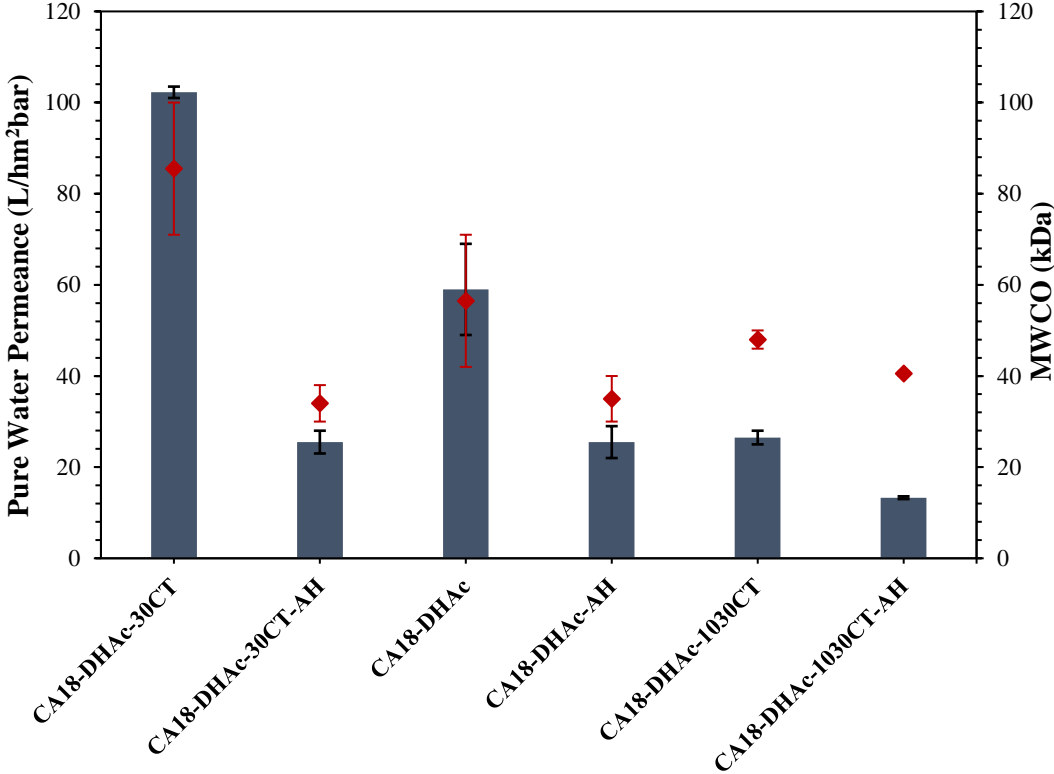


Figure C. 1. Performance results of CA18-DHAc membranes and alkaline hydrolysis parts with different thicknesses

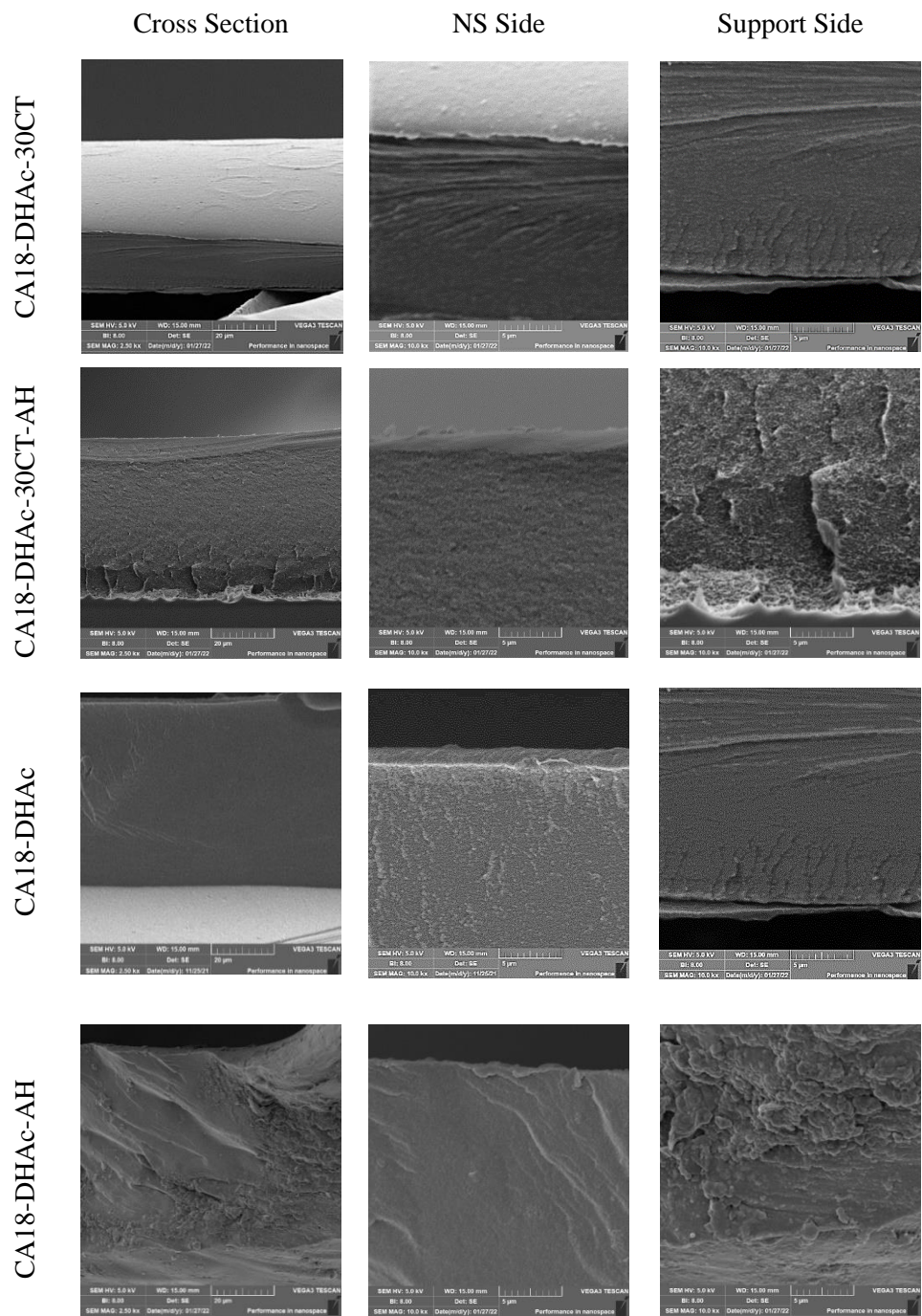
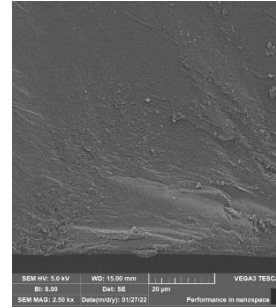
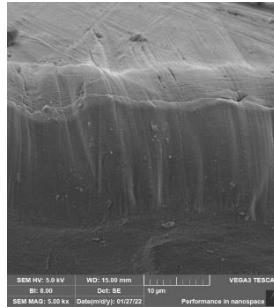
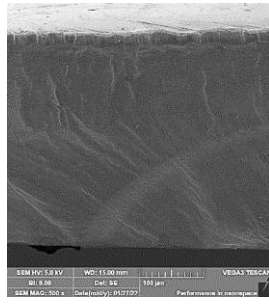


Figure C. 2. Morphologies of CA18-DHAc membranes and alkaline hydrolysis parts with different thicknesses (cont'd)

CA 18-DHAc-1030CT



CA 18-DHAc-1030CT-AH

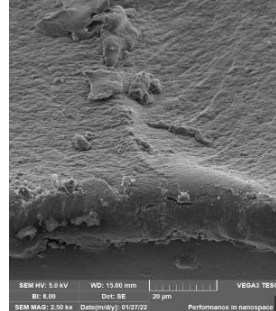
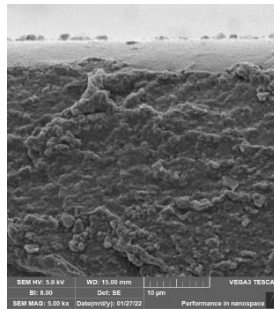
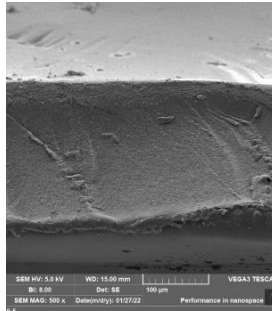


Figure C. 2. (cont'd)

D. Average Pore Size and Effective Skin Layer Thickness Estimation by Ferry-Renkin Equation

The average pore size (r_p) of UF membranes can be estimated by Ferry-Renkin equation shown in equation (1) derived for the screen filter model¹. As seen from the equation, the average pore size of membranes were obtained from the membrane's rejection (R) of a solute of known radius (a).

$$R = \left[1 - 2 \left(1 - \frac{r_D}{r_p} \right)^2 + \left(1 - \frac{r_D}{r_p} \right)^4 \right] \times 100 \% \quad (1)$$

To calculate the average radius of pores, the hydrodynamic radius of dextran molecules was calculated with the molecular weight (M_S) of dextran molecules at 90% rejection (MWCO) by using equation (2). The calculated r_D and r_p values for membranes with different casting thicknesses (CT) are tabulated in Table D.1.

$$\log(r_D) = 0.47 \log(M_S) - 1.513 \quad (2)$$

Table D. 1. Calculated hydrodynamic radius of dextran molecules (r_D) and average pore diameters (r_p) of CA18-DHAc membranes with different thicknesses

Membrane	Average MWCO, Da	Radius of Dextran (r_D), nm	Avr. Radius of Pore (r_p), nm
CA18-DHAc-30CT	85500	6.38	8.3
CA18-DHAc-250CT	56500	5.25	6.8
CA18-DHAc-1030CT	48000	4.87	6.3

Using these average pore sizes (r_p) and permeance of membranes (P), the effective selective layer thicknesses (δ) of CA18-DHAc membranes were estimated by modified Hagen-Poiseuille equation for convective flow through the membrane pores as shown in equation (3),

$$P = \frac{1}{8} \frac{r_p^2 \varepsilon}{\tau \delta \eta} \quad (3)$$

where the τ is tortuosity and ε is porosity of membranes were assumed as 2.5 and 0.05 for CA18-DHAc membranes, respectively. The dynamic viscosity of water (η) at 25 °C was used (0.001 kg/ms). The effective selective layer thickness of membranes are listed in Table D.2.

Table D. 2. Effective selective layer thickness of membranes of CA18-DHAc

Membrane	PWP (L/hm ² bar)	Selective Layer Thickness (μ m)
CA18-DHAc-30CT	101	0.6
CA18-DHAc-250CT	59	0.7
CA18-DHAc-1030CT	26.5	1.3

E. CA18-DHAc Hollow Fiber Membranes with Different Bore Liquids

Table E. 1. Spinning conditions for CA18-DHAc hollow fiber membranes fabricated by different bore liquids

Membrane Code	Bore Liquid	Air Gap (cm)	PDFR/BLFR (mL/min)	Pulling Speed (m/min)
2AG-DW-FF	80% DMSO 20% Water			
2AG-50D50W-FF	50% DMSO- 50% Water	2	3.8/1.9	Freefall
2AG-W-FF	Water			
2AG-50EG50W-FF	50% Ethylene Glycol 50% Water			

Table E. 2. Performance tests of CA18-DHAc hollow fiber membranes fabricated by different bore liquids

Membrane	Pure Water Permeance ($\text{Lh}^{-1}\text{m}^2\text{bar}^{-1}$)	MWCO (kg mol^{-1})
2AG-DW-FF	4 ± 2	10 ± 1
2AG-50D50W-FF	3	6.5
2AG-W-FF	1	*
2AG-50EG50W-FF	0.2	*

*MWCO test couldn't be conducted due to lower PWP.

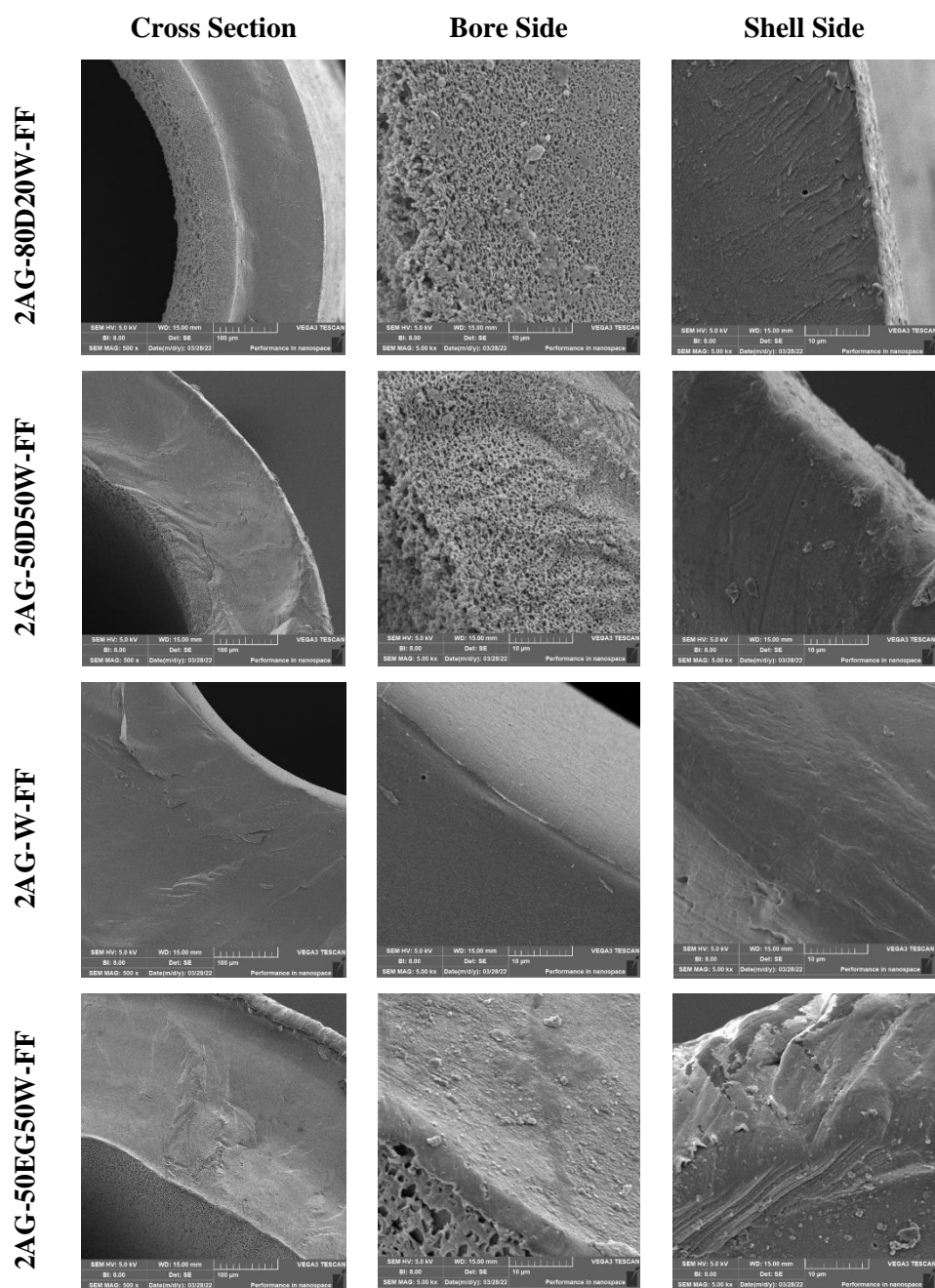


Figure E. 1. SEM Images of CA18-DHAc hollow fiber membranes fabricated by different bore liquids

F. Polymer Solutions for Cloud Point Measurements

CA18-D System (Cloud Point: 10.3 wt. % water)

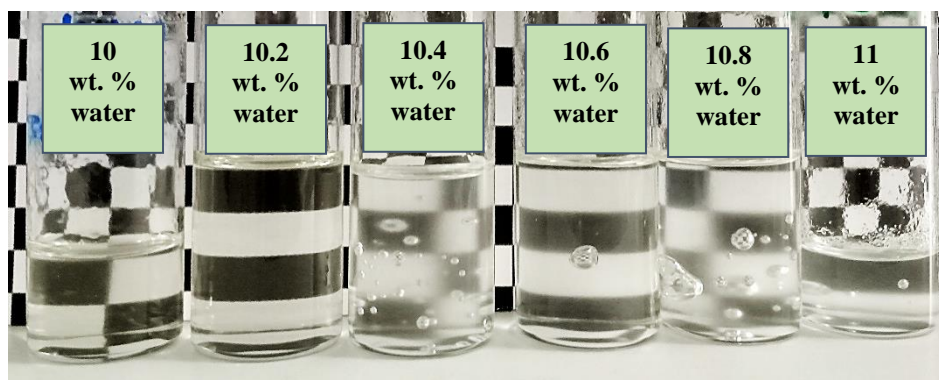


Figure F. 1. CA18-D polymer solutions with different water concentrations for cloud point measurement

CA18-DA System (Cloud Point: 13.3 wt. % water)

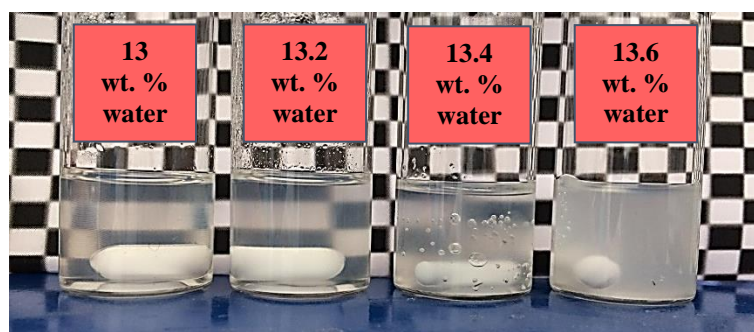


Figure F. 2. CA18-DA polymer solutions with different water concentrations for cloud point measurement

CA18-DHAc System (Cloud Point: 8.1 wt. % water)



Figure F. 3. CA18-DHAc polymer solutions with different water concentrations for cloud point measurement

G. Viscosity of Polymer Solutions

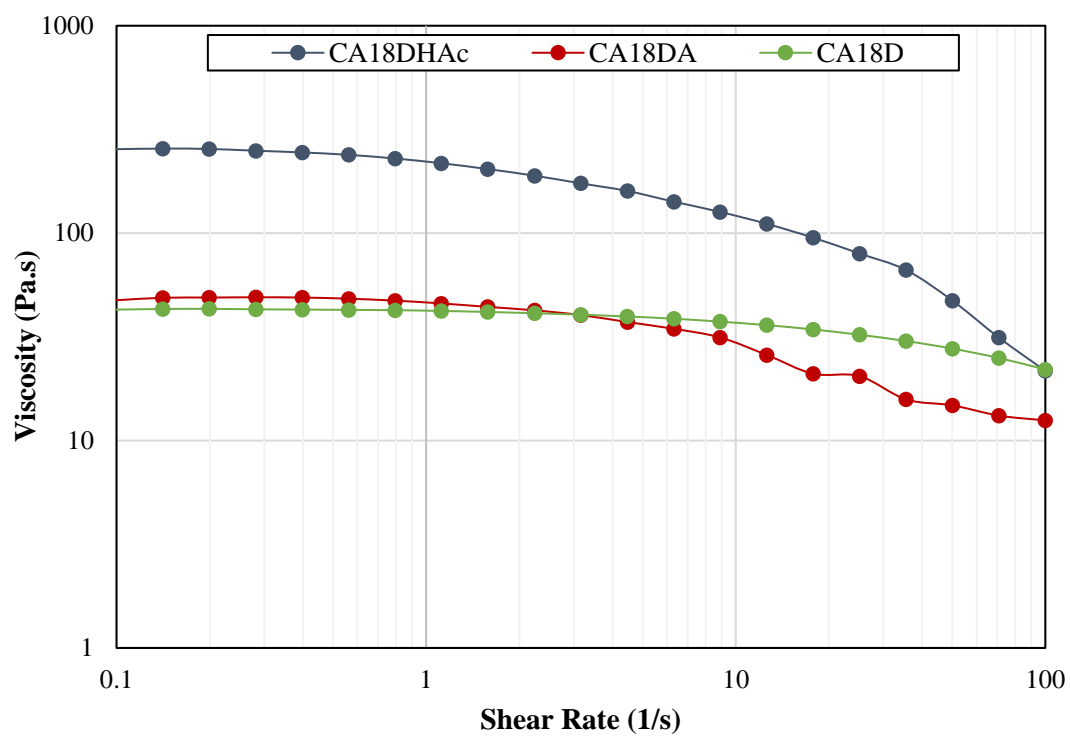


Figure G. 1. Viscosities of polymer solutions at different shear rates

H. Excess Gibbs Free Energy Calculation for Solvent-Water Systems

Excess Gibbs free energy (\underline{G}^{ex}) of solvent-water systems were calculated by equation (1),

$$\underline{G}^{ex} = RT \sum_{i=1}^k x_i \ln \gamma_i \quad (1)$$

Since the experimental data are not available for all solvent-water systems, the activity coefficients of components (γ_i) in the mixture were estimated via the UNIFAC model,

$$\ln \gamma_i = \ln \gamma_i^C + \ln \gamma_i^R$$

where, γ_i^C is combinatorial activity coefficient and γ_i^R is residual activity coefficient. The γ_i^C part was calculated by equation (2),

$$\ln \gamma_i^C = \ln \frac{\Phi_i}{x_i} + 5q_i \ln \frac{\theta_i}{\Phi_i} + l_i - \frac{\Phi_i}{x_i} \sum_j x_j l_j \quad (2)$$

Φ_i : volume fraction of component i

θ_i : surface area fraction of component i

x_i : mole fraction of component i

$$\Phi_i = \frac{r_i x_i}{\sum_j r_j x_j}$$

$$\theta_i = \frac{q_i x_i}{\sum_j q_j x_j}$$

$$l_i = 1 - r_i + 5(r_i - q_i)$$

r_i : molecular volume of component i

q_i : molecular surface area of component i

$$r_i = \sum_k v_k^{(i)} R_k$$

$$q_i = \sum_k v_k^{(i)} Q_k$$

$v_k^{(i)}$ is the number of k chemical groups present in component i , and R_k and Q_k values are listed in Table H. 1. for subgroups of component.

Table H. 1. R_k and Q_k values for groups included by solvents and components ⁶⁹

Components	Subgroup	$v_k^{(i)}$	R_k	Q_k
DMSO	DMSO	1	2.8266	2.472
Acetone	CH ₃	1	0.9011	0.848
	CH ₃ CO	1	1.6724	1.488
Acetic Acid	CH ₃	1	0.9011	0.848
	COOH	1	1.3013	1.224
Water	H ₂ O	1	0.9200	1.400

The γ_i^R part was calculated by equation (3),

$$\ln \gamma_i^R = \sum_k v_k^{(i)} [\ln \Gamma_k - \ln \Gamma_k^{(i)}] \quad (3)$$

$$\ln \Gamma_k \text{ (or } n \Gamma_k^{(i)}) = Q_k \left[1 - \ln \left(\sum_m \Theta_m \Psi_{mk} \right) - \sum_m \frac{\Theta_m \Psi_{km}}{\sum_n \Theta_n \Psi_{nm}} \right]$$

Θ_m : area fraction of group m

Ψ_{mn} : group interaction parameter

$$\Theta_m = \frac{Q_m X_m}{\sum_n Q_n X_n}$$

X_m : mole fraction of group m

$$X_m = \frac{\sum_j v_m^{(j)} x_j}{\sum_j \sum_n v_n^{(j)} x_j}$$

$$\Psi_{mn} = \exp\left(\frac{-a_{mn}}{T}\right)$$

a_{mn} : binary interaction parameter between two subgroups,

$a_{mn} \neq a_{nm}$ and $a_{mm} = 0$, the interaction parameters for solvent-water systems are listed in Table H. 2.

Table H. 2. Interaction Parameters for subgroups in the components⁶⁹

Interaction parameters for DMSO-Acetone-Water System			
$a_{\text{DMSO-CH}_3}$	50.49	$a_{\text{CH}_3\text{-DMSO}}$	526.5
$a_{\text{DMSO-CH}_3\text{CO}}$	110.4	$a_{\text{CH}_3\text{CO-DMSO}}$	-44.58
$a_{\text{DMSO-H}_2\text{O}}$	-240.0	$a_{\text{H}_2\text{O-DMSO}}$	-139
$a_{\text{CH}_3\text{-CH}_3\text{CO}}$	476.4	$a_{\text{CH}_3\text{CO-CH}_3}$	26.76
$a_{\text{CH}_3\text{-H}_2\text{O}}$	1318	$a_{\text{H}_2\text{O-CH}_3}$	300
$a_{\text{CH}_3\text{CO-H}_2\text{O}}$	472.5	$a_{\text{H}_2\text{O-CH}_3\text{CO}}$	-195.4
Interaction parameters for DMSO-Acetic Acid-Water System			
$a_{\text{DMSO-CH}_3}$	50.49	$a_{\text{CH}_3\text{-DMSO}}$	526.5
$a_{\text{DMSO-COOH}}$	-180.2	$a_{\text{COOH-DMSO}}$	-463.6
$a_{\text{DMSO-H}_2\text{O}}$	-240.0	$a_{\text{H}_2\text{O-DMSO}}$	-139
$a_{\text{CH}_3\text{-COOH}}$	663.5	$a_{\text{COOH-CH}_3}$	315.3
$a_{\text{CH}_3\text{-H}_2\text{O}}$	1318	$a_{\text{H}_2\text{O-CH}_3}$	300
$a_{\text{COOH-H}_2\text{O}}$	-66.17	$a_{\text{H}_2\text{O-COOH}}$	-14.09
Interaction parameters for DMSO-Water System			
$a_{\text{DMSO-H}_2\text{O}}$	-240.0	$a_{\text{H}_2\text{O-DMSO}}$	-139

I. Shear Rate Calculations

- Between the casting bar and glass plate during casting of a polymer solution

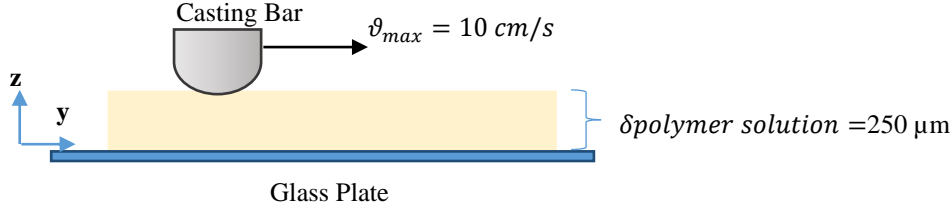


Figure I. 1. Schematic drawn of casting of polymer solution on a glass plate

Since the distance between the glass plate and casting bar is very close, polymer solution was assumed to flow in parallel plates. The velocity profile for Newtonian fluid flowing in parallel plates is in equation (1). Velocity profile at casting system was calculated for Newtonian fluid for a quick estimation since the results for shear rate at the spinneret wall were calculated as very similar in Newtonian and non-Newtonian assumptions. The shear rate is derivative of equation (1) with respect to z as shown in equation (2).

$$v_{zy} = z \frac{v_{zy,max}}{\delta} \quad (1)$$

$$\dot{\gamma} = \frac{dv}{dz} = \frac{v_{max}}{\delta} \quad (2)$$

The velocity of casting bar during (upper plate) was assumed as 10 cm/s. The thickness of fluid layer (polymer solution) is 250 μm .

$$\dot{\gamma} = \frac{v_{max}}{\delta} = \frac{0.1 \text{ m/s}}{250 * 10^{-6} \text{ m}} = 400 \text{ s}^{-1}$$

- At the outer wall of the spinneret

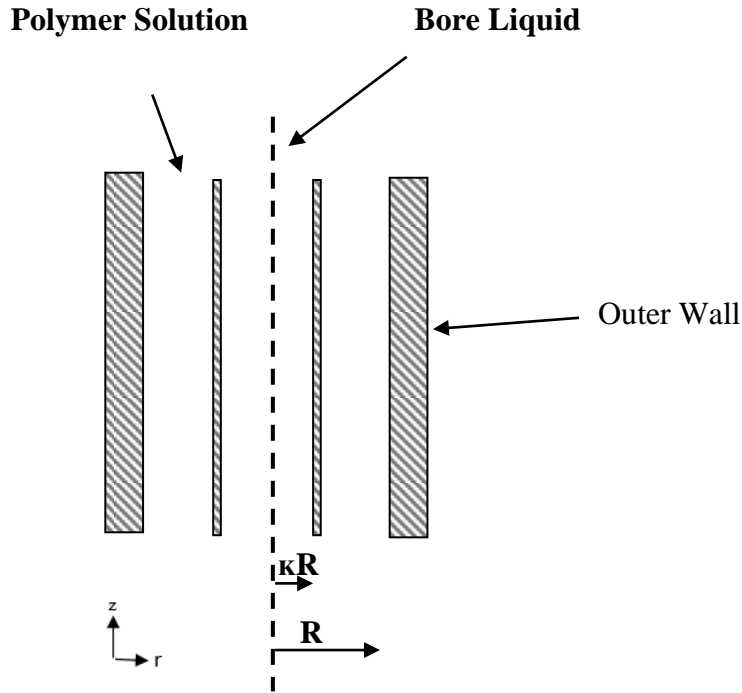


Figure I. 2. Basic illustration of inside of the spinneret

During hollow fiber spinning, the polymer solution was fed through the annular space shown in Figure I. 2. The z-component of Couchy stress equation was considered in cylindrical coordinates in equation (3)

$$0 = \frac{-1}{r} \frac{d}{dr} (r\tau_{rz}) - \frac{dP}{dz} \quad (3)$$

$$\frac{-1}{r} \frac{d}{dr} (r\tau_{rz}) = \frac{dP}{dz} = c1 \text{ (constant)}$$

After integration,

$$\tau_{rz} = \frac{-dP}{dz} \frac{r}{2} + \frac{c1}{r}$$

Boundary Condition: at $r=\lambda R$ (is the radius of maximum velocity), $\tau_{rz} = 0$

$$0 = \frac{-dP \lambda r}{dz} \frac{1}{2} + \frac{c1}{\lambda r}$$

$$c1 = \frac{dP \lambda R^2}{dz} \frac{1}{2}$$

$$\tau_{rz} = \frac{-dP r}{dz} \frac{1}{2} + \frac{dP \lambda R^2}{dz} \frac{1}{2}$$

$$\tau_{rz} = \frac{-\Delta P}{2L} \left(r - \frac{\lambda R^2}{2} \right) \quad (4)$$

The power law model in equation (5) was used for CA18-DHAc polymer solution.

$$\eta = -m\gamma^{n-1} \quad (5)$$

$\lambda R \leq r \leq R$; as r increased, ϑ_z decreased so,

$$\gamma = \frac{d\vartheta_z}{dr} < 0$$

$$\eta = -m \left(-\frac{d\vartheta_z}{dr} \right)^{n-1} \quad (6)$$

$$\tau_{rz} = -\eta \frac{d\vartheta_z}{dr} \quad (7)$$

Equation (6) was substituted into equation (7),

$$\tau_{rz} = m \left(-\frac{d\vartheta_z}{dr} \right)^{n-1} \left(-\frac{d\vartheta_z}{dr} \right)$$

$$\tau_{rz} = m \left(-\frac{d\vartheta_z}{dr} \right)^n \quad (8)$$

Equation (8) is equal to equation (4),

$$\tau_{rz} = \frac{-\Delta P}{2L} \left(r - \frac{\lambda R^2}{2} \right) = m \left(-\frac{d\vartheta_z}{dr} \right)^n \quad (9)$$

When the equation (9) was simplified for shear rate expression,

$$\dot{\gamma} = \frac{d\vartheta_z}{dr} = \left(\frac{\Delta Pr}{2mL}\right)^{1/n} \left[1 - \left(\frac{\lambda R}{r}\right)^2\right]^{1/n}$$

At the outer wall of the spinneret, where the $r=R$, the shear rate was expressed by equation (10)

$$\dot{\gamma} = \left|\frac{d\vartheta_z}{dr}\right| = \left(\frac{\Delta PR}{2mL}\right)^{1/n} [1 - (\lambda)^2]^{1/n} \quad (10)$$

Instead of Hagen-Poiseuille equation, the volumetric flow rate in terms of pressure differences across the length L was expressed as follow ⁷⁴.

$$Q = \int_{\kappa R}^R 2\pi r \vartheta_z dr = \pi R^3 \left(\frac{\Delta PR}{2mL}\right)^{1/n} \int_{\kappa}^1 [\lambda^2 - \rho^2]^{\frac{n+1}{n}} \rho^{-1/n} d\rho$$

$$\left(\frac{\Delta PR}{2mL}\right)^{1/n} = \frac{Q}{\pi R^3} \frac{1}{\int_{\kappa}^1 [\lambda^2 - \rho^2]^{\frac{n+1}{n}} \rho^{-1/n} d\rho} \quad (11)$$

Equation (11) was substituted into equation (10), and shear rate at the outer wall of the spinneret ($r=R$) was expressed in equation (12),

$$\dot{\gamma} = \left|\frac{d\vartheta_z}{dr}\right| = \frac{Q}{\pi R^3} \frac{[1 - (\lambda)^2]^{1/n}}{\int_{\kappa}^1 [\lambda^2 - \rho^2]^{\frac{n+1}{n}} \rho^{-1/n} d\rho} \quad (12)$$

Where $\rho = r/R$, and n is power law constant of the CA18-DHAc polymer solution obtained by rheological data (log shear rate vs. log viscosity graph) in Figure I. 3.

The linearized form of equation (5),

$$\log \eta = \log m + (n - 1) \log \dot{\gamma}$$

From the graph,

$$\text{Slope} = n-1 = -0.2664$$

$$n = 1-0.26 = 0.74$$

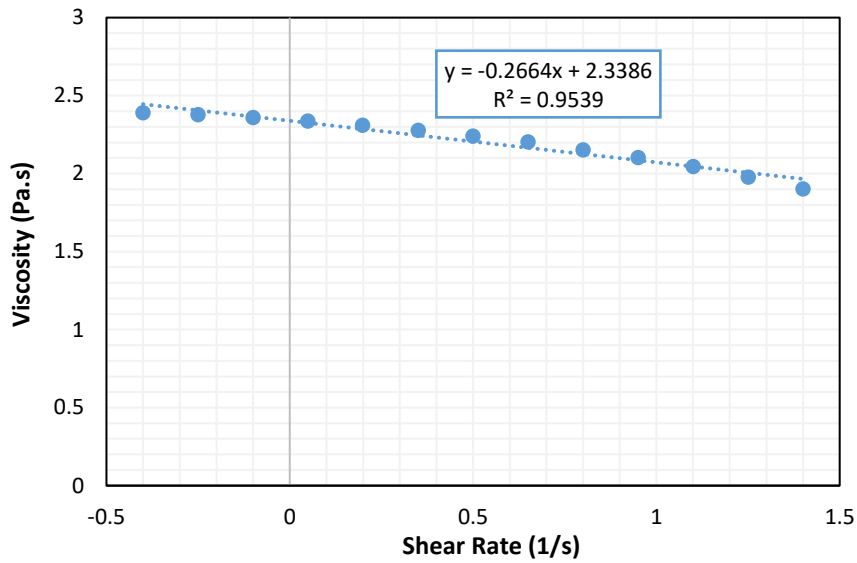


Figure I. 3. Viscosity versus shear rate graph of CA18-DHAc polymer solution

λ was found by the following equation that is the equation for Newtonian fluid; however, the same one may be used for non-Newtonian fluid since the dimensions of spinneret are small,

$$2\lambda^2 = \frac{1 - \kappa^2}{\ln\left(\frac{1}{\kappa}\right)}$$

- inside radii of spinneret: $\kappa R = 0.65 \text{ mm}$
- outside radii of spinneret: $R = 1.5 \text{ mm}$

$$\kappa = \frac{\kappa R}{R} = 0.43$$

$$2\lambda^2 = \frac{1 - 0.43^2}{\ln\left(\frac{1}{0.43}\right)}$$

$$\lambda^2 = 0.49$$

When the constants are substituted into equation (12) and the integral part of it was solved by Simpsons 1/3 rule ($h=0.057$),

$$\int_{\kappa}^1 [\lambda^2 - \rho^2]^{\frac{n+1}{n}} \rho^{-1/n} d\rho = \int_{0.43}^1 [0.49 - \rho^2]^{2.37} \rho^{-1.37} d\rho = 0.032$$

When $Q = 12 \text{ cm}^3/\text{min}$,

$$\dot{\gamma} = \left| \frac{d\vartheta_z}{dr} \right| = \frac{Q}{\pi R^3} \frac{[1 - (\lambda)^2]^{1/n}}{\int_{\kappa}^1 [\lambda^2 - \rho^2]^{\frac{n+1}{n}} \rho^{-1/n} d\rho}$$

$$\dot{\gamma} = \frac{12 \text{ cm}^3/\text{min}}{3.14 (0.15^3) \text{ cm}^3} \frac{[1 - 0.49]^{1.37}}{0.032}$$

$$\dot{\gamma} = 14255 \frac{1}{\text{min}} = 237 \text{ 1/s}$$

When $Q = 3.8 \text{ cm}^3/\text{min}$,

$$\dot{\gamma} = 4514 \frac{1}{\text{min}} = 75 \text{ 1/s}$$